GLOBULAR CLUSTERS

A Photometric Study of Some Southern Clusters

K.K. Searia

Thesis submitted to the
Madurai University
for the Degree of
Doctor of Philosophy

Indian Institute of Astrophysics

January 1980

Certificate from the Supervisor

I certify that the thesis entitled "GLOBULAR CLUSTERS - A Photometric study of some southern clusters" by K.K. Scaria is a record of the research carried out by him at the Indian Institute of Astrophysics. The candidate has worked on this thesis under my supervision since January 1975. I declare that the thesis has not previously formed the basis for the award of any Degree, Diploma, Associateship, Fellowship or similar title.
The thesis contains an account of research carried out by the candidate on some aspects of the intensity distributions in globular clusters, especially in some of the brightest such objects located in the Southern Hemisphere. Techniques involving photoelectric and photographic procedures form the basis of many of the inferences of kinematic behaviour and stellar distribution.

M K V Bappu

(M.K.V. Bappu)
Director
Indian Institute of Astrophysics

ACKNOWLEDGEMENTS

All the observational material used for this work was obtained with the 102cm reflector at the Kavalur field station of the Indian Institute of Astrophysics. Most of the reduction was done when I was stationed at Kodaikanal.

I was initiated into the subject of Photoelectric Photometry and Equidensitometry of Globular Clusters by Dr. M.K.V. Bappu, Director, Indian Institute of Astrophysics in 1975. The work was carried out under his able guidance. No words can express my thanks for the ever helpful inspiration and guidance provided by him during the entire course of this work. His constant advice in the matter of reduction and the interpretation of the results helped me in completing the work. I am also grateful to Mrs. Bappu for the keen interest she has shown in my work.

I am thankful to Mr. T.P. Prabhu and Mr. A.V. Raveendran for their help in the processing of the data. I am also thankful to Dr. R. Rajamohan, Dr. N. Kameswara Rao, Mr. M. Parthasarathy and Mr. P. Venkatakrishnan for their helpful suggestions during the course of the work.

Mr. L. Peter, Mr. F. Gabriel, Mr. Alfred Charles, Mr. A. Mani, Mr. M. Irulappan and Mr. A. Michael rendered all the required help in making the auxilliary equipments for the observation and the reduction of the data. I am grateful to every one of them.

I am grateful to Mr. R. Sivashanmugam for making my stay in Kavalur field station very pleasant during the many trips I have made for observations with the telescope.

The entire thesis was typed by Mr. A.Md. Batcha. All the diagrams were prepared by Mr. S. Muthukrishnan and Mr. A. Selvaraj. Mr. Monappa made xerox copies of all the diagrams. Mrs. and Mr. Krishnamoorthy did the binding of the thesis. My sincere thanks are due to each one of these individuals. I am also grateful to Mrs. A. Vagiswari for the cooperation she offered in completing the work.

I am grateful to Prof. W. Liller of Harward Observatory for lending me the photographs of 47 Tucanae for equidensitometry.

Everybody in the Institute showed keen interest in this work and I gratefully acknowledge the help they rendered to me.

CONTENTS

CONTENTS

SUMMARY

Globular clusters form a spherical system around the centre of the galaxy. Harlow Shapley observed that the stars in globular clusters are quite different from those seen in galactic clusters in that the blue giants and super-giants are completely absent in them. We infer from this behaviour, in the light of work done in the last few decades, that globular clusters have large ages. The colour-magnitude diagrams of globular clusters are very important for comparison with theories on stellar evolution. Also globular clusters are of great importance in the field of stellar dynamics. The distribution of stars of different colours, in such a cluster, is of importance for an inference of the dynamical properties of these spherical systems.

The evolution of stars and their distribution in the cluster are related to each other. There is evidence to show that, in globular clusters, the giants have larger concentration towards the centre. There is also evidence to show that the fainter stars in a globular cluster have a wider spatial distribution when compared to the red giants. The RR Lyrae stars show less concentration towards the centre of the cluster. The brightest stars in globular clusters are red giants, which occupy the tip of the giant

branch in the HR diagram. The bluest stars in the cluster are, in general, the horizontal branch stars. If the RR Lyrae stars show less concentration towards the centre, it is perhaps because, they have attained larger velocity dispersion due to mass loss while evolving from the giant branch to the horizontal branch. Since all the stars in the horizontal branch are in a more advanced stage of evolution than the giants in the cluster, the horizontal branch stars could have lost much mass. This mass loss could give a different spatial distribution to the horizontal branch stars.

Such differences in star distribution are best studied near the centre, where the time of relaxation is the smallest for the cluster. But, unfortunately, due to the large density of stars in the inner regions, the study of individual stars is impossible. Hence, such differences are best studied from colour gradients over the cluster. In the work described in this thesis, we have made a colour gradient study over the giant globular cluster Omega Centauri. We have also carried out multicolour equidensitometry of the cluster for a study of two dimensional colour distribution.

Chapter I gives a comprehensive history of early work done on globular clusters. Points which are relevant to the

present work have been explained in detail. We have described the kind of photometric observations available for globular clusters, especially on surface photometry. A detailed description of the theoretical model presented by King for brightness distribution in globular clusters is made. The merits and demerits of the model are pointed out. This chapter also gives a detailed account of the chemical inhomogeneities seen in globular clusters with special emphasis on the inhomogeneities observed in the giant globular cluster Omega Centauri. We have presented the data available on the rotation of Omega Centauri and its effect on the form of cluster. Also described herein are characteristics of intensity distribution seen in elliptical galaxies and the relationship with their rotational characteristics.

In Chapter II, we describe the five colour photoelectric surface photometry done on the globular cluster Omega Centauri. A filter system for five colour photometry which can be used with an S20 surface photomultiplier tube is described. Full details are given about the transformation of the instrumental system to the standard U B V R I system of Johnson. Using Hartwick's luminosity function for the globular cluster M92 we have estimated

the sampling errors in UBVR and I bands and also for U-B, B-V, V-R and R-I colours. Kings theoretical model has been used to calculate the core-radius of the cluster. We have shown that the values of core-radius change with the wavelength band used for the surface photometry. The U-B/B-V diagram was used to find the UV excess over the cluster with Hyades main sequence as reference. It has been shown that the increase in UV excess between 2'.5 and 5' from the cluster centre, is due to an increase in the contribution from bluer stars. Observations made by other investigators on individual stars have been cited to prove our conclusions. The photometric data have been used to show the B-I colour change over the cluster along the major and minor axis.

In the third chapter, we describe the multicolour isodensitometry done on Omega Centauri. A detailed description is given about the method of obtaining isophotes, the making of isophote maps and the reduction of axial ratios and position angles from the equidensity contours. The results obtained are compared with the photometric results of Chapter II. We have shown that the increase in ellipticity of the cluster between 2'.5 and 5' from the centre of the cluster, is due to the blue bulge around the core of the cluster.

We have also done equidensitometry on 47 Tuc, another giant globular cluster in our galaxy. The results of equidensitometry, are compared with the photometric results obtained for the cluster by other investigators. These results are used to confirm our earlier conclusions.

In chapter IV, we have employed the technique of photographic subtraction, to obtain the spatial distribution of blue and red stars in the cluster. The surface brightness due to the horizontal branch stars has been calculated. The bulge which gives the large blue contribution in the annular region from 2'.5 to $\lesssim$ 5' of arc has been brought out in the photograph which gives a direct proof for the presence of the blue bulge around the centre.

In the final chapter, we have given the results of the above investigation and discussed possible observations needed for further elucidation of the conclusions reached.

CHAPTER I

THE NATURE OF GLOBULAR CLUSTERS

1.1 **Introduction:** Globular Clusters are large stellar aggregates that are almost spherical in shape, have linear diameters in the range of 10 to 120 pc and masses of the order of 10^5 to 10^6 $M_\odot$. They are known to contain large numbers of evolved stars, which is an indication of their age ($\lesssim 10^{10}$ years). Shapley (1917) was the first to show the uniqueness of the colour-magnitude diagram of globular clusters. He found that the most luminous group of stars in each cluster had high colour-indices and these colour-indices decrease with decreasing luminosity. This is a trend quite opposite to what is seen in the young galactic clusters. Since Shapley's measures were confined to cluster giants ($M_v < +1$), the relationship between the H-R diagrams of galactic and globular clusters remained unnoticed.

Cuffey, Greenstein and Hackenberg made further attempts to study C-M diagrams of globular cluster stars in the thirties. With the advent of photoelectric techniques and the development of yellow sensitive plates of greater speed and low reciprocity failure, the study of the fainter members of the globular clusters became

possible. Arp et al (1953) gave colour-magnitude diagrams for M92 which extended from the red giant branch, at absolute photovisual magnitude of -3 to a segment of the main sequence, at absolute photovisual magnitude of +4. They showed how the giant sequence branches off from the main sequence in globular clusters. The cluster type variables fell in a distinct gap in the horizontal branch between P-V = +.12 mag and P-V = +.23 mag, which is completely devoid of non-variable stars.

Baade's (1944) work on M31 and its two elliptical companions M32 and NGC 205, gave rise to the two population concept. The galactic clusters and stars in the solar neighbourhood, which have small velocity dispersion of space motions and show a distribution confined to the disc of the galaxy, belonged to a category that was recognized to be relatively young. Globular cluster stars and stars which have high velocity dispersion in their space motions, and which show almost a spherical galactic distribution were considered to be old objects. Colour-magnitude diagrams of globular clusters are qualitatively very similar, but significant differences exist among them. Sandage (1953) has shown the striking differences that exist in the colour-magnitude diagrams of M3 and M92, the most striking being the stretching along the colour-index

axis of the M3 diagram, as compared to that for M92, resulting in the colour differences of the giant, subgiant asymptotic and main sequences in the two clusters. Schwarzschild explains this in terms of differences in the abundance of heavy elements between M3 and M92. Arp (1959) has shown that the UV excess measured in a U-B/B-V diagram at B-V = 1.0 is a good indicator of metal abundance in the cluster. Preston (1959) has established a parameter of metal abundance by differencing the spectral types of RR Lyrae stars, as determined by their hydrogen lines on one hand and the metallic H and K lines on the other hand. This parameter ΔS has a range of values that represent clusters with metal abundances that vary from low to high values. Morgan (1959) has measured metallicity from integrated spectra and his results match well with the results of the other methods mentioned above.

Morgan (1959) finds that the earliest spectral type of globular clusters can be early F with spectra that show extremely weak metallic lines. On passing towards globular clusters of successively later spectral type, the metallic absorptions become more and more similar to those in stars of the solar neighbourhood. Several globular clusters have been found to simulate spectra of strong lined stars. Based on the metallic line intensities,

globular clusters are divided into 8 groups by Morgan ranging from the extremely weak lined clusters (e.g. M92) to those that have strong metallic lines. The radial inhomogeneity in metal abundance of our galaxy, is clearly seen in Morgan's results. It is well known that there exists large differences in metal abundance between the halo and disc populations in our galaxy. One also finds the metal rich globular clusters to be more concentrated towards the centre of the galaxy (Morgan 1959). This has been taken to indicate a decrease of metallicity with increasing radial distance from the centre.

Baade has shown the similarity in stellar content between globular clusters and the more massive elliptical and dwarf galaxies. Strom et al (1976) have found in several elliptical and SO galaxies that the colour-indices (U-B), (B-V) and (V-K) decrease outward from the nucleus. In flattened systems, the observed colour gradients were the greatest along the minor axis. They have noted the decrease in metallicity with increasing distance from the nucleus of the galaxy. The (U-B) index, shows a weak correlation with (V-K) as well as other metallicity indicators. Thus the (U-B) index can be used as a probe for the study of metallicity changes in E and SO galaxies.

The structure of a globular cluster and its stellar content are very much related to each other. If there is any equipartition of energy in these clusters, we should find a stratification of cluster stars, the large mass stars concentrating towards the centre and low mass stars keeping away. Harding (1965) has shown that the globular cluster Omega Centauri rotates about its minor axis and that the cluster is quite elliptical in form. Michie (1964) finds that a rotating cluster will show flattening because of mixing of orbits due to stellar encounters. In the inner regions where encounters are very effective, some stars will obtain sufficient energy to escape and many more will acquire enough energy to be thrown out into bound orbits of high energy and low angular momentum. These stars carry away much energy from the inner regions. The decrease in velocity dispersion will make the core contract, and the loss of angular momentum will cause the rotation at the centre to decrease. This in turn should produce a smaller ellipticity. Michie also points out that in a rotating cluster, it is easier for a star to escape, if the peculiar velocity is in the direction of rotation.

King (1974) discusses the different aspects of the structure of round stellar systems, the kind of

observations available and the merits and demerits of all available observations. He points out that relaxation through stellar encounters should create differences in distribution between low and high mass stars. The relaxation time of globular clusters is small when compared to their age and hence these objects should show mass segregation. King (1962) points out the difficulty in observing this feature in clusters. The density distribution in a stellar system is related to the velocity distribution in it. Hence, there will be a concentration of low velocity stars near the centre of the cluster, which means that brightness distribution near the centre is dominated by the light from large mass stars. The low mass stars are easily seen in the envelope. But here the bright stars are few. Thus we cannot observe both the low mass and high mass stars over the same region of the cluster with equal certainty. As theory predicts, the contribution to the surface brightness from the low mass stars increases and that from the massive stars decreases, with distance from the cluster centre. Surface photometry, which can be carried out to faint limits, should show this relative change, when the cluster is observed in different colours. Another way to look for mass segregation is to search for evolved stars, like RR

Lyrae stars, which have lost mass due to evolution and then relaxed to a higher degree of velocity dispersion. Their spatial distribution in the cluster would demonstrate the segregation.

I.2 Distribution of light in globular clusters: To study the distribution of light in globular clusters, one has to use different techniques, for the central and the outer regions. For the dense central regions, we use photoelectric or photographic photometry whereas for the outer regions, it is possible to use star counts. Star counting is the best way of reaching the tidal limit of the cluster. Gascoigne and Burr (1956) made concentric aperture photoelectric measures of surface brightness, colour and integrated magnitude, of the two giant globular clusters Omega Centauri and 47 Tuc in the P and V bands. They report that for 47 Tuc, the centre is redder than the outer regions by P-V = 0.17 magnitude. Kron and Mayall (1960) made concentric aperture photoelectric measurements of sixty seven galactic globular clusters in V band. They also give the integrated (P-V) and (V-I) colours of these clusters. King (1966) made a very extensive study of nine bright northern globular clusters in B and V bands. He has carried out an exhaustive discussion on the statistical fluctuations in observed surface

brightness and colours due to random distribution of the individual stars. Illingworth and Illingworth (1976) made detailed photoelectric surface photometry of ten centrally concentrated southern clusters using small aperture drift scans as well as centred aperture photometry in B and V bands. Star counts were made to extend the distribution to the outer regions of the cluster. The observed distributions are compared with King's theoretical models to derive core-radii, tidal radii, total magnitudes and other basic parameters for the observed clusters. Twentyfour globular clusters have been studied by Chun and Freeman (1979) in U, B and V bands. They report that eight of the clusters observed, show an increase in reddening towards the centre. Da Costa (1979) has carried out centred aperture photometry and small aperture drift scans for four southern globular clusters in U, B and V bands, to get surface brightness profiles. Again star counts have been used to extend the profiles to tidal limits. Peterson and King (1975) have derived core-radii for 43 globular clusters and core-radii, limiting radii and richness factor for 37 globular clusters, using all the available data on globular cluster surface photometry.

In a series of papers King (1962, 1966) has derived a theoretical model which fits well the density

distributions in globular clusters, galactic clusters and Sculptor-type dwarf elliptical galaxies. The distribution of stars in the outer regions of a cluster is influenced by the tidal forces of the galaxy. This gives a limitation to the maximum possible radius of a globular cluster which is derived from an approximate formula (King 1962).

$$r_{lim} = R_p \, (M/3.5\ Mg)^{\frac{1}{3}} \qquad .. \quad (1.1)$$

where R_p is the distance of the cluster at perigalacticon, M, the mass of the cluster and Mg, the mass of the galaxy. The internal energy of the cluster determines the stellar distribution in the central regions and hence the core-radius of the cluster. A third parameter affecting the stellar distribution in the cluster, is the number factor which is determined by its total mass. Using the above three parameters, King (1962) arrives at an empirical formula for the surface brightness (f) distribution over the cluster, which is given by

$$f = k\left[\frac{1}{\left[1+\left(\frac{r}{r_c}\right)^2\right]^{1/2}} - \frac{1}{\left[1+\left(\frac{r_t}{r_c}\right)^2\right]^{1/2}}\right]^2 .. \quad (1.2)$$

where r_t is the tidal radius, r_c is the core-radius, k is the number factor and $C = r_t/r_c$ is the concentration class of the cluster. Using a wide range of data, King has shown that the above equation is consistent with distribution of stars seen over globular and galactic clusters and also Sculptor type dwarf elliptical galaxies. The equation fails for giant elliptical galaxies. The extreme values of concentration $C = r_t/r_c$ seen in globular clusters are 3½ and 125. These concentration values correlate fairly well with the concentration classes given by Kron and Mayall (1960), but do not correlate well with Shapley's (1930) concentration classes (I to X).

King remarks that there is no evidence to show that ellipticities observed in some clusters have any influence on the radial density law. Another disadvantage of the law is that it assumes the same mass for all the stars, which is not true. The bright and faint stars do not have the same distribution in the cluster. Equipartion of energy will give higher velocities to less massive stars and these fainter stars will show less concentration towards the centre of the cluster. Near the cluster limit, the distribution of low and large mass stars will be the same, as the tidal cut off operates equally on all stars, regardless of mass. But nearer to the centre bright and

and faint stars should show differences in distribution. This can be observed only in clusters of very low central concentration. Results of star counts on NGC 5053 show that the low mass stars are more widely spread than the large mass ones. They have a r_c value, 1.3 times larger than that for large mass stars. The equation represents the density distribution of bright and faint stars, provided proper r_c and k values are chosen.

King (1962) points out that all the clusters obey the same law, because, though born under varying conditions, they have become similar under the influence of a regularising agency or a relaxation process. There are three kinds of relaxation processes possible: (1) Relaxation through stellar encounters (2) Relaxation through initial mixing during the time of formation of the system and (3) Relaxation following mass loss due to evolution of stars. Globular clusters have relaxation times quite small compared to their age and the first process is more favoured. The third kind of relaxation is important in very old stellar systems where mass loss due to stellar evolution is substantial. King points out that, there is enough evidence to show that relaxation takes place even before any major mass loss has started and the chances are that the relaxation in these systems, is first produced by initial

mixing and is then continued by stellar encounters. No observational evidence has so far been produced, to show a tendency towardsequipartion of energy in a stellar system that is younger than one time of relaxation.

I.3 Radial colour gradients and chemical inhomogeneities in globular clusters: Observations, both spectroscopic and photoelectric, show chemical inhomogeneities in globular clusters. Large differences are seen not only from cluster to cluster, but also within the same cluster. Morgan (1959) has shown from integrated spectra that the globular clusters nearer to the centre of the galaxy have larger metallicity as compared to clusters farther away. Bohm-Vitense et al (1963) find that the metal deficiency in globular clusters increases with increasing distance Z from the galactic plane. Pierre Demarque (1979) has shown that the heavy elements in globular clusters increase systematically with their age. The ages for the clusters he has studied range from 14-16 x 10^9years (M92) to 10 x 10^9years (M71). The age for 47 Tuc is 10-11 x 10^9years. Martin (1937) has pointed out that RR Lyrae stars are less concentrated towards the centre of the cluster in Omega Centauri. Oosterhoff found a similar phenomenon in M5, M3 and M15 also show similar characteristics in the distribution of RR Lyrae stars. Oort and van Herk (1959) have

tried to explain this feature on the basis of mass loss while the stars have evolved from the tip of the giant branch to the horizontal branch. Clusters like M3, Omega Centauri, M5 and M15 are rich in RR Lyrae stars whereas other clusters have few or none at all.

Dickens and Bell (1976) and Mallia (1977) observe that the s-process elements (barium and strontium) are enhanced in some stars of globular clusters, by a factor of more than thirty. It is considered that this enhancement is due to mixing effects which occur during the late stages of stellar evolution. Wallerstein and Pillachowski (1978) have studied C, N and O abundances in globular clusters M3, M5, M10, M13 and M71 using CO bands at 2.3 microns and the [OI] line at 6300Å. They find that in M3 and M5, carbon and oxygen (or both) have a higher abundance, as compared to M10 and M13. Kraft (1978) reports evidence for non-homogeneity in metal abundances of giant stars in several globular clusters. Differences in the value of $[A/H] \equiv \log (A/H)_* - \log (A/H)_\odot$, from star to star, within the same cluster is cited.

Omega Centauri is classified as a metal poor cluster of Morgan Class II. The cluster is well known for its wide upper giant branch with $\Delta (B-V) \gtrsim 0.4$ mag (Cannon

and Stobie, 1973). Bell and Dickens (1974) reports the presence of CH stars in the cluster. This is the only cluster which contains both CH and CN stars. They point out that stars on the red side of the upper giant branch, have abnormally strong CN bands. Bessell and Norris (1976) suggest that this elliptical cluster might have acquired considerable angular momentum at the time of formation and since there was an excess of angular momentum per unit mass, some of the stars might have developed fast rotating cores. These rotating cores could be producing the necessary mixing for the enhancement of CN and CH bands. Freeman and Rodgers (1975) found a spread of about 0.6 in Ca/H for twenty five RR Lyrae stars in this cluster. They suggest that this could be an indication of primordial inhomogeneity in calcium abundance. Three of the RR Lyrae stars showed very enhanced Ca/H value that was comparable to the metal abundance seen in metal rich clusters like 47 Tuc. Freeman also points out some of the important features noticed in globular clusters (but not yet explained). Clusters like Omega Centauri and M3 show different radial distributions for bright giants and RR Lyrae stars. Since the relaxation time for Omega Centauri is $\simeq 3 \times 10^9$ years (Peterson and King 1975), which is much larger than the giant-RR Lyrae evolution time ($\lesssim 10^8$ years, Iben 1974) the dynamical relaxation after the mass loss cannot be an

explanation for the above peculiarity in distribution. The colour changes seen in some of the clusters are too large to be explained by equipartion of energy over stars of different masses (Freeman 1975). Some clusters with Fe/H = 2.0 have stars with strong TiO bands. The M stars seen in Omega Centauri have composition similar to population I stars. Freeman and Rodgers suggest that the above features seen in globular clusters, show some of the clusters to be chemically inhomogeneous. They hypothesise that heavy element enrichment occurs in the formation of globular clusters, that it is a function of cluster mass and that it is most evident in the most massive, but initially metal weak cluster, Omega Centauri. Norris and Bessell (1975) observe that the ultraviolet colour excess for stars in Omega Centauri is more for bluer stars than for the redder stars. One possible explanation suggested by them is the contribution from faint stellar-background.

I.4 Ellipticity in the form of Globular Clusters: Many of the globular clusters are not spherical. The largest ellipticity observed is for the cluster M19 with an axial ratio of 0.4 (Shapley 1927). Lindsay (1956) has measured the ellipticity in Omega Centauri by star counts and finds the outer regions to be very elliptical. The ellipticity in blue light decreases towards the centre whereas it

increases in the near infrared. Also the ellipticity in blue is less than what it is in red from the star counts. The innermost equidensity contour of Lindsay has semi-major and semi-minor axes of 16.7' and 13.3' respectively. Dickens and Woolley (1967) find that the cluster ellipticity increases from the centre to the outer regions and reaches a maximum at a, the semi-major axis $\lesssim$ 5 minutes of arc and then decreases again further out. Sistero and Fourcade (1970) used the Sabattier technique to obtain the equidensity contours for Omega Centauri in the B band. Their five contours show the rotation of the position angle of the major-axis and also the increase in the ellipticity of the cluster with distance from the centre. Hogner et al (1973) used the same technique to study the ellipticity in M92, in U, B, V and R bands. Kadla et al (1976) obtained axial ratios and position angles of the major axis, for M3, M5, M13 and M15 in U, B, V and R bands. A change in ellipticity and orientation of the major axis has been observed in all the clusters.

Rotation of the position angle of major axis and change in ellipticity have been observed in galaxies also. Richter and Hogner (1963) have shown that the axial ratio b/a and position angle ϕ of the major axis in M31, M32 and NGC 205, change with distance from the centre.

Peterson, Ford and Rubin (1977) have studied the change in b/a and ϕ in the nucleus of M31 and shown that these changes are not due to the presence of emission regions. One well widened spectrum in blue light, of the centre of the galaxy did not show evidence of any emission within $r \lesssim 18''$. Schwarzschild (1974) has shown that the position angle of the major axis within the 3 arc second region of the centre in M31, is different from that for the rest of the galaxy. Feibelman (1979) showed that ϕ in the nuclear regions of M51 also changes with distance from the centre. He points out the similarity between the plot of ellipses he obtained for the centre of M51, and Linshu's (1964, 1966) kinematic density waves of spiral form shown by Toomre (1977). Photographic surface photometry is presented for 16 elliptical galaxies by King (1978). In four ellipticals the orientation of the major axis shifts significantly with radius. Ellipticities increase outward in some galaxies, while in some others ellipticities decrease outward. Peterson (1978) has studied rotation of ten early type galaxies. The angular velocities in the central regions of NGC 4406 and 4472 which have round centres, are much lower than those in NGC 4621 or 4649 where centres are elliptical.

I.5 Rotation in Omega Centauri: Harding (1965) has shown that Omega Centauri rotates around its minor axis. Taking 5.2 kpc as the distance of Omega Centauri from the sun (Arp 1965), Harding writes the rotation law for Omega Centauri as

$$v/r = 0.87 \text{ kms/sec/pc/cosec } i$$

This is a low estimate of rotation as the stars selected for the velocity measurements are far away from the cluster centre where the rotational velocities are relatively low. Also the tilt of the axis of rotation to the line of sight needs to be taken into account. The effect of rotation on ellipticity is not very well understood. Dickens and Woolley (1967) suggest that the inner parts of Omega Centauri are in solid body rotation. They have developed a first order theory to explain the observed ellipticity in the inner parts of the cluster. The agreement of observation with theory is fairly good which shows that rotation flattens the cluster. On the other hand Illingworth (1977) has compared the rotation data for thirteen ellipticals with the oblate models of Gott (1973, 1975), Larson (1975) and Wilson (1975) and finds that on the average most elliptical galaxies have one third the peak rotational velocities required for these models.

He suggests that rotation plays, at the most, a minimal role in the observed flattening of these elliptical galaxies. He also points out that surprisingly one elliptical galaxy in his list, rotates with velocity consistent with its flattening.

CHAPTER II

PHOTOELECTRIC PHOTOMETRY OF OMEGA CENTAURI

II.1 Introduction: We have used photoelectric and photographic techniques to study some of the characteristics of the cluster Omega Centauri and compare them with other globular clusters. The following are the different observations we have made to achieve this end.

a) Spot photoelectric measurements of Omega Centauri along the major and minor axis in UBVR and I bands.

b) Equidensitometry of the cluster in B, V and Infrared bands.

c) The use of photographic subtraction techniques to study the distribution of blue and red stars in the cluster Omega Centauri.

d) Equidensitometry of some globular clusters in the V band.

In this chapter we deal with the photoelectric observations on Omega Centauri. The bulk of the photoelectric data available in the literature for globular clusters are in the U, B and V bands. But for old stellar systems like

globular clusters, there is a predominance of light in the longer wavelengths and hence the R and I bands would be valuable sources of information. These bands, unlike U and B bands, are relatively line free. Hence, we have preferred to use 5-colour photometry. Also, the interstellar absorption in R and I bands for globular clusters is almost nil.

Omega Centauri is a very good candidate for a colour gradient study, because it is the most massive cluster in our galaxy. It has the largest core-radius among the brightest galactic globular clusters. The surface intensity does not vary so fast as it does in the case of other globular clusters. Omega Centauri has a large core radius when compared to the other giant globular cluster 47 Tucane. The cluster is 15° above the galactic plane. Even though it is relatively close to the galactic plane, there is no evidence of non-uniform reddening over the cluster. From star count data Lindsay (1956) suggested that there may be some absorbing material about 45 minutes of arc away from the centre of the cluster to the east. This absorbing material is far from our region of interest, which is the brightest part of the cluster. Also Cannon and Stobie (1973), Freeman and Rodgers (1975) and Norris and Bessel (1975) have shown from observations on the horizontal and giant branches of the cluster, that there is no large scale differential inter-stellar reddening across the cluster.

They estimate $\Delta E\ (B-V) \leq 0.04$. The major axis of the cluster is inclined to the East-West direction only by about 10°. Hence, we take the East-West scan as representative of intensity gradients along the major axis and the North-South scan as indicative of similar behaviour along the minor axis. The relaxation time of the cluster is quite large, but since the cluster age is greater than one relaxation time (Peterson and King 1975), it has had enough time to reach a state of dynamical equilibrium. We infer this from the fact, that the surface density distribution in the cluster also, matches well with King's models, with fits similar to these obtained for the other globular clusters. The basic parameters of the cluster represented in Table II-1 are taken from Peterson and King (1975).

Table II-1

Some Parameters of Omega Centauri

α 1950	δ 1950	l" deg	b" deg	V_r kms^{-1}	Distance in kpc from Sun	Distance in kpc from Gal.	$(m-M)_V$
$13^h23^m.8$	-47°13'	309	+15	+230	5.4	8.0	14.1

r_{core} (pc)	r_{tidal} (pc)	Integrated V	Central brightness in mag/sq. min. of arc	E(B-V)	Spectral Type	Concentration Class (Shapley)
3.8	86.7	3.54	7.84	0.11	F7	VIII

II.2 Instrumentation: The photometry on the cluster was done with the 102 cm reflector at Kavalur. A dry-ice cooled EMI 9558B tube was used as the detector at the f/13 Ritchey Chretien focus. This was followed by pulse counting equipment and an on-line computer. Measurements with a bright star at different points in the field through the largest aperture showed that the response of the detector unit is flat over the full field of the detector.

Concentric aperture photometry is usually applied to study the surface brightness in a cluster. Since Omega Centauri has an appreciable ellipticity, concentric aperture measures are not likely to yield reliable gradients of brightness in the cluster. Hence, aperture photometry was planned along two directions in the cluster. To get good spatial resolution, one should scan the cluster with as small an aperture as possible. But, if the aperture is

made too small, the large sampling errors will make the measurements unreliable. Hence, we have chosen an aperture of about 60 seconds of arc as a compromise. The area of the diaphragm was determined photoelectrically and with the diaphragm was determined photoelectrically and with the help of an Abbe Comparator.

Table II-2

Measurements with Abbe Comparator			Photoelectric Measurements		
Diameter of diaphragm used for measurements in mms	Scale of the field in arc secs/mm	Diameter of the diaphragm used for spot measurements in arc secs.	Diameter of the smaller diaphragm in mms	Ratio of the counts obtained for the night sky through the smaller diaphragm and the diaphragm used for spot measurements	Diameter of the diaphragm used for the spot measurements in arc secs.
2.545	23.18	58.99	0.597	18.20	59.00

The 102 cm telescope has an excellent drive system. The star changing device on the telescope, is a programmable facility that moves the telescope in R.A. and DEC., in the forward or reverse direction by known amounts from a reference point and with an accuracy of one second of arc.

By programming the system suitably to move the telescope in R.A. and DEC., the object in the field can be scanned along any required direction. The backlash in the telescope is $<$ 1 second of arc. This is easily checked by setting the telescope on a star, moving the telescope in some direction using the star changing device, and then bringing the telescope back to the star by reversing the direction of motion of the telescope. The star is never off the centre of the field by more than the diameter of the seeing disc of the star. Thus we have a very accurate way of locating the exact position of the aperture on the cluster with reference to a star in the field. The star marked P on Plate 1 which is a reproduction from a 102 cm plate at the Ritchey-Chretien focus is used as the reference star for scanning the cluster in the East-West direction and the star marked Q was used as the reference star for scanning the cluster in the North-South direction. The centre obtained by our equidensitometry on Omega Centauri was compared with the path of the scan on the cluster. It was found that the scan path is about ten seconds of arc to the west and five seconds of arc to the south of the cluster centre. This was not considered very serious, as the diaphragm size we use for scanning the cluster, is 59" of arc in diameter. Plate 1 shows the path of the aperture while scanning the cluster, when the transparent grid provided along with it

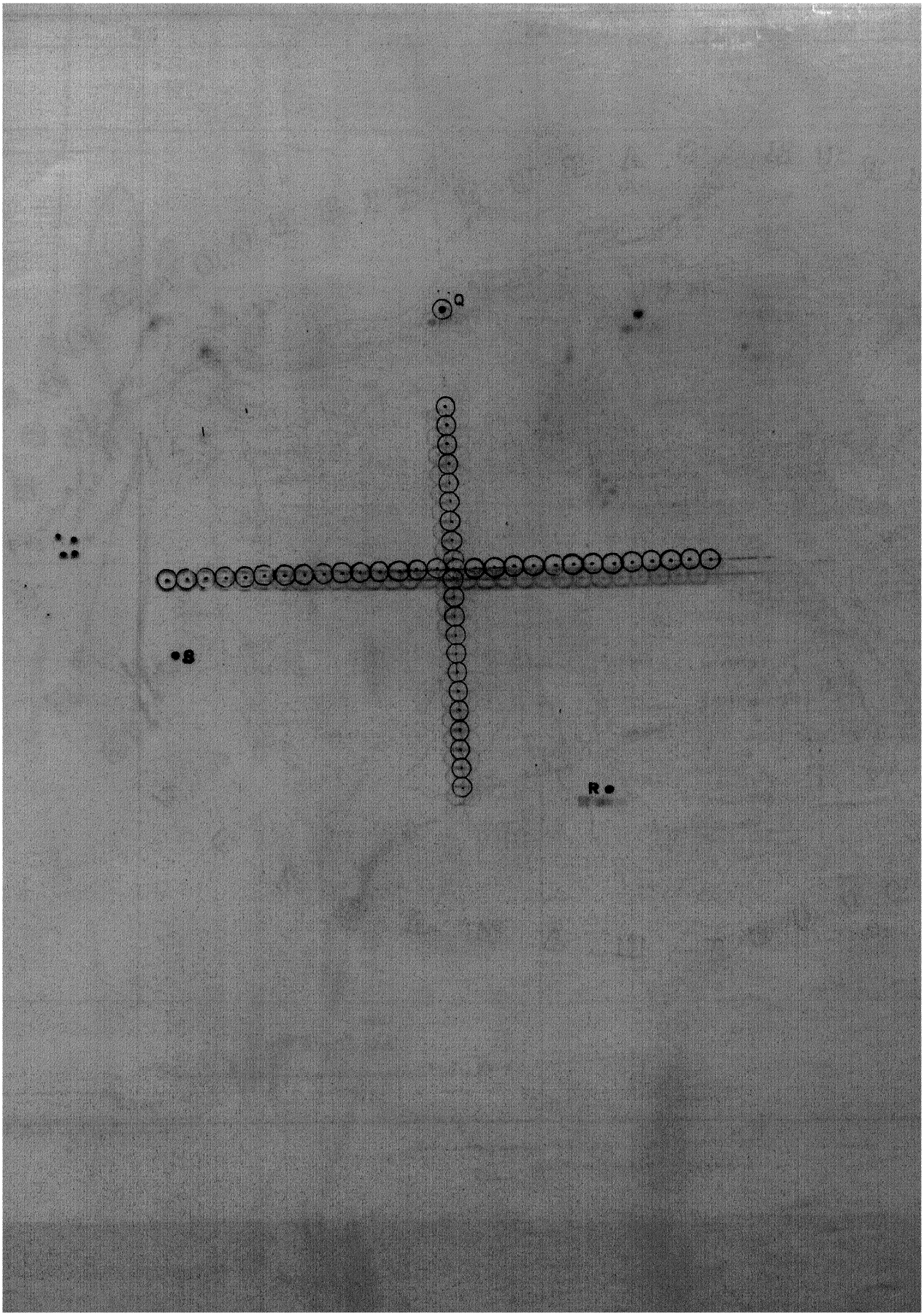
Q
S
R

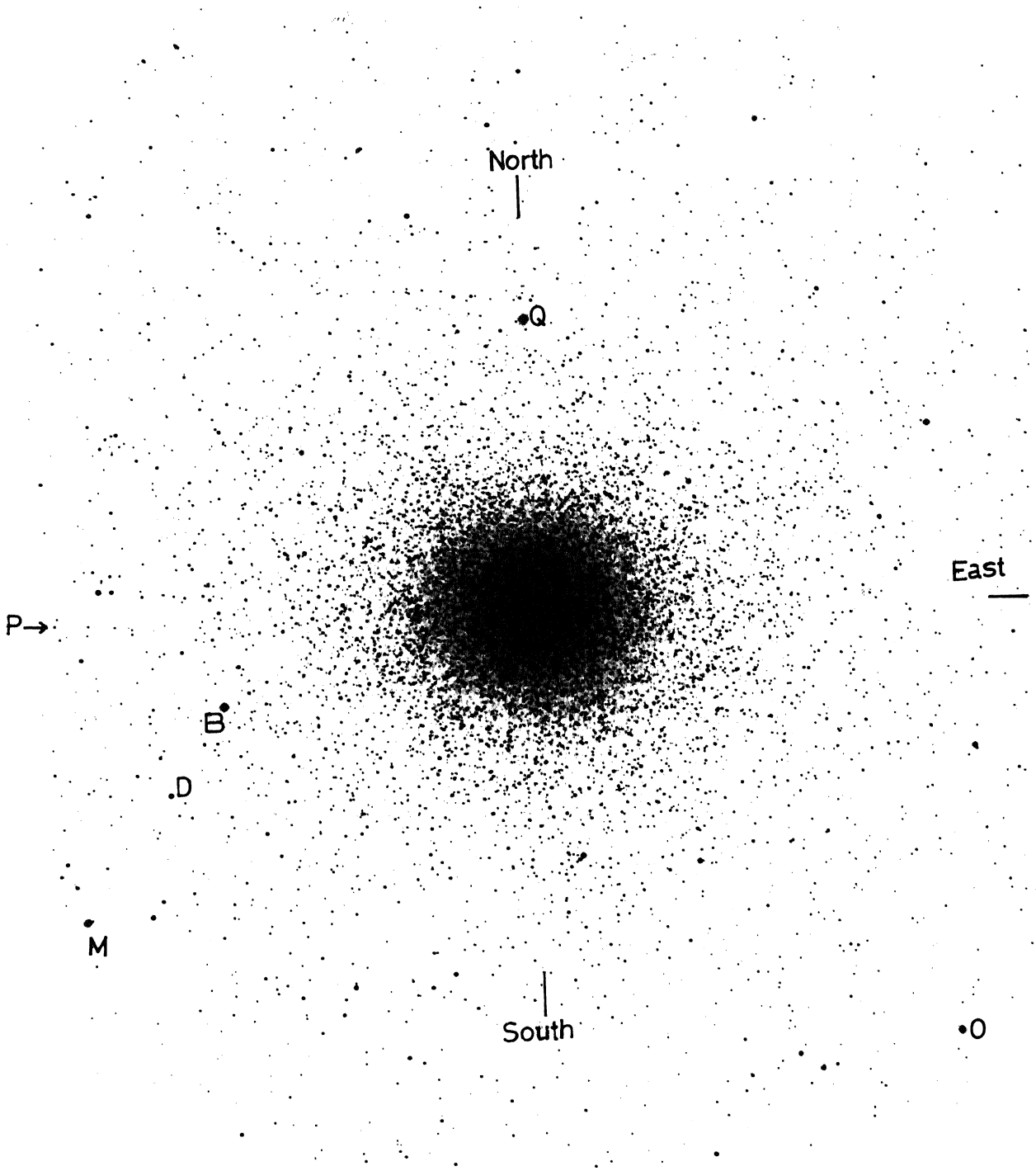

PLATE I

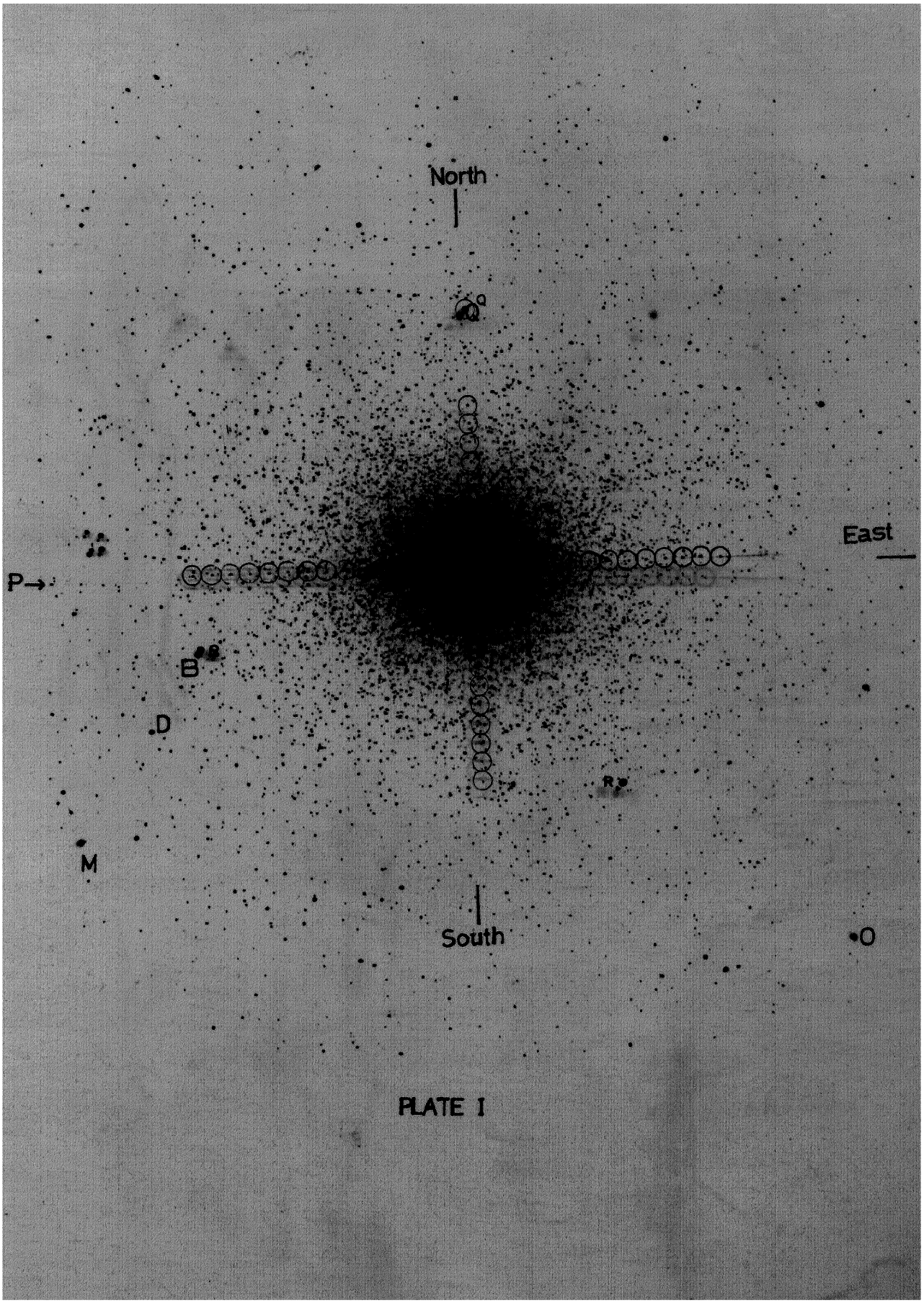

PLATE I

is matched with the reference stars. After taking counts over three aperture positions, the telescope is made to retrace the path to the reference star to see whether there was any drift in the telescope during the time of observation. Such drift, if any, was less than a second of arc. For the central regions of the cluster, 5 second counts were made and for the faint outer regions 10 and 15 second counts have been made. The counts for the U band became comparable to the sky counts when the aperture was 8 to 10 minutes of arc from the centre of the cluster. Since the sky counts have been well determined, the counts obtained for the cluster are very reliable even at these distances. Each count is a mean of two values. The stability of the counts was very good as judged by the fact that counts for a certain zone were almost the same for observations made on two different nights. If any sudden jump in the counts is noticed, such spots have been repeated once again. The time taken for one set of observation in UBVR and I bands over one position of the cluster is about 70 seconds, in the 5 seconds mode. The nights used for the observations were very good and the counts had high reproducibility. Because of the large declination, the cluster was observed every day for only about two hours around the time of culmination. Most of the remainder of the night was used for calibration of the system.

The standard detector for Johnson's UBV system is the cooled or uncooled 1P21 photomultiplier. For the R, I bands, the observations have to be made with an S1 surface. We have used an S20 surface EMI 9558B for the observations, with a suitable filter system. The tube cuts off at about 8800Å. For the RI bands, the performance of the S20 surface is not equivalent to that of the S-1 surface. But the lower noise and higher sensitivity of the S20 surface makes it more suitable for the UBVRI photometry. The filter combinations are the same as the ones used by Fernie (1974) except that in R combination, RG8 was used in place of RG6. These combinations are given in Table II-3.

Table II-3

Filter Combinations

Band	Combination.
U	UG2 (2mm) + BG18 (2mm)
B	BG12 (4mm) + BG18 (2mm) + GG 4 (1mm)
V	DG14 (3mm) + BG18 (2mm)
R	OG550 (2mm) + RG8 (1mm)
I	BG3 (1mm) + RG610 (2mm)

The standard UBV filters used with 1P21 tube cannot be utilised with the S20 surface because of the large red

leaks. In the present filter system, the red-leak is cut off by BG18 to better than one per cent. This photometric system was tested with the 102cm reflector telescope at Kavalur. Fifteen to twenty standard stars were selected from the list of Iriarte et al (1965), to calibrate the UBVRI filter system. Fernie's observations show that the transformation equations of the system to Johnson's system are not dependent on the luminosity class of the observed stars. The I band is much affected by the early wavelength cut off of the S20 surface compared to the S1 surface. This makes the transformation slope coefficient quite large for the I band. But the atmospheric extinction in this band is very low and the overall accuracy of the measured value is as good as it is in the other bands. Transformation was found to be somewhat non-linear at the extreme blue end of the relation. But observations on the cluster Omega Centauri do not include very blue objects and hence this small non-linearity at the blue end does not affect the observations to any extent. Each night the standard stars have been observed immediately after the observations on the cluster, to determine the transformation coefficients.

II.3 Observations: The observations on the cluster were made on four consecutive nights in the month of May 1979. The cluster was scanned once each night along the major and

minor axis. The surface brightness counts along the major axis have been taken at 30 locations of the aperture and along the minor axis at 22 positions. The locations of the aperture on the cluster, at the time of observation, can be seen by matching the transparency included along this paper with plate 1. Two relatively star free positions have been chosen near the cluster for sky observations. After each set of five colour observations, the telescope is moved to the two positions for evaluation of sky brightness. Two comparison stars located in the cluster were measured, after every three sets of five-colour observations. The comparison stars are B and D marked on Plate 1. They have been used by Arp (1958), Geyer (1965) and Dickens and Woolley (1966). At least 10 observations were obtained on the comparison stars during the night. About 15 standard stars picked from the list of Iriarte et al (1965) have been observed during each night for the transformation to the Johnson UBVRI system. Atmospheric extinction coefficients were determined each night for all the bands, and the mean value has been used in the reduction. The change in the extinction coefficients from night to night was $\lesssim$ 0.02 magnitude in V band. Figures II-1a to II-1d show the residuals of the transformations to the standard system obtained during one night's run on the standard stars.

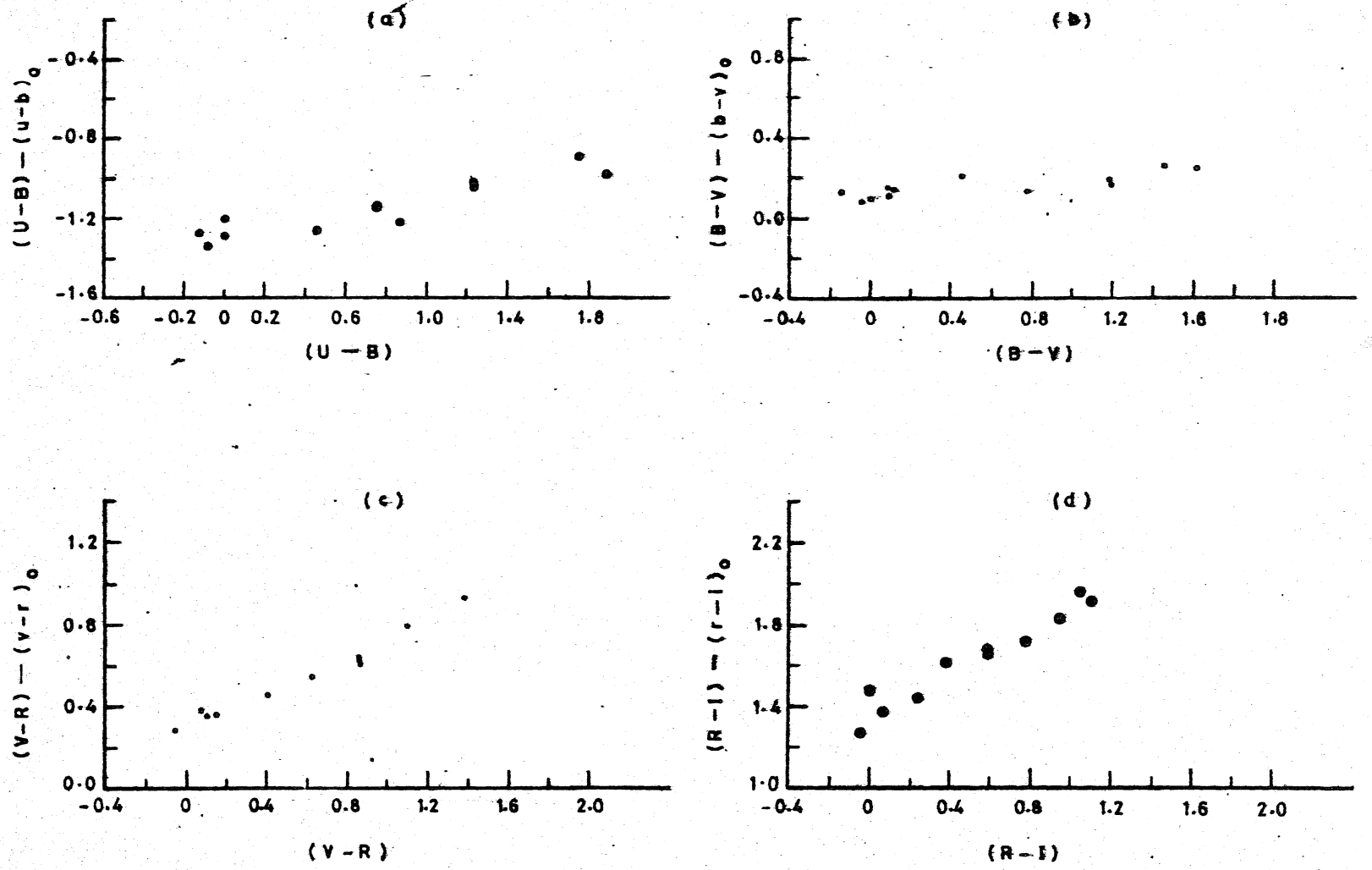
(a)
(U-B) − (u-b)o
-0·4
-0·8
-1·2
-1·6
-0.6
-0.2
0
0.2
0.6
1.0
1.4
1.8
(U − B)
(b)
(B-V) − (b-v)o
0.8
0.4
0.0
-0.4
0
0.4
0.8
1.2
1.6
1.8
(B − V)
(c)
(V-R) − (v-r)o
1.2
0.8
0.4
0.0
-0.4
0
0.4
0.8
1.2
1.6
2.0
(V - R)
(d)
(R-I) − (r-i)o
2.2
1.8
1.4
1.0
-0.4
0
0.4
0.8
1.2
1.6
2.0
(R - I)

FIG. II−1

The standard deviations for the residuals are given below:

(U-B)	=	0.030 mag.
(B-V)	=	0.020 "
(V-R)	=	0.025 "
(R-I)	=	0.050 "
(V)	=	0.020 "

Figures II-2a and II-2b show the (B-V) colour and V magnitudes for the major axis obtained on two different nights. The scatter near the brightest part of the cluster is negligible. The larger scatter as we go out from the cluster centre is due to larger sampling errors and also partly due to centering. Even a difference of one second of arc in the centering of the diaphragm may bring in a bright star into the field or take it out. This will show a scatter in the counts because of the low surface brightness of the cluster in this region. In the region outside the bright part of the cluster, the brightest stars are the red stars and they contribute most of the light to the surface brightness there. Hence, the colour of the cluster is becoming increasingly red as we go away from the centre.

II.4 Evaluation of Errors in Photometry: We now consider the various sources of error that can contribute to the uncertainty in these photoelectric measurements. King (1966) and Illingworth and Illingworth (1976) have made a

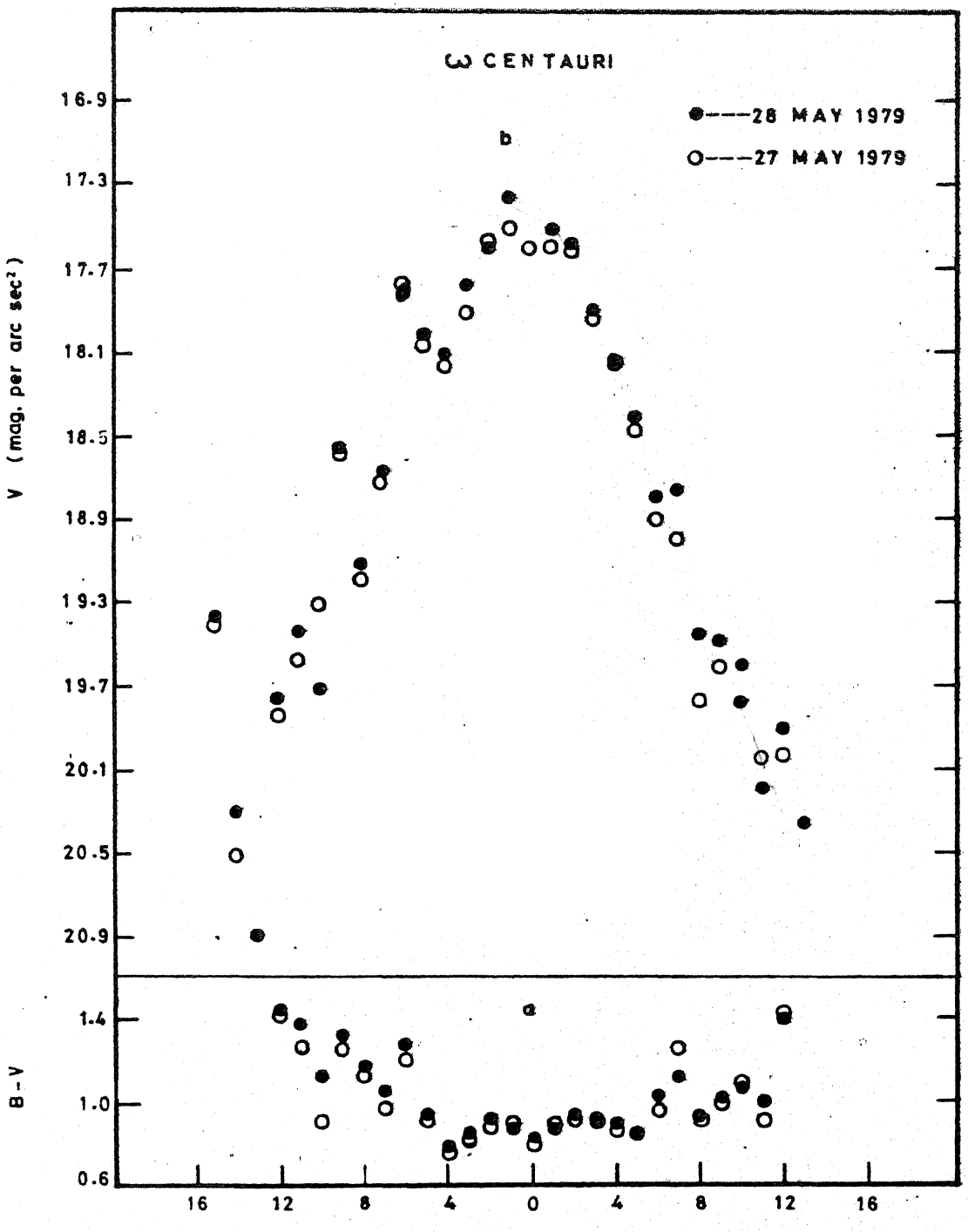
ω CENTAURI
●---28 MAY 1979
○---27 MAY 1979
b
a
V (mag. per arc sec²)
B-V
16.9
17.3
17.7
18.1
18.5
18.9
19.3
19.7
20.1
20.5
20.9
1.4
1.0
0.6
16
12
8
4
0
4
8
12
16
DISTANCE FROM THE CENTRE OF THE CLUSTER IN ARCMINUTES

FIG. II-2

detailed study of the problem. They have shown that the sampling and centering errors are the most important ones. In our photometric observations on Omega Centauri, only the sampling error is likely to be the principal contributor. We, therefore, consider this in detail.

An unavoidable source of error in surface brightness photometry of globular clusters comes from the random fluctuations in the number of luminosity distributions of the stars in the cluster (King 1966). The mean relative error σ/L is proportional to $L^{-\frac{1}{2}}$ where L is the total luminosity given by $L = \Sigma_i L_i N_i$. σ/L is given by the equation:

$$\sigma/L = \sum_i (L_i^2 N_i)^{\frac{1}{2}} / \Sigma L_i N_i \qquad .. (II.1)$$

This error σ/L can be calculated using any luminosity function available for globular clusters.

Similarly sampling errors affect the colours. If L_b and L_v are the total luminosities in the blue and visual bands, the integrated colour

$$C = 2.5 \log L_v/L_b \qquad .. (II.2)$$

The mean error σ_c in (B-V) colours will be given by

$$\sigma_c^2 = (1.085)^2 \Sigma N_i (L_{vi}/L_v - L_{bi}/L_b)^2 \qquad .. (II.3)$$

where L_{vi} is the visual luminosity for stars of class i etc (Chun and Freeman, 1979). Using such equations and following King, sampling errors in any colour can be calculated using the available luminosity functions of globular clusters. King (1966) Illingworth and Illingworth (1976) and Chun and Freeman (1979) have used the luminosity function given by Sandage (1957) for the cluster M3, for calculating the sampling errors $(\sigma/L)_V$, $(\sigma/L)_B$, σ_{B-V} and σ_{U-B}. These values have been used by them in their UBV surface photometry of globular clusters.

Since, we are doing photometry in UBVR and I bands, we need sampling errors for R and I bands also. Instead of taking the luminosity function of a metal rich cluster like M3, we have chosen the luminosity function available in UBVR and I bands for the metal poor cluster M92. This cluster is comparable to Omega Centauri in both metal abundance and geometrical form. M92 has a published luminosity function by Hartwick (1970). Sandage (1970) has published UBV photometry for stars in M92 in the range V = 16.26 to V = 22.26. Cathey (1974) has UBVR photometry from V = 12.19 to V = 15.41 and Rusev (1972) has BVI photometry for stars in M92 in the range V = 12.16 to V = 14.19. Using the above data we have estimated the sampling errors as explained in the following section.

Hartwick's (1970) luminosity function has a step size of 0.1 magnitude between V = 11.9 and V = 21.1. We have calculated the sampling errors in V magnitudes directly by using equation II-1. In order to estimate the sampling errors in the rest of the bands, we treated each step in V magnitude as a box consisting of identical stars with constant colours. The horizontal branch and the red giant branch were treated separately. For each of these boxes, we estimated the mean colours U-V, B-V, R-V, and I-V using the published photometry cited above. Due to the limitation in the published photometry, one could obtain the colours R-V only for $V \leq 15.5$ and I-V only for $V \leq 14.5$ while U-V and B-V were available for the entire range of $V \leq 21.1$. These colours were used in estimating the luminosity in UBVR and I bands for stars in each box with a given V magnitude to the limits of available photometry. The sampling errors were then derived using equation II.1 to these limits. The errors in colours were also derived similarly using equation II.3. The limits of available photometry, which have forced us to truncate the luminosity function in each band or colour, are enumerated below:

Case A : U, B, V band and U-B, B-V colours for the full range of $V \leq 21.1$

Case B : R band V-R colour for stars $V \leq 15.5$

Case C : I band and R-I colour for stars $V \leq 14.5$

In order to estimate the sampling error in R, I, V-R and R-I for the full range ($V \leq 21.1$), we have studied the effect of truncating the luminosity function at $V \leq 15.5$ and $V \leq 14.5$ in the case of U, B, V, U-B and B-V. Table II-4 lists the value of $(\sigma/L)_{10^m.0}$ for these three cases while Table II-5 lists the values of $\sigma_c/(\sigma/L)_{B,\ 10^m.0}$. The ratios of Case A to Case B, and Case A to Case C are also shown in the columns A/B and A/C respectively. The values for U, B, V, U-B and B-V are computed directly in all the three cases. The values corresponding to R and V-R are computed directly only for Case B and C. The values for I and R-I are directly computed only for Case C. A comparison of $(\sigma/L)_{10}$ in U, B and V shows that the ratios A/B and A/C slowly increase as one moves to longer wavelengths. This increase is due to the relative increase in the contribution of the brighter stars to the total luminosity without a comparable increase in σ. This implies that the relative contribution of fainter stars to the total (σ/L) increases with wavelength. However, the rate of increase in A/B and A/C slows down as one moves to longer wavelengths. We assume an estimated value of A/B = 0.76 and A/C = 0.65 for the bands R and I. These are shown in

Table II-4

$(\sigma/k)_x$ reduced to $10^m.0$

X	A V 21.1	B V 15.5	C V 14.5	A/B	A/C
U	0.0609	0.0925	0.106	0.658	0.572
B	0.0883	0.122	0.145	0.723	0.611
V	0.1650	0.219	0.255	0.752	0.646
R	(0.270)	0.358	0.414	(0.76)	(0.65)
I	(0.38)	(0.43)	0.500	(0.76)	(0.65)

Table II-5

$\sigma_C / (\sigma/L)_B$

C	A V 21.1	B V 15.5	C V 14.5	A/B	A/C
U-B	0.49	0.39	0.31	1.3	1.6
B-V	0.48	0.38	0.28	1.3	1.7
V-R	(0.35)	0.26	0.20	(1.3)	(1.7)
R-I	(0.30)	(0.38)	0.29	(1.3)	(1.7)

parameters in II-4. The resultant estimates of the total (σ/L) in R and I bands are also shown in parantheses in II-4.

The corresponding ratios A/B and A/C do not vary appreciably between U-B and B-V colours. Hence, we assume the values of A/B = 1.3 and A/C = 1.7 for the colours V-R and R-I. These values as well as the estimates of total errors in V-R and R-I appear in parantheses in Table II-5.

The values of $(\sigma/L)_{10^m.0}$ and $\sigma_c/(\sigma/L)_{B,\ 10^m.0}$ computed by us may be compared with the values derived for M3 in a few bands by previous investigators. Illingworth and Illingworth (1976) derive a value of $(\sigma/L)_V$ which equals 0.141 when reduced to $10^m.0$. This is 17 per cent smaller than our estimate. Similarly the value of Chun and Freeman (1979) for $(\sigma/L)_B$ which equals 0.103 after reduction to $10^m.0$ is about 15 per cent smaller than our value. The errors in colours obtained by the latter authors are $\sigma_{U-B}/(\sigma/L)_B = 0.46$ and $\sigma_{B-V}/(\sigma/L)_B = 0.51$. These values are 6.5 per cent smaller and 6.5 per cent larger respectively, when compared to our values. These departures are indicative of errors introduced by using different model luminosity functions. We will use the estimates of Case A listed in Tables II-4 and II-5 in our analysis of the errors.

II.5 Results of Photoelectric Scans: Table II-6 gives the results of the aperture scans along the major axis. In this table, column 1 gives r, the distance of the aperture from the cluster centre in minutes of arc. The letter E or W with the numbers shows whether the location is to the east or west of the centre. Columns 2 and 3 give the (U-B) colours and the corresponding sampling errors. Only the sampling errors have been calculated, as the other errors shown in the previous section are too small for this cluster. Columns 4 and 5 give the (B-V) colours and the corresponding sampling errors. Columns 6 and 7 give the V surface brightness expressed in magnitudes per square second of arc and the corresponding sampling errors. Columns 8 and 9 give (V-R) colours and the corresponding sampling errors. Columns 10 and 11 give the (R-I) colours and the corresponding sampling errors. Column 12 gives the R magnitudes expressed in magnitude per square second of arc and Column 13 gives the B-I colours. In Table II-7, we give similar data for the scan along minor axis.

Figure II-3 shows the colours U-B, B-V, V-R and R-I along with the brightness in the V band over the cluster along the major axis. The bumps seen in the wings of the brightness profile are inherent in the cluster. Similar bumps have been seen by Gascoigne and Burr (1956) for Omega Centauri and 47 Tuc. We notice changes in colour wherever

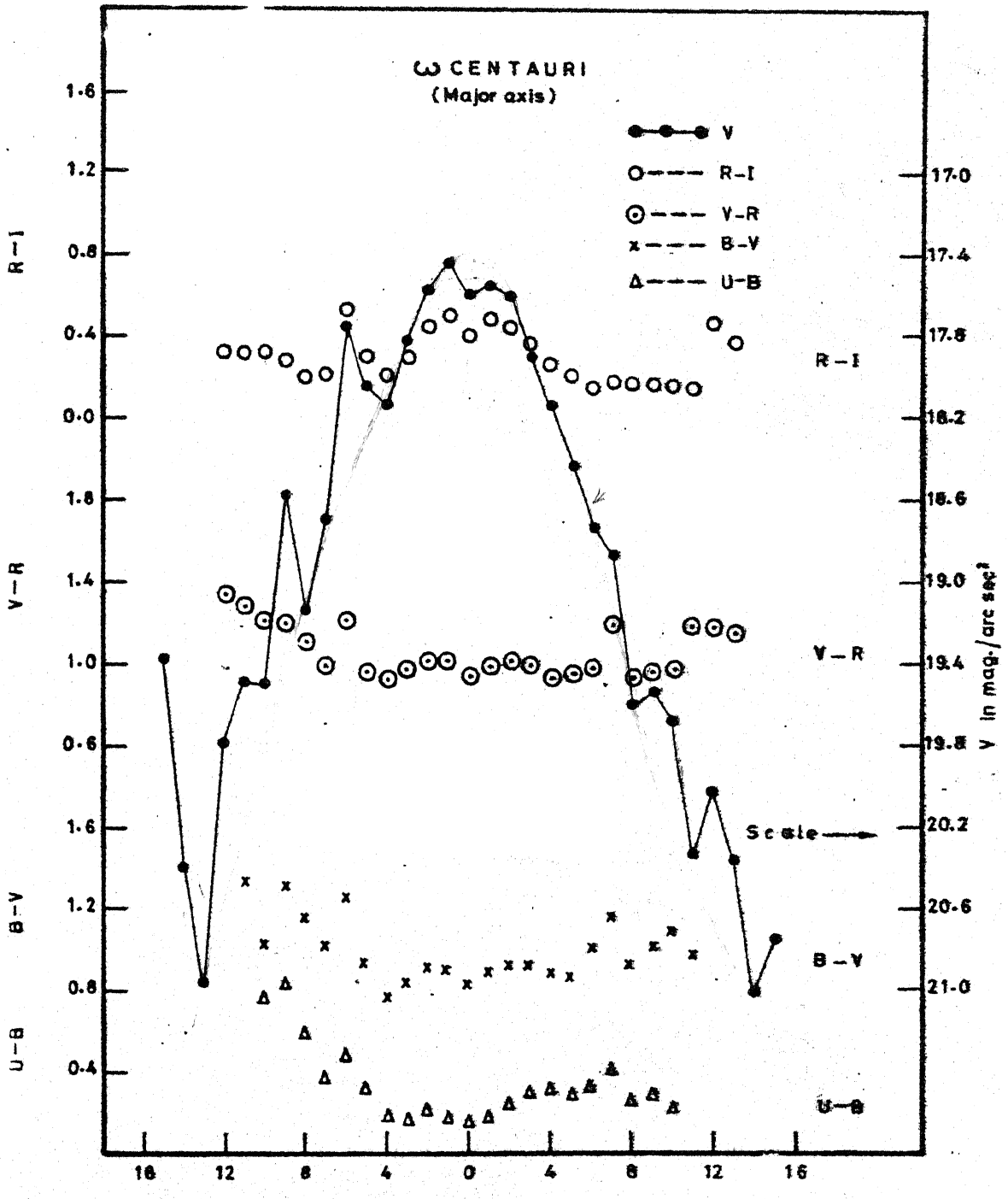

DISTANCE FROM THE CENTRE OF THE CLUSTER IN ARCMINUTES

FIG. II-3

Table II-6

Spot measurements along the major axis of Omega Centauri

r in min. of arc	U-B	σ U-B	B-V	σ B-V	V	σ V	V-R	σ V-R	R-I	σ R-I	R	B-I
14W			1.62	0.13	20.40	0.24	1.46	0.09	0.44	0.08	18.94	3.52
13W			2.11	0.27	20.97	0.31	1.76	0.15	0.70	0.13	19.21	4.57
12W	1.60	0.09	1.43	0.09	19.79	0.18	1.34	0.06	0.32	0.22	18.45	3.09
11W	0.77	0.07	1.33	0.07	19.49	0.16	1.28	0.05	0.31	0.09	18.21	2.92
10W	0.76	0.07	1.02	0.07	19.51	0.16	1.21	0.05	0.32	0.08	18.30	2.55
9W	0.83	0.05	1.30	0.06	18.58	0.10	1.20	0.03	0.28	0.07	17.38	2.78
8W	0.58	0.06	1.15	0.06	19.14	0.13	1.10	0.04	0.20	0.05	18.04	2.45
7W	0.37	0.05	1.02	0.04	18.70	0.11	0.98	0.03	0.21	0.06	17.72	2.21
6W	0.48	0.03	1.25	0.03	17.75	0.07	1.21	0.02	0.53	0.05	16.54	2.99
5W	0.32	0.03	0.93	0.03	18.05	0.08	0.96	0.02	0.30	0.03	17.09	2.19
4W	0.18	0.03	0.76	0.03	18.14	0.08	0.92	0.02	0.21	0.03	17.22	1.89
3W	0.16	0.03	0.84	0.03	17.83	0.07	0.97	0.02	0.30	0.03	16.86	2.11
2W	0.21	0.03	0.91	0.02	17.58	0.03	1.01	0.02	0.44	0.03	16.57	2.36
1W	0.17	0.02	0.89	0.02	17.44	0.06	1.01	0.02	0.50	0.03	16.43	2.40
0	0.15	0.03	0.82	0.02	17.60	0.07	0.94	0.02	0.40	0.02	16.66	2.16
1E	0.17	0.03	0.88	0.02	17.55	0.06	0.98	0.02	0.48	0.02	16.57	2.34
2E	0.23	0.03	0.92	0.03	17.60	0.07	1.01	0.02	0.44	0.03	16.59	2.37
3E	0.29	0.03	0.91	0.03	17.91	0.08	0.99	0.02	0.36	0.03	16.97	2.26
4E	0.30	0.03	0.88	0.03	18.14	0.08	0.93	0.02	0.26	0.03	17.21	2.07
5E	0.28	0.04	0.85	0.04	18.44	0.10	0.95	0.02	0.21	0.03	17.49	2.01
6E	0.32	0.05	1.00	0.05	18.84	0.11	0.98	0.03	0.15	0.04	17.86	2.13
7E	0.42	0.05	1.16	0.05	18.87	0.12	1.20	0.03	0.18	0.05	17.67	2.54
8E	0.25	0.07	0.92	0.06	19.60	0.16	0.93	0.04	0.17	0.05	18.67	2.02
9E	0.28	0.07	1.01	0.06	19.54	0.16	0.96	0.05	0.17	0.07	18.58	2.14
10E	0.22	0.07	1.08	0.07	19.68	0.17	0.98	0.05	0.16	0.07	18.70	2.22

Table II-6 - continued

r in min. of arc.	U-B	σ_{U-B}	B-V	σ_{B-V}	V	σ_{V}	V-R	σ_{V-R}	R-I	σ_{R-I}	R	B-I
11E			0.79	0.09	20.34	0.23	1.19	0.05	0.15	0.07	19.15	2.31
12E			1.42	0.10	20.03	0.20	1.18	0.05	0.47	0.10	18.85	3.07
13E			1.71	0.13	20.36	0.23	1.16	0.07	0.37	0.10	19.20	3.24
14E					21.01	0.31	1.29	0.10	0.15	0.14	19.72	4.03

Table II-7

Spot measurements along the minor axis of Omega Centauri

r in min. of arc	U-B	σ U-B	B-V	σ B-V	V	σ V	V-R	σ V-R	R-I	σ R-I	R	B-I
8.5N			1.10	0.09	20.16	0.21	0.88	0.07	0.15	0.09	19.28	2.13
7.5N			1.50	0.13	20.50	0.25	0.76	0.09	0.13	0.13	19.74	2.39
6.5N			1.24	0.09	19.99	0.20	0.93	0.07	0.56	0.09	19.06	2.73
4.5N	0.35	0.05	0.89	0.05	18.86	0.11	0.92	0.03	0.07	0.05	17.94	1.88
3.5N	0.32	0.04	0.85	0.04	18.82	0.11	0.90	0.03	0.07	0.05	17.62	2.12
2.5N	0.23	0.03	0.90	0.03	17.84	0.07	1.00	0.02	0.38	0.03	16.84	2.28
1.5N	0.12	0.02	0.83	0.02	17.76	0.07	0.90	0.02	0.36	0.03	16.86	2.09
.5N	0.16	0.02	0.90	0.02	17.37	0.06	0.99	0.02	0.52	0.03	16.38	2.41
0	0.15	0.02	0.82	0.02	17.60	0.07	0.94	0.02	0.40	0.03	16.66	2.16
.5S	0.21	0.02	0.88	0.02	17.58	0.07	0.97	0.02	0.50	0.03	16.61	2.35
1.5S	0.29	0.02	0.95	0.02	17.79	0.07	1.00	0.02	0.38	0.03	16.69	2.43
2.5S	0.33	0.03	0.96	0.03	18.09	0.08	1.04	0.02	0.27	0.03	17.05	2.27
3.5S	0.22	0.05	0.94	0.05	18.94	0.12	0.98	0.04	0.21	0.05	17.96	2.13
4.5S	0.22	0.05	1.21	0.05	18.74	0.11	1.10	0.04	0.23	0.05	17.64	2.54
5.5S	0.33	0.07	1.08	0.07	19.62	0.16	0.93	0.05	0.30	0.07	18.69	2.31
6.5S	0.22	0.08	1.13	0.08	19.86	0.18	0.97	0.06	0.07	0.08	18.89	2.17
7.5S	0.50	0.12	1.67	0.12	20.18	0.21	1.33	0.09	0.25	0.12	18.85	3.25
8.5S			1.77	0.14	20.40	0.24	1.07	0.10	0.11	0.14	19.33	2.95
9.5S			2.35	0.20	20.62	0.26	1.08	0.14	0.27	0.20	19.54	3.70
10.5S			1.71	0.16	20.82	0.29	0.83	0.12			19.99	

absorbing features are seen. The absorption near the centre shows a change of 0.3 magnitude in (R-I) colour. In the U-band profile of the cluster, the bumps are not very prominent. Figure II-4 shows the surface brightness variation in V band over the cluster along the minor axis. The colours U-B, B-V, V-R and R-I also are plotted in this figure. Minor axis also shows the bumps on both sides of the surface brightness profile, similar to the ones seen along the major axis. The absorption at the centre of the cluster makes the determination of the surface brightness at the centre very difficult. This is an important parameter in the determination of the core-radius of the cluster. Gascoigne and Burr (1956) and later Da Costa (1979)have used concentric aperture measures for the determination of surface brightness at the centre (f_o). We have used the results of Gascoigne and Burr and of Da Costa along with our results, to derive the surface brightness value at the centre, f_o, for the cluster. Tables II-8 and II-9 give the surface brightness in U, B, V, R and I bands expressed in units of U, B, V, R or I = 10 mag/arc sec^2. Column 1 gives log r where r is the distance from the centre in arc minutes. Column 2 gives the values of log f where r is the surface brightness at r minutes of arc away from the centre along the major or minor axis. Log f values presented in Table II-8 are the mean of log f values for the east and

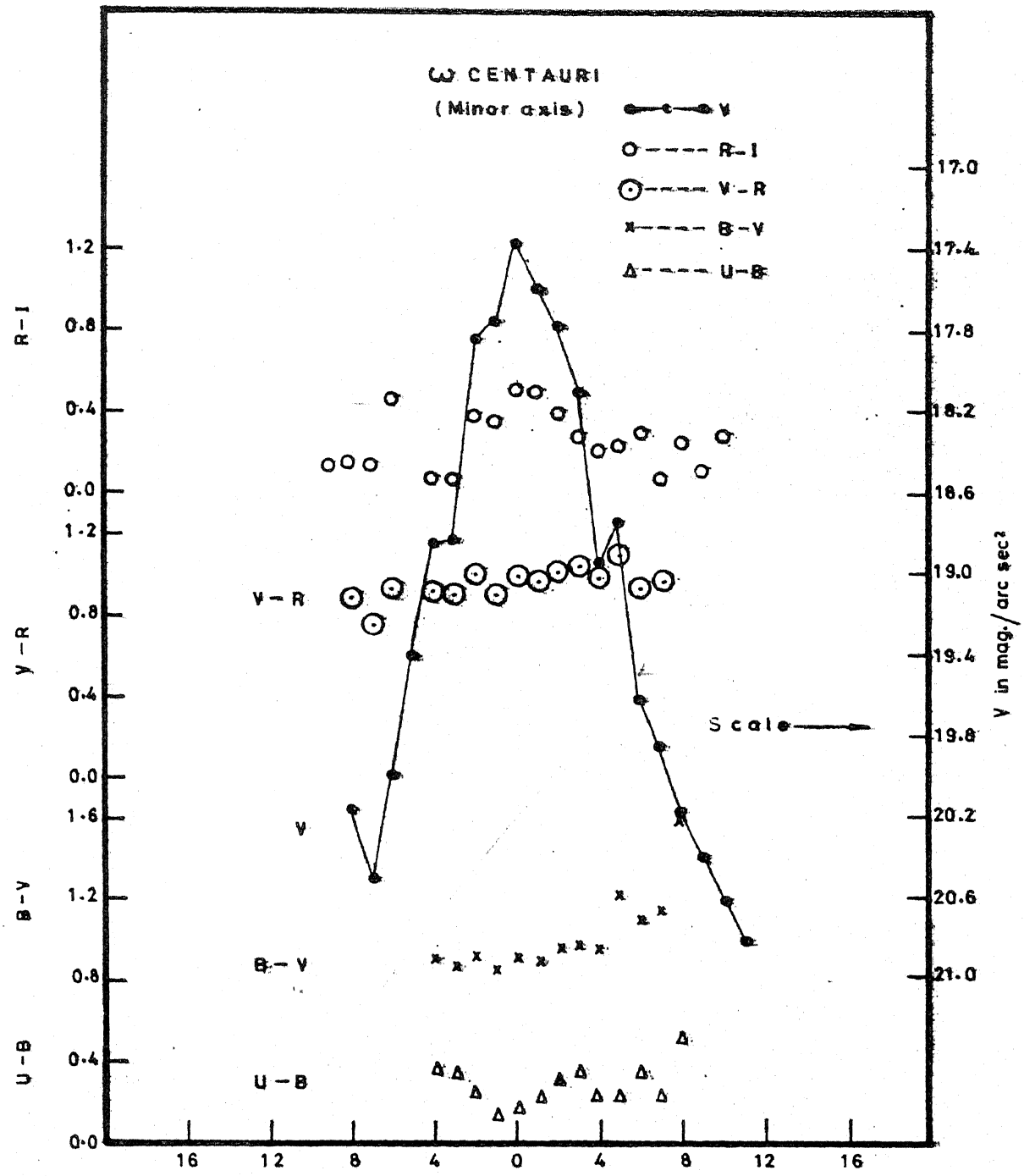

DISTANCE FROM THE CENTRE OF THE CLUSTER IN ARCMINUTES

FIG. II-4

Table II-8

Surface brightness over Omega Centauri in U B V R and I bands along the major axis

log r	log f	log r	log f	log r	log f
U Band		**B Band**		**V Band**	
0	-3.388	0	-3.320	0	-2.964
0.301	-3.485	0.301	-3.397	0.301	-3.031
0.477	-3.587	0.477	-3.496	0.477	-3.146
0.602	-3.679	0.602	-3.583	0.602	-3.255
0.699	-3.775	0.699	-3.654	0.699	-3.298
0.778	-3.929	0.778	-3.937	0.778	-3.537
0.845	-4.109	0.845	-3.951	0.845	-3.515
0.903	-4.289	0.903	-4.163	0.903	-3.749
0.954	-4.333	0.954	-4.221	0.954	-3.817
1.000	-4.475	1.000	-4.259	1.000	-3.838
1.041	-4.832	1.041	-4.524	1.041	-4.136
1.079	-4.948	1.079	-4.534	1.079	-3.964
		1.140	-4.828	1.114	-4.388

log r	log f	log r	log f
R Band		**I Band**	
0	-2.560	0	-2.360
0.301	-2.630	0.301	-2.451
0.477	-2.754	0.477	-2.622
0.602	-2.885	0.602	-2.801
0.699	-2.916	0.699	-2.814
0.778	-3.145	0.778	-3.085
0.845	-3.079	0.845	-3.001
0 .903	-3.343	0.903	-3.269
0.954	-3.433	0.954	-3.365
1.000	-3.401	1.000	-3.349
1.041	-3.660	1.041	-3.600
1.079	-3.460	1.079	-3.362
1.114	-3.682	1.114	-3.574
1.146	-3.732	1.146	-3.714

Table II-9

Surface brightness over Omega Centauri along the minor axis

log r	log f	log r	log f	log r	log f
U Band		B Band		V Band	
-0.301	-3.408	-0.301	-3.334	-0.301	-2.978
0.176	-3.543	0.176	-3.461	0.176	-3.105
0.398	-3.704	0.398	-3.572	0.398	-3.184
0.602	-4.006	0.602	-3.894	0.602	-3.514
0.740	-4.413	0.740	-4.281	0.740	-3.849
0.813	-4.445	0.813	-4.445	0.813	-3.973
0.875	-4.941	0.875	-4.771	0.875	-4.137
0.929	-4.561	0.929	-4.687	0.929	-4.113
		0.978	-5.189	0.978	-4.249
				1.021	-4.328
R Band		I Band			
-0.301	-2.586	-0.301	-2.382		
0.176	-2.705	0.176	-2.577		
0.398	-2.776	0.398	-2.648		
0.602	-3.116	0.602	-3.058		
0.740	-3.477	0.740	-3.357		
0.813	-3.591	0.813	-3.465		
0.875	-3.719	0.875	-3.643		
0.929	-3.723	0.929	-3.671		
0.978	-3.817	0.978	-3.709		
1.021	-3.996				

west wings. Log f values shown in Table II-9 are the mean of log f values for the north and south wings. Some of the values which represent the bumps in the surface brightness profile, have not been included while taking the mean values of log f. The log f values given here have been corrected for aperture smoothing, using an approximate equation similar to the one used by Illingworth and Illingworth (1976) for concentric aperture measures. In figures II-5a to II-5d, we have plotted log f against log r (r in arc minutes) for the U, B, V, R and I bands for locations along the major axis. In Fig. II-5e, we have plotted measures of Gascoigne and Burr and of Da Costa (1979) along with our observational results for the V band. The correction applied by Da Costa for the ellipticity in Omega Centauri has not been included in these values, so that the values plotted here represent the surface brightness along the major axis. The plot gives the value for log f_o = -2.775 where f_o is the surface brightness at r = 0 and is expressed in units of V = 10.0 mag/arc sec^2. From Table II-6 and II-7, we have taken the U-B, B-V, V-R and R-I colours for the centre of the cluster and these values have been used to calculate the value of log f_o in the U, B, R and I bands.

Table II-10 gives the mean colours for the centre of the cluster and log f_o values in U, B, V, R and I bands.

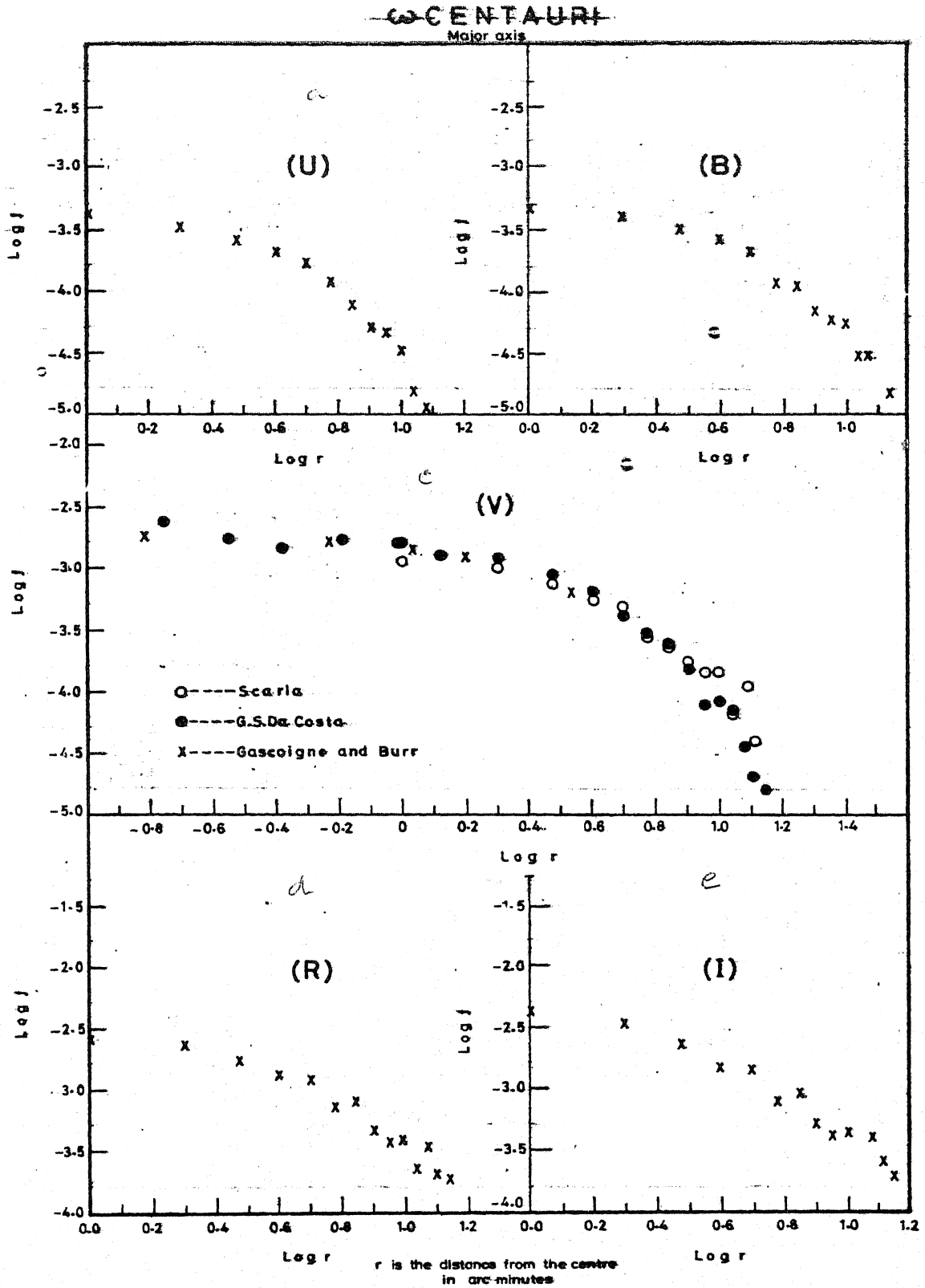

r is the distance from the centre in arc-minutes

FIG. II-5

Table II-10

Mean Colour at the centre in mag.			log f_o in units of 10.0 mag/arc sec^2
U-B	=	0.16	U = -3.187
B-V	=	0.87	B = -3.123
V-R	=	0.97	V = -2.775
			R = -2.387
R-I	=	0.46	I = -2.203

In Figures II-6a to II-6e, we have plotted r against log f/f_o for U, B, V, R and I bands for the major axis and in Figures II-7a to II-7e, we have plotted r against log f/f_o for U, B, V, R and I bands for the minor axis. Using equation I.1, we have calculated r_c for the cluster in U, B, V, R and I bands. The calculations have been done for the major and minor axis separately. The fits for the different surface brightness profiles are shown in the figures by continuous lines. As the surface brightness data available is limited to a small distance from the cluster centre, accurate values for r_t could not be obtained and hence only r_c values have been calculated. The fits show two points near the centre showing brightness less than what the fit demands. This is because of the distortion of the surface brightness profile by the absorbing feature at the centre. In Table II-11 first column gives r_c values

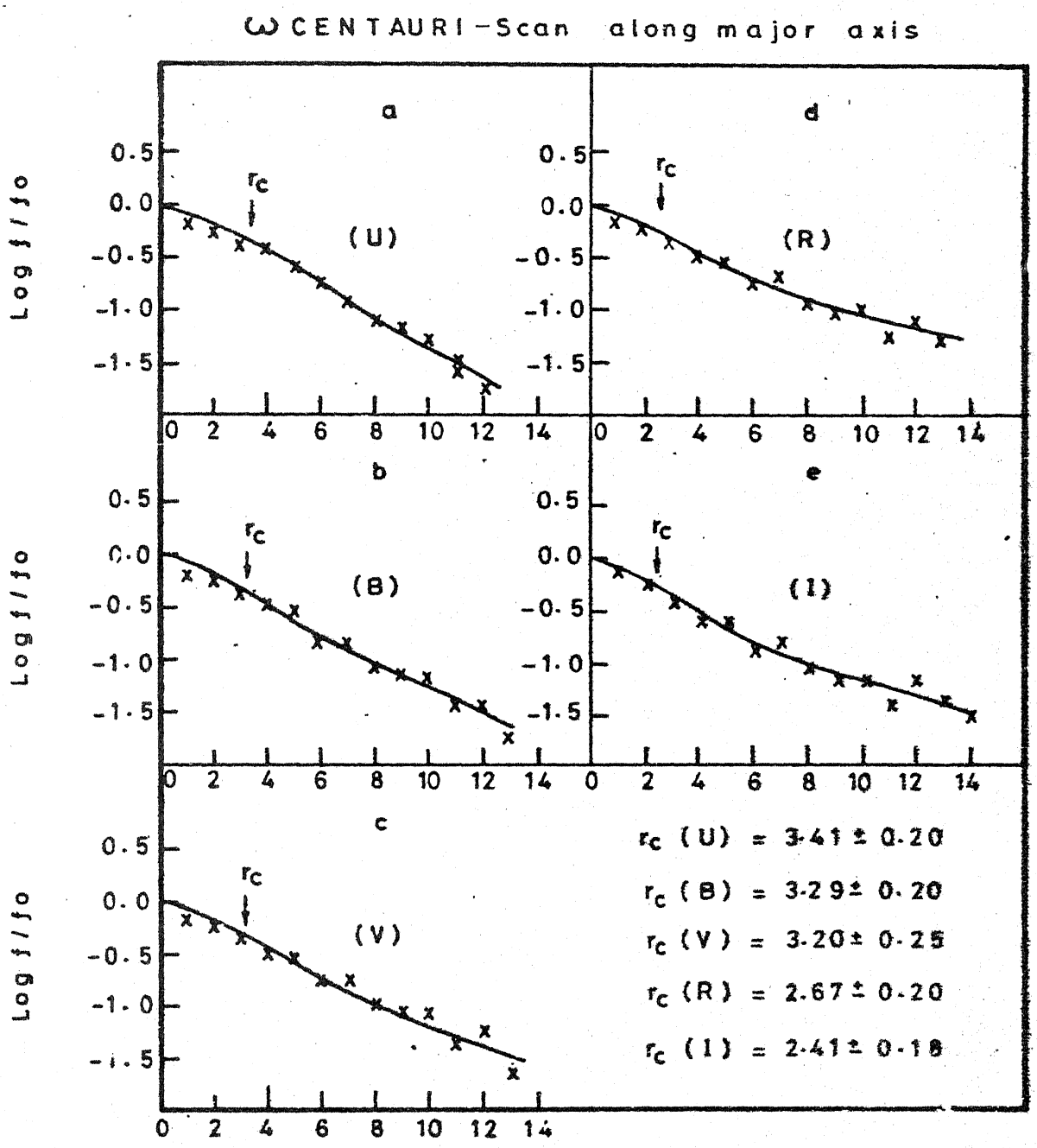
ω CENTAURI – Scan along major axis
a
(U)
d
(R)
b
(B)
e
(I)
c
(V)
r_c
Log f / fo
r in arcminutes
r_c (U) = 3·41 ± 0·20
r_c (B) = 3·29 ± 0·20
r_c (V) = 3·20 ± 0·25
r_c (R) = 2·67 ± 0·20
r_c (I) = 2·41 ± 0·18

FIG. II-6

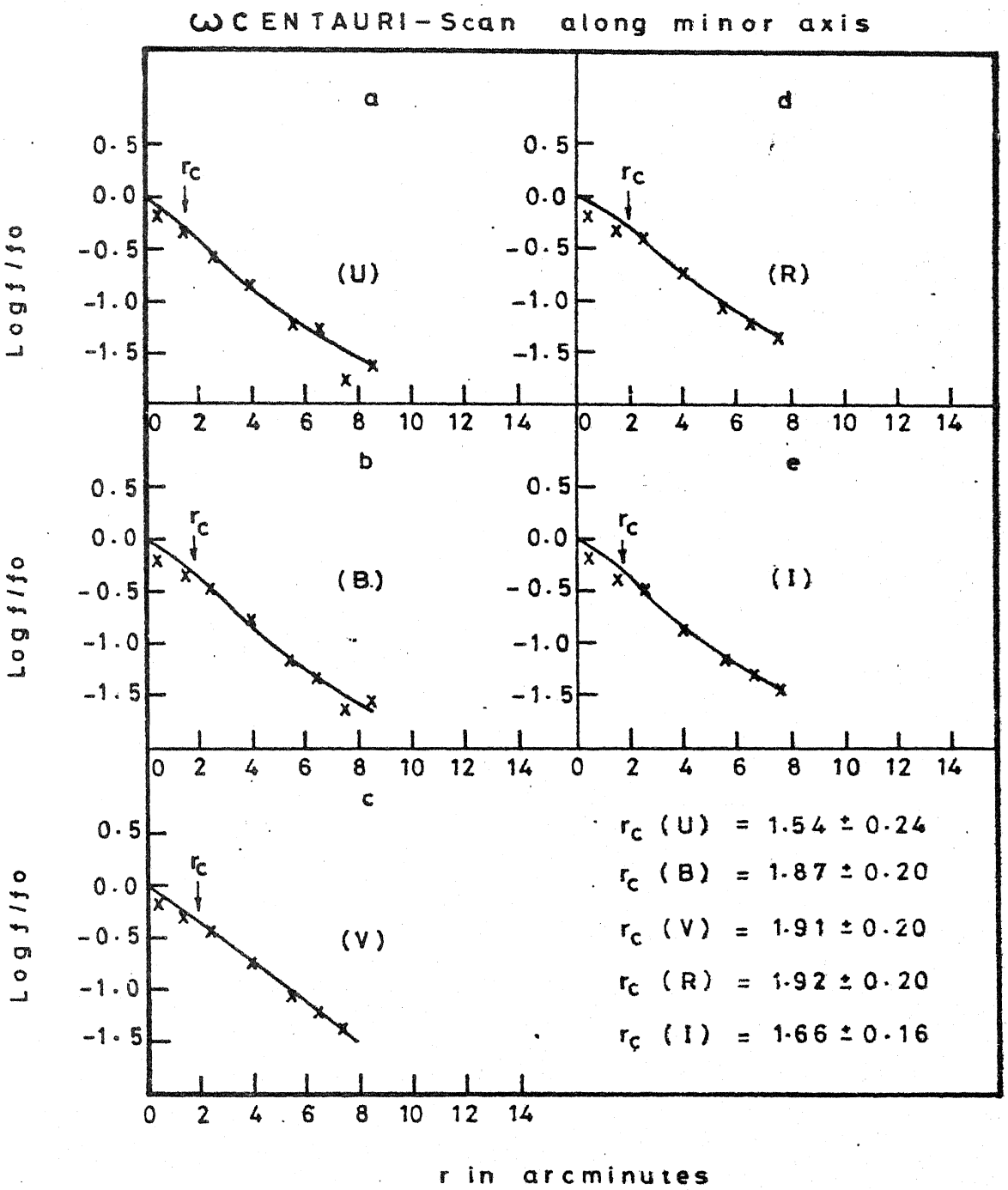
ω CENTAURI – Scan along minor axis
a
d
b
e
c
(U)
(R)
(B)
(I)
(V)
r_c
0·5
0·0
-0·5
-1·0
-1·5
0 2 4 6 8 10 12 14
Log f / fo
r in arcminutes
r_c (U) = 1·54 ± 0·24
r_c (B) = 1·87 ± 0·20
r_c (V) = 1·91 ± 0·20
r_c (R) = 1·92 ± 0·20
r_c (I) = 1·66 ± 0·16

FIG. II-7

obtained for U, B, V, R and I bands along the major axis, second column gives r_c values for the minor axis in U, B, V, R and I bands and the third column gives the ratio of the r_c values obtained for the major axis and minor axis.

Table II-11

Core-radii in U, B, V, R and I bands for the cluster Omega Centauri

Band	r_c (Major axis)	r_c (Minor axis)	$\frac{r_c \text{ (Major)}}{r_c \text{ (Minor)}}$
U	3.41 ± 0.20	1.54 ± 0.24	2.21
B	3.29 ± 0.20	1.87 ± 0.19	1.76
V	3.20 ± 0.25	1.91 ± 0.20	1.68
R	2.67 ± 0.20	1.92 ± 0.20	1.39
I	2.41 ± 0.18	1.66 ± 0.16	1.45

This table gives the colour dependance of the value of r_c. There is a gradual decrease in the value of r_c from the U band to the I band, along the major axis. The r_c values for the minor axis behave just in the opposite way except for the I band. The 3rd column in Table II-11 gives the ratio of the core-radius along the major axis to that along the minor axis in the respective bands. The ratio decreases fast from the U band to the R band and the tendency is for the ratio to increase in the I band.

r_c values obtained by different investigators for Omega Centauri in the V band are given in Table II-12. Our value included in the table is the mean of the values obtained for the major and minor axis.

Table II-12

r_c (King 1962)	= 2'.45
r_c (Peterson and King 1975)	= 2'.40
r_c (Da Costa 1979)	= 2'.63
r_c (Scaria)	= 2'.56

This table shows the agreement of our value with the values obtained for r_c by others. From Table II-11, it is very clear that, there is an increase in the flattening of the cluster, as we go towards shorter wavelength side. But in the longer wave length side, the cluster presents a more spherical shape. It is interesting to note here what has been observed by Dickens and Woolley (1966) in the radial distribution of blue stars in the outer annulus of Omega Centauri (8' to 22'). The counts for the stars have been made in two sectors 315°-45°, 135°-225° and 45°-135°, 225°-315° denoted by major and minor axis respectively. The counts have been corrected for the field stars. They find a larger concentration of bright horizontal branch stars in the major axis sectors. They suggest that this

could be a chance grouping. But our results given above show that this may not be a chance grouping. It is worth mentioning here that Strom et al (1976) have observed that colour gradients in E and S0 galaxies appear to be greatest along the minor axis.

Figure II-8 shows the distribution of (B-I) colour along the major and minor axis. The curve is symmetrical around the centre. The curve can be divided into 3 parts. Region A_1 A_2 has an uniform colour of about B-I = 2.45 mag. This region has a diameter of 5 minutes of arc. Beyond A_1 and A_2, the cluster is becoming bluer and reaches a maximum blueness at B_1 and B_2. The difference in B-I colour, between the centre and this zone is 0.45 magnitude. This blue zone around the cluster has a width of about 3 minutes of arc and extends, along the major axis, from 2.5 to $\lesssim$ 5'.0 from the cluster centre. Along the minor axis this zone does not extend so much as it does along the major axis. Beyond zone B_1 B_2, the cluster again becomes red. The change in colour is rather sharp. The arrows in Figure II-8 show the region where the cluster shows sudden change to redder colour. The effect of these three zones on the equidensity contours of the cluster are explained in Chapter III.

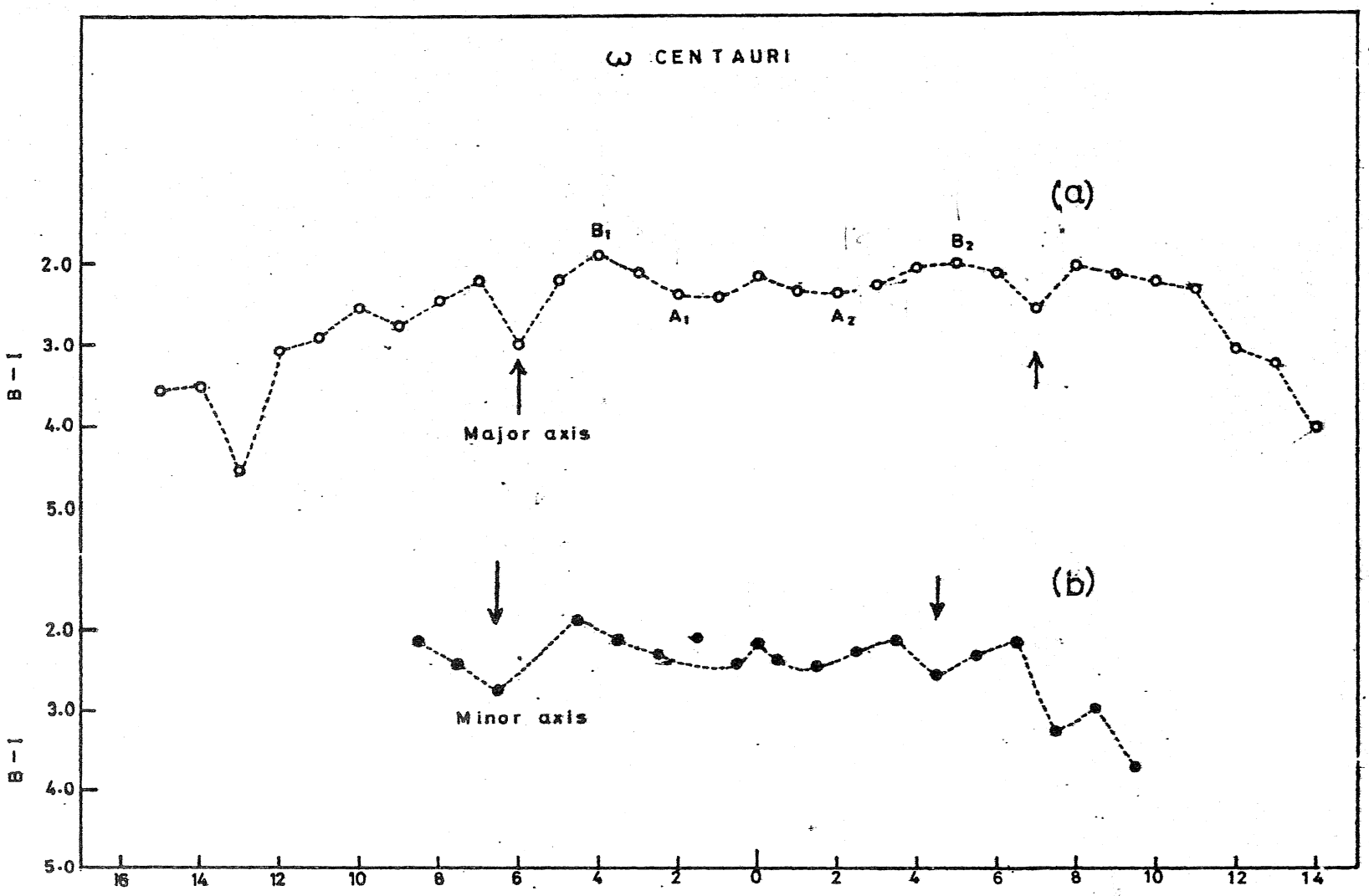

r, Distance from the centre of the cluster in arcminutes

FIG. II-8

Figure II-9 shows U-B/B-V relation for the observed regions on the cluster. The filled circles represent points along the major axis and crosses are for points along the minor axis. The number near each point shows the distance of the point from the cluster centre in minutes of arc. The continuous line is the intrinsic relation (Eggen and Sandage 1965) for the main sequence, shifted by $E_{B-V} = 0.11^m$ and $E_{U-B} = 0^m.08$ for space reddening.

In Figure II-10, we have plotted the values of $\delta(U-B)$, the ultraviolet excess for each point read against the (B-V) of that point, over the reference sequence. The abscissa shows the distance r, of the point from the cluster centre. The figure shows that from r = 0 to r = 2'.5 the UV excess is constant at 0.26. Beyond r = 6', the UV excess keeps decreasing with increasing distance from the cluster centre. Between r = 2'.5 and r = 6' the UV excess shows a sudden increase. In Figure II-8, this is the region where the cluster becomes bluer by 0.45 mag. in B-I colour. The mean ultra-violet excess of the central region over the reference sequence is $\lesssim$ 0.26 mag. The UV excess obtained by Dickens and Woolley (1966) for Omega Centauri giants is $\lesssim$ 0.28 mag, in good agreement with our result. Around 6' from the cluster centre, the UV excess is similar to what it is at the centre. Beyond 6' from the centre, the UV excess decreases with increasing distance from the cluster centre.

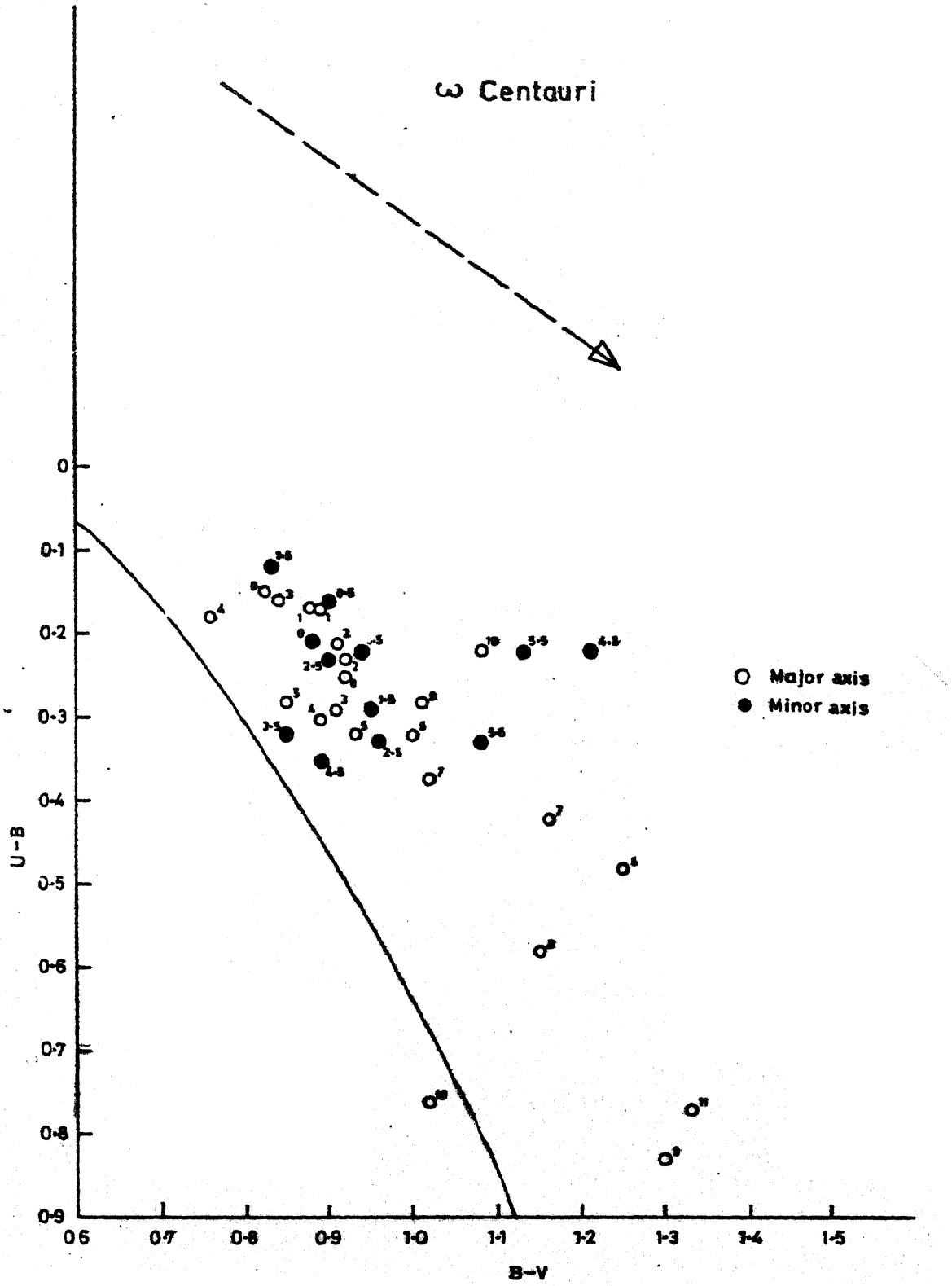
ω Centauri
O Major axis
● Minor axis
U-B
B-V
0
0·1
0·2
0·3
0·4
0·5
0·6
0·7
0·8
0·9
0·6
0·7
0·8
0·9
1·0
1·1
1·2
1·3
1·4
1·5

FIG. II-9

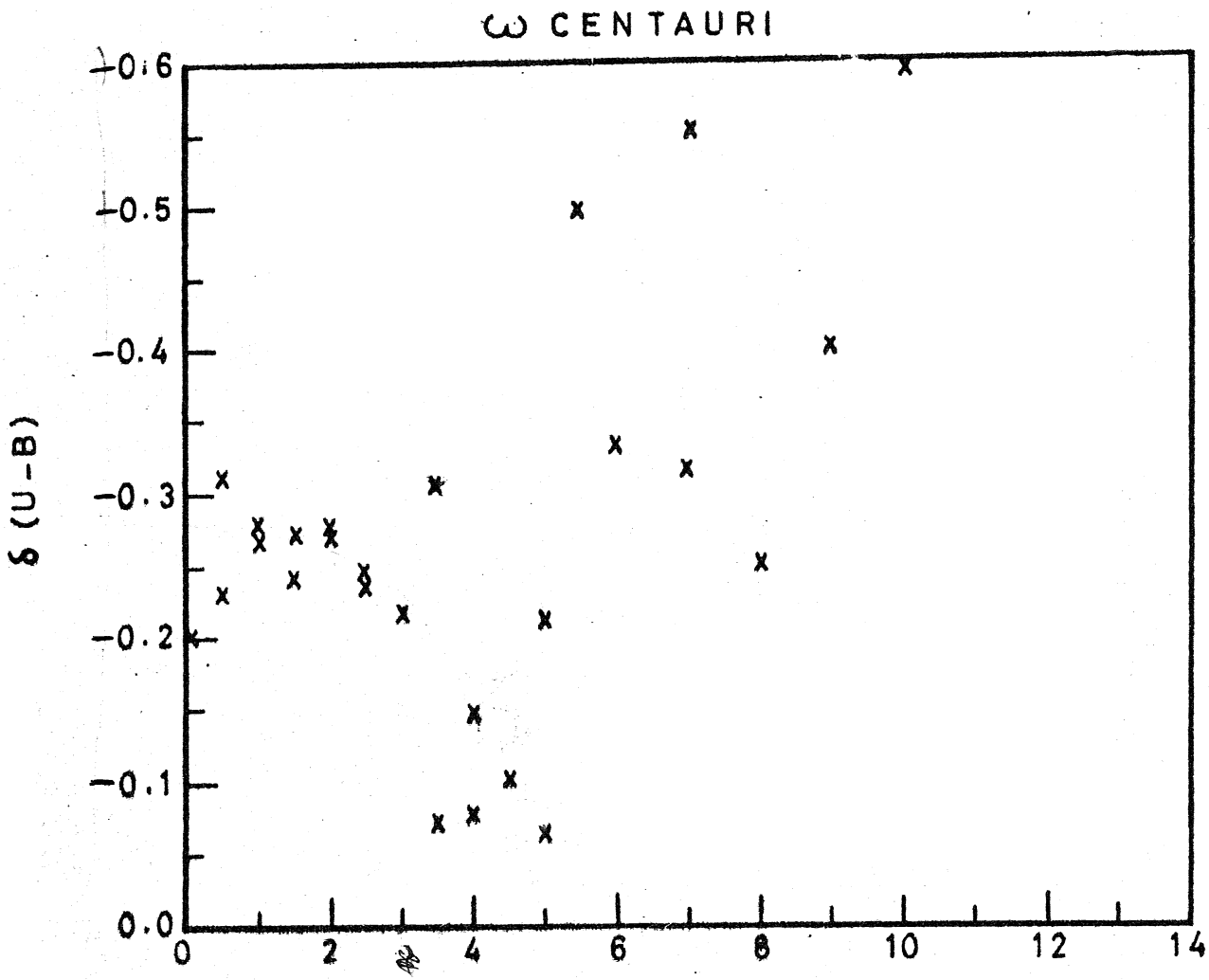
ω CENTAURI
-0.6
-0.5
-0.4
-0.3
-0.2
-0.1
0.0
δ (U-B)
0
2
4
6
8
10
12
14
r Distance from the centre in arcminutes

FIG. II-10

The presence of a large number of red stars around the cluster has been observed by Dickens and Woolley (1966). They give counts of the blue and red stars in Omega Centauri to show the radial distributions of these stars. The blue stars are defined by stars with B-V < 0.3 mag and the red stars have B-V > 0.3 mag. The total red star count for the region 7' to 11' from the cluster centre is 917 and for the blue stars, the count is 298. Most of these red stars are much brighter than the blue stars in the cluster and hence the contribution to surface brightness by these red stars, is very much larger than what the counts show. The kind of kinks shown by arrows in Fig. II-8 are seen in several clusters observed by Strauss (1978). The (B-I) colour and the UV excess, are about the same for the stars at the centre and the stars which give rise to these kinks in B-I colour. The zone between these two regions present a different picture by showing a bluer colour and a larger UV excess.

Three colour photometry by Sandage and Walker (1966) on M92 shows that stars belonging to the sub-giant sequence can be separated from the asymptotic branch stars in a U-B/B-V diagram. The difference in U-B between subgiant and asymptotic branch stars ranges from δ(U-B) = 0.08 mag to δ(U-B) = 0.37 mag when read at constant B-V. The

observed effect is too large to be explained by changing surface gravity in model atmospheres. UBV photometry on M3 by Johnson and Sandage (1956) and UBV photometry on Omega Centauri by Geyer (1966) show the same effect. But this photometric difference is not seen in the spectral features of the stars belonging to these two groups. A moderate resolution spectrophotometry survey by Strom and Strom (1971) revealed no difference in the spectral energy distribution except for wavelengths below the Balmer jump. They point out that the differences in δ(U-B) between the asymptotic giant branch stars and the red giant stars can be explained by a surface gravity difference resulting from the observed luminosity difference between them and a mass loss not exceeding 0.2 dex. Strom and Strom also show that δ(U-B) is dependant on the radial distance of the individual stars from the cluster centre. For the red giants in M92, Strom and Strom (1971) get UV excess 0.24. This matches well with our value of 0.26 for the region around the centre of Omega Centauri. Strom and Strom get UV excess of 0.04 for the asymptotic giant branch stars. This compares well with our value of .10 for the intermediate region in the cluster Omega Centauri.

From our results, we can show that the systematic change of δ(U-B) with distance from the centre, is partly

due to contribution from a bulge of unresolved stars around the core. The contribution from this bulge is highest between $r \simeq 2.5'$ and $r \lesssim 5'$. This is clearly seen in the composite photograph of the cluster shown in Plate IV. The details of the photograph are given in the next chapter. The radial dependence of $\delta(U-B)$ observed by Strom and Strom (1971) is easily explained by the contribution to the surface brightness by the bulge around the inner core. Thus the larger UV excess in the intermediate region can be due to two reasons. One possibility is that there is a larger concentration of asymptotic giant branch stars in this zone. The other possibility is that the bulge around the core seen in Plate IV has large UV excess. Probably both together contribute to the observed result.

II.6 R/(R-I) relation: Fig. II-11 is a plot of R, the surface brightness in mag/arc sec^2 against (R-I) colour, over the cluster along the major and minor axis. Major axis points are shown by open circles and minor axis points are shown by filled circles. The numbers marked near each point show their distance from the centre of the cluster. The diagram shows the cluster to be the reddest at the centre. Since the contribution to the surface brightness from the red stars is decreasing and that from the bluer stars is increasing, we can see the colour of the cluster

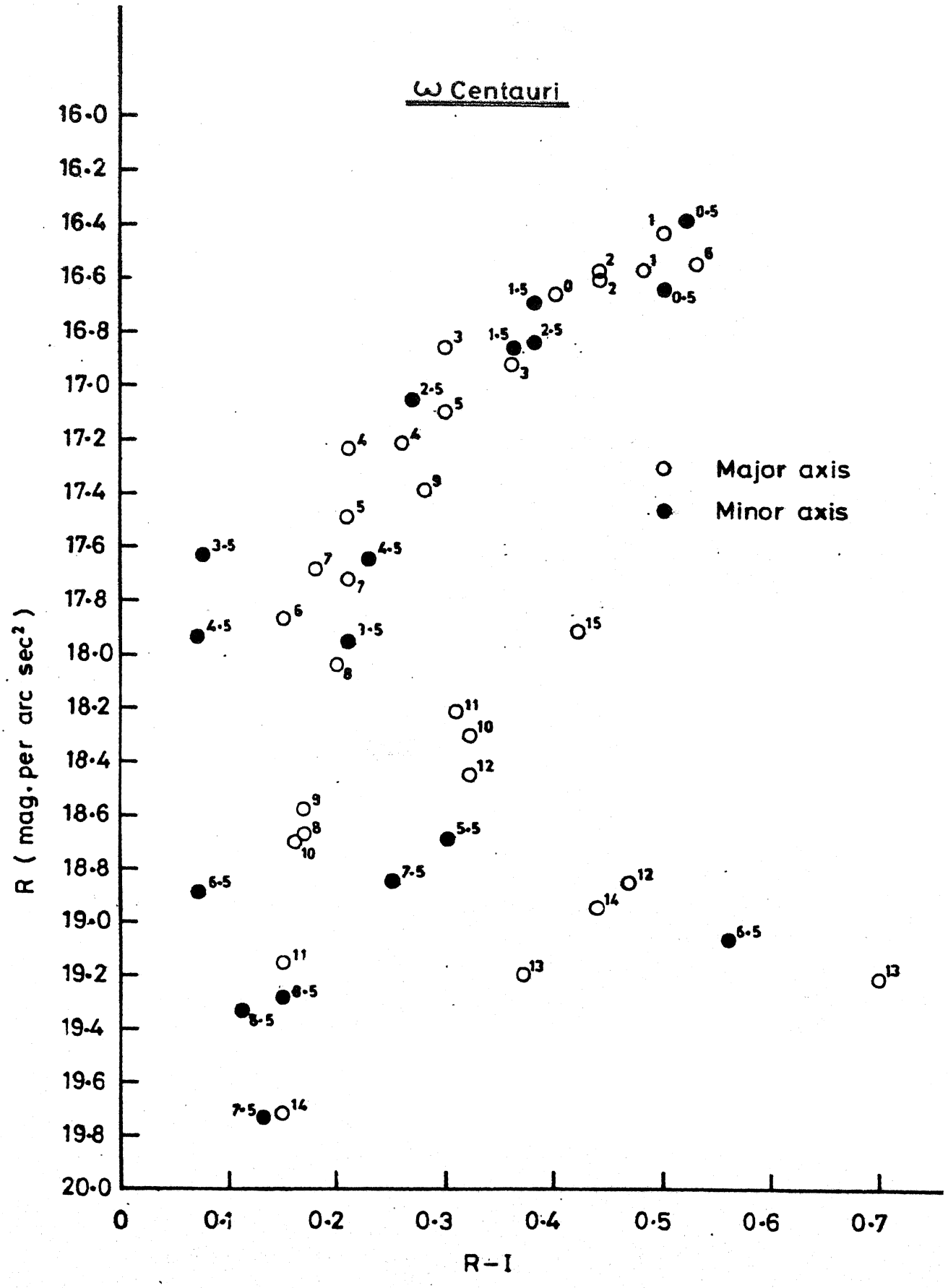
ω Centauri
Major axis
Minor axis
R (mag. per arc sec²)
R – I
16·0
16·2
16·4
16·6
16·8
17·0
17·2
17·4
17·6
17·8
18·0
18·2
18·4
18·6
18·8
19·0
19·2
19·4
19·6
19·8
20·0
0
0·1
0·2
0·3
0·4
0·5
0·6
0·7

FIG. II-11

becoming bluer as we go from centre to the outer regions. The change is very gradual and is the same for both the major and minor axis. Bessell and Norris (1976) observe a large width for the giant branch when plotted in the V / (B-V) plane. But the R / R-I plane gives a very narrow giant branch. The R/(R-I) plot shows a width of about 0.05 magnitude for the dense regions of the cluster. This value is similar to what Bessell and Norris obtained for the giants in Omega Centauri.

In the next chapter, we show how this change in distribution of colour, changes the equidensity contours of the cluster.

CHAPTER III

ISODENSITOMETRY OF OMEGA CENTAURI AND 47 TUCANAE

III.1 **Introduction:** Our aperture photometry and photometry of individual stars done by others show an increase in the giant population towards the centre of the cluster. Similar results have been noticed for a few other clusters. For the metal rich globular cluster NGC 6171, Dickens and Rolland find that, red giant stars are more concentrated towards the centre than stars on the horizontal branch. From our photometric results, we have seen that the inner region of Omega Centauri has a uniform colour upto a distance of 2.5' of arc from the cluster centre. Beyond this the cluster gets bluer and reaches a maximum around 4' from the cluster centre, after which again the cluster becomes redder. We have seen that these are variations created by the peculiar distribution of red giants, the asymptotic giant branch stars and the horizontal branch stars. The central region is the reddest and has a uniform colour in B-I, because there is a uniform distribution of red giants in this region. The cluster is equally red beyond six minutes from the centre. Between 2'.5 and 6' the cluster is bluer which shows a larger concentration of bluer stars in this zone. The effect of these peculiar

distributions of the stars will show up in the results of multicolour equidensitometry done on the cluster.

Omega Centauri is well known for its large ellipticity. This fact has been studied by Lindsay (1956) in the outer regions of the cluster through star counts. He has pointed out that the ellipticity is not the same in blue and red colours for the cluster. The ellipticity is found to decrease as we come closer to the cluster centre. But his counts do not come closer than 15' from the centre. For the dense inner regions, star counting techniques are not possible. If we try to reduce the crowding in the central parts of the cluster by under exposing the plate, we would only obtain the distribution of the brightest members of the cluster and neglect the fainter members which actually form the bulk of the mass in the cluster. To study, therefore, the ellipticity in the denser regions of the cluster, we have to use the technique of equidensitometry. There are many methods available to obtain equal intensity contours on a photographic plate. Some of these procedures are photographic and some photoelectric.

In the photoelectric domain, we have the hunting or scanning type of isophotometers. In the photographic field, the Sabattier effect has been usefully exploited to obtain

isophotal contours. The merits and demerits of both the methods have been well analysed by Hodge and Brownlee (1966) and Breido and Ermoshina (1969). They point out the simplicity of the photographic method.

Detailed accounts of procedure and technique of Sebattier effect are given by Lan and Krug in their monograph. The astronomical applications of this technique have been studied in detail by Richter and Hegner (1963). They have applied it in their study on the ellipticity of the galaxies M31, M32 and NGC 205. Sources of errors and the accuracy of the results have been studied and they have come to the conclusion that the Sabattier technique is a very sound and reliable method of obtaining isophotes. They find that the attainable minimum distance between two isophotes is 0.1 arc minutes on M31, M32 and NGC 205. Objects with diameters of about 0.5 arc minutes can be described with good accuracy by three or four equidensity contours. The effectiveness of the Sabattier technique in many astronomical problems have been demonstrated by Bappu (1978).

III.2 <u>Details of the Sabattier technique of equidensitometry:</u> Equidensity contours refer to regions of equal transparency or equal blackening on the photographic plate. This is obtained by special copying process using the Sabattier

effect. Sabattier effect is the photographic reversal effect which occurs, when one exposes an exposed plate, after a brief development, to a uniform diffuse light once again, and then continues with the full development. In this process, the parts of the plates, which had not been blackened during the first exposure and development, are blackened by the second exposure and subsequent development, whereas the other parts which got developed first, remain unaffected by the second exposure and development. When the second diffuse light exposure is made just sufficient, so that it does not cause total reversal, a certain narrow blackened region of the original plate can be brought out as an equidensity line. In this process, the gamma value of the film used should be high, 5 to 6. Also a contrast developer should be used. By suitably choosing the gamma value of the plate used, and the proper exposure time while copying, the equidensity lines, can be moved to any desired density level of the original plate.

The first order equidensity contours are generally broad and cover a large range of density levels. By taking second order and then third order equidensity lines, one can go upto the plate limit of the original photograph, which is set by the grain size in it.

III.3 Sources of Error in Photographic Equidensitometry: For good accuracy in isodensitometry, the source of light in the enlarger unit should be very uniform over the full field of the plate. The uniformity of the illumination was checked in our equipment to an accuracy of two per cent and was found to be very uniform. Since, the object of our study is not larger than two or three centimetres in size on the original photographs, the error caused by non-uniform illumination is practically nil. The source of light used for the second exposure is a 25W bulb kept at a distance of two metres from the plate and is covered by opal glass. This keeps the illumination uniform over a large area. The film which was used is "ORWO" FO6 sheet film. It has a high gamma value and is fairly thick.

III.4 The Determination of equal density contours: The plates that we have used for the equidensitometry of Omega Centauri cover a field of 45 minutes of arc and the densest region of the cluster covers about 20' of arc of this field. We have used the stars in the outer regions of the cluster to match the different contours while making the map. The problem in doing this is that, when we are giving the second exposure, to get the equidensity contour, these stars also will undergo the same process experienced by the cluster and hence in the place of star images, rings

will develop. In later stages of processing, these rings will get split further and it may not be possible to use them at all to match the contours. To avoid this difficulty, we have used a mask to cover the field stars and hence while giving the second exposure, the stars outside the cluster, will not get sabattiered and will remain as black points on a clear background or clear points on a dark background, depending on the stage of equidensitometry. A sample set of equidensity contours is shown in plate II. It shows the equidensity contours after three stages of processing. The stars seen are carried through all these stages. Since all these stars are available in all sets of equidensity contours, there is no difficulty involved in matching the contours. The sets of contours, for map making, are selected in such a way, that the outermost contour in one set matches well with the innermost contour of the next set. Always these overlapping contours match to the finest detail seen in them, which shows the high accuracy of the process. Plate III is a map prepared this way of Omega Centauri. The E-W and N-S directions are marked on the plate.

III.5 Diffusion of Stellar Images in the Plate: For obtaining isodensity contours, we need continuity of density levels. Except in the central regions of a globular cluster,

b

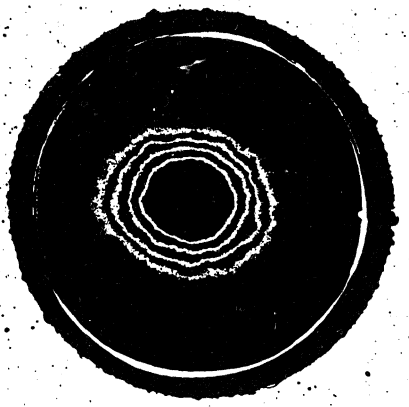

a

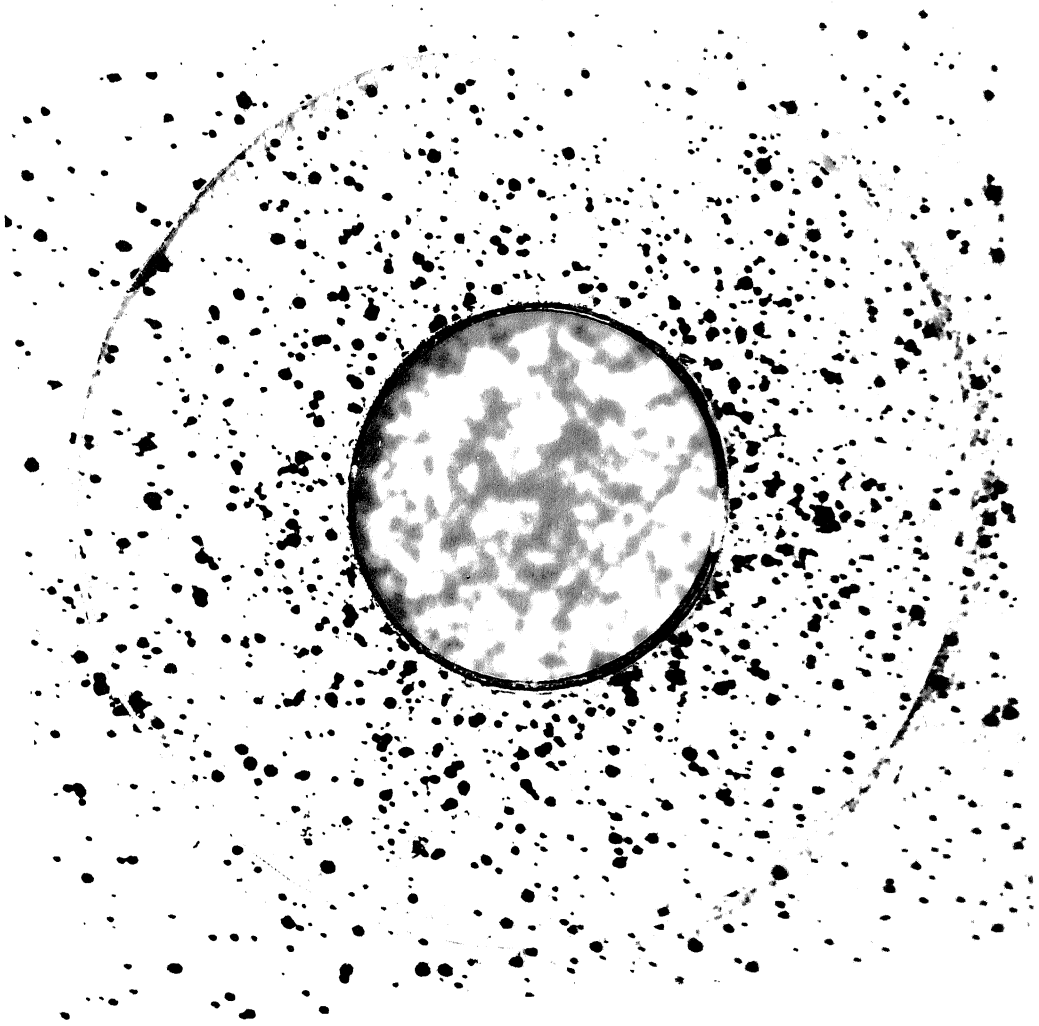

PLATE II

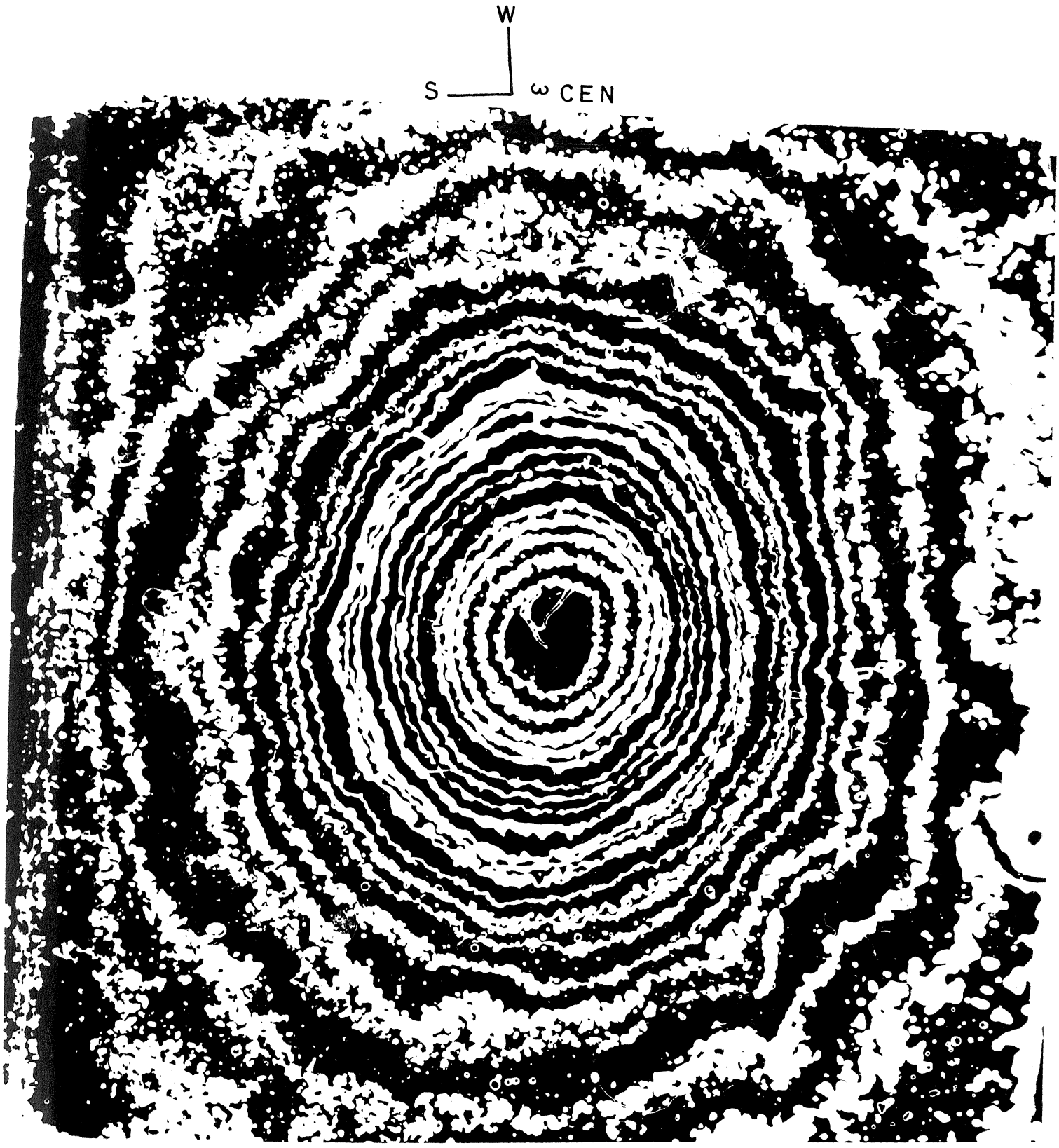

PLATE III

the stars are resolved and hence a direct application of the Sebattier technique will give only a collection of small rings, corresponding to the isophotes of stellar images. The resultant equidensity contours of the cluster are too irregular to measure. Hence, while making the graded exposures of the cluster, for covering regions of different density levels, a thin diffuser is introduced between the film and the original plate (Sistero and Fourcade 1970). The diffuser increases the size of the stellar image by a factor of about three and hence all the stars get smeared out to give the effect of an out of focus photograph of the cluster. Since, we want only the cluster to be defocussed and the outer stars to be left out as they are, we have used a diffuser as shown in plate II. The central circular portion of the plate is the ground portion and the remaining part of the plate is clear glass. The plate also keeps the film pressed well to the holder while taking the graded exposures and avoids any chance of film buckling. In plate II, the diffuser is shown against the background of a star field. The details of the central regions of the star field are not lost. Only the images of the stars get defocussed.

in some clusters like M92 and M5, the b/a vs a curve show well defined regions of minimum ellipticity close to the centre and well defined regions of maximum ellipticity at some distance away from the cluster centre. The position angle of the inner region is different from that of the outer region in both these clusters. The differing behaviours of b/a and ϕ in different wavelength bands at distances less than 1' of arc from the centre, are attributed to different distributions of giants and sub-giants.

Our photometric results have shown, that in the cluster Omega Centauri, there are concentric zones of differing colours and are demonstrated by Fig. II-8, in B-I colour. We have obtained photographs of the cluster Omega Centauri in B, V and Infra-red bands. The details of the photographs are given in Table III-1. As explained before, we have obtained isodensity contours in B, V and infra-red bands for the cluster.

Table III-1

Details of plate-filter combination used at the 102cm R-C reflector

Kavalur Plate No.	Emulsion	Filter	Scale of Plate	Exposure time	Approx. limiting Magnitude	Image size of faintest stars
C311	103aO	GG11	40"/mm	30 mts.	19.0	20
C43	103aD	C3384	40"/mm	35 mts.	17.9	25
C280	1 N	RG8	40"/mm	90 mts.	18.5	30

For each contour we have measured x, y coordinates for 72 points on the contour at 5° intervals, along with the x, y coordinates of 2 reference stars of the cluster. The measures are done using a Zeiss Ascocord two coordinate comparator. A computer programme made for the purpose, first translates the arbitrary coordinate system used for measurement, to a new coordinate system, such that the origin coincides with the position of one of the reference stars. The new reference system is, then, rotated, so that the x-axis coincides with the direction of the line joining the two reference stars. The coordinates are scaled down

taking the distance between the two reference stars as unity. The x, y values are then fitted to a second degree equation of the kind

$$X^2 + BXY + CY^2 + DX + EY + F = 0$$

by the method of least squares. The solution of the normal equations are done using the matrix inverse method. The properties of the ellipse are derived from the coefficients B, C, D, E and F. The errors are calculated by a method given by Denning (1943).

The results have been obtained using two sets of reference stars. Both sets give exactly the same results. The computer programme gives the axial ratio b/a, position angle ϕ, area within each contour, the x and y coordinates of the centre of each contour and the respective errors. The origin for the coordinate system is the star marked O in plate I and the x-axis is the line joining O and M where M is the second reference star and is marked in plate I. Since all the distances are normalised to the distance OM on every plate, the small differences in the scales of the plates taken in B, V and infra-red bands will not cause any error in the results. Knowing the distance of OM in arc minutes, all the distances can be reduced to arc minutes. In the B band, seven contours have been

reduced using a different set of reference stars and hence their x, y coordinates and origin are different from those for the other contours.

Table III-2 to III-4 give the data regarding the equi-density contours obtained for the B, V and infra-red bands. III-2 is for the B band, III-3 is for the V band and III-4 is for infra-red band. In each table, the first column gives the serial number of the contour, the number increasing outward from the cluster centre. Columns 2 and 3 give the semi-major axis (a) and semi-minor axis (b) in arc minutes. Columns 4 and 5 give the x-coordinate of the centre of the cluster with star O as the origin and OM as the x-axis and the corresponding error in the least squares fit. Columns 6 and 7 give the y-coordinate of the cluster centre with star O as the origin and OM as the x-axis and the corresponding error. Column 8 gives the distance between the reference stars which gives a check on the scale of the plates used. Since, this distance is taken as unity in the reductions, the plate scale does not come into the picture. Small differences in the scale of the photographs taken in B, V and infra-red bands will not create any uncertainty in the values derived for each contour and for each band. Columns 9 and 10 give log a and log b where a and b are in minutes of arc. Columns 11 and 12 give the axial ratio b/a

Table III-2

Blue Plate

S. No.	a	b	X_0	σX_0	Y_0	σY_0	Distance OM
1	2	3	4	5	6	7	8
1	2.2616	2.0134	22.177	0.008	16.828	0.004	41.999
2	2.9009	2.5233	22.258	0.004	16.724	0.004	41.979
3	3.0132	2.7194	22.177	0.008	16.806	0.004	42.016
4	3.5007	3.1182	22.299	0.008	16.765	0.004	41.971
5	3.6850	3.2330	22.177	0.018	16.806	0.004	41.999
6	3.8177	3.2627	22.299	0.008	16.684	0.008	41.979
7	4.4649	3.8166	13.632	0.012	24.216	0.009	28.591
8	4.5416	3.8173	22.177	0.012	16.765	0.008	41.947
9	5.0722	4.2283	22.177	0.012	16.765	0.008	41.963
10	5.2252	4.4395	22.096	0.012	16.724	0.008	41.985
11	5.3571	4.5785	13.687	0.015	24.188	0.012	28.591
12	5.5987	4.8054	13.604	0.015	24.160	0.012	28.593
13	5.8462	5.0140	22.177	0.016	16.765	0.012	41.963
14	5.9137	5.0609	13.632	0.018	24.216	0.015	28.591
15	5.9902	5.2207	22.096	0.016	16.806	0.012	42.017
16	6.2712	5.4011	13.632	0.015	24.188	0.012	28.593
17	6.4004	5.5621	22.136	0.012	16.765	0.012	41.985
18	6.5644	5.7001	22.096	0.012	16.765	0.008	42.009
19	6.9729	6.0423	22.136	0.012	16.724	0.012	41.985
20	7.2724	6.3064	22.055	0.012	16.765	0.012	42.016
21	8.0541	6.7988	22.258	0.018	16.562	0.012	42.009
22	8.8647	7.5092	22.055	0.018	16.765	0.020	42.016
23	9.5247	7.9735	22.177	0.024	16.480	0.020	42.009
24	10.7520	8.8370	22.299	0.032	16.724	0.024	42.016

Table III-2 - continued

log a	log b	b/a	σ b/a	Area	σ Area	ϕ	$\sigma\phi$
9	10	11	12	13	14	15	16
0.3544	0.3039	0.890	0.006	14.306	0.079	124°.5	1.6
0.4625	0.4020	0.870	0.004	22.996	0.077	105°.1	0.8
0.4790	0.4345	0.903	0.005	25.743	0.120	100°.8	1.5
0.5442	0.4939	0.891	0.004	34.293	0.123	98°.0	1.0
0.5664	0.5096	0.877	0.003	37.428	0.112	96°.2	0.7
0.5818	0.5136	0.855	0.004	39.132	0.132	100°.7	0.7
0.6498	0.5817	0.855	0.005	53.535	0.214	100°.5	0.8
0.6572	0.5818	0.841	0.005	54.465	0.208	100°.4	0.7
0.7052	0.6262	0.834	0.005	67.377	0.280	101°.3	0.7
0.7181	0.6473	0.850	0.005	72.876	0.303	100°.3	0.8
0.7289	0.6607	0.855	0.005	77.055	0.338	101°.3	0.9
0.7481	0.6817	0.858	0.005	84.521	0.355	100°.5	0.9
0.7669	0.7002	0.858	0.005	92.089	0.431	101°.8	1.0
0.7719	0.7042	0.856	0.005	94.024	0.437	99°.5	1.0
0.7774	0.7177	0.872	0.005	98.247	0.410	100°.4	1.0
0.7974	0.7325	0.861	0.005	106.410	0.417	99°.6	0.8
0.8062	0.7452	0.869	0.004	111.840	0.378	97°.1	0.8
0.8172	0.7559	0.868	0.003	117.551	0.378	100°.2	0.7
0.8434	0.7812	0.867	0.004	132.363	0.504	97°.4	0.9
0.8617	0.7998	0.867	0.004	144.082	0.540	101°.8	0.8
0.9060	0.8324	0.844	0.005	172.027	0.827	101°.4	0.9
0.9477	0.8756	0.847	0.005	209.126	0.969	100°.6	0.9
0.9789	0.9017	0.837	0.005	238.589	1.126	103°.8	0.9
1.0315	0.9463	0.822	0.006	298.500	1.442	106°.1	0.8

Table III-3

Visual Plate

S. No.	a	b	X_0	σX_0	Y_0	σY_0	Distance OM
1	2	3	4	5	6	7	8
1	1.1967	1.0950	22.205	0.008	16.989	0.008	41.341
2	1.6684	1.5259	22.157	0.004	17.046	0.004	41.365
3	1.9268	1.7563	22.108	0.004	17.095	0.004	41.301
4	2.0370	1.8323	22.177	0.008	17.095	0.004	41.292
5	2.5762	2.2861	22.177	0.004	17.054	0.004	41.347
6	2.6771	2.3727	22.177	0.004	17.054	0.004	41.365
7	3.5430	3.1129	22.124	0.008	17.009	0.008	41.365
8	3.5919	3.1564	22.128	0.008	17.013	0.008	41.347
9	3.8124	3.3782	22.218	0.012	16.977	0.012	41.309
10	3.9483	3.4901	22.258	0.012	16.969	0.008	41.330
11	3.9772	3.4531	22.185	0.008	17.005	0.008	41.365
12	4.0903	3.5422	22.169	0.012	16.989	0.008	41.347
13	4.3438	3.7823	22.218	0.012	16.969	0.008	41.309
14	4.7068	3.9776	22.169	0.012	16.956	0.008	41.325
15	5.0462	4.3947	22.161	0.012	16.977	0.012	41.335
16	5.2008	4.4334	22.104	0.012	16.956	0.012	41.295
17	5.5259	4.7770	22.136	0.012	17.009	0.012	41.285
18	5.6976	4.9554	22.128	0.016	16.997	0.012	41.325
19	6.1741	5.2964	22.079	0.016	16.997	0.012	41.305
20	6.5538	5.6488	22.035	0.016	17.017	0.012	41.335
21	7.2517	6.3365	22.022	0.024	17.017	0.020	41.335
22	7.7322	6.5221	22.059	0.028	16.964	0.024	41.325
23	8.6433	7.2521	21.933	0.028	16.887	0.024	41.305
24	8.8948	7.4869	22.116	0.032	16.978	0.024	41.325
25	10.8930	9.0266	21.567	0.040	16.439	0.032	41.305

Table III-3 - continued

log a	log b	b/a	σ b/a	Area	σ Area	ϕ	$\sigma\phi$
9	10	11	12	13	14	15	16
0.0780	0.0394	0.915	0.016	4.133	0.063	102.3	5.1
0.2223	0.1835	0.915	0.007	7.998	0.048	109.6	2.1
0.2848	0.2446	0.912	0.006	10.631	0.054	125.9	1.8
0.3090	0.2630	0.900	0.006	11.726	0.063	128.3	1.7
0.4100	0.3391	0.887	0.004	18.503	0.069	112.4	1.0
0.4277	0.3752	0.886	0.004	19.955	0.063	111.1	0.9
0.5494	0.4932	0.879	0.004	34.649	0.131	101.5	1.0
0.3553	0.4992	0.879	0.004	35.618	0.147	98.1	1.1
0.5812	0.5287	0.886	0.007	40.461	0.243	104.1	1.7
0.5964	0.5428	0.884	0.005	43.291	0.191	98.1	1.2
0.5996	0.5382	0.868	0.005	43.146	0.181	98.6	0.9
0.6118	0.5493	0.866	0.005	45.517	0.199	98.4	1.0
0.6379	0.5778	0.871	0.005	51.615	0.270	101.7	1.3
0.6727	0.5996	0.845	0.004	58.816	0.217	98.9	0.7
0.7030	0.6429	0.871	0.005	69.670	0.305	97.4	1.0
0.7161	0.6467	0.852	0.005	72.436	0.300	99.4	0.9
0.7424	0.6792	0.865	0.005	82.929	0.361	98.0	1.0
0.7557	0.6951	0.870	0.005	88.700	0.414	100.1	1.1
0.7906	0.7240	0.858	0.005	102.732	0.429	98.8	0.9
0.8165	0.7520	0.862	0.005	116.306	0.483	97.5	0.9
0.8604	0.8018	0.874	0.005	144.358	0.871	98.9	1.4
0.8883	0.8144	0.844	0.007	158.431	0.994	96.0	1.2
0.9367	0.8605	0.839	0.007	196.922	1.135	99.1	1.1
0.9491	0.8743	0.842	0.008	209.213	1.328	93.3	1.2
1.0372	0.9555	0.829	0.008	308.903	1.931	98.5	1.1

Table III-4

Infra-red Plate

S. No.	a'	b'	X_{centre}	X_{centre}	Y_{centre}	Y_{centre}	Distance OM
1	2	3	4	5	6	7	8
1	1.7449	1.5504	22.258	0.012	16.521	0.012	42.7798
2	2.2470	1.9902	22.218	0.008	16.602	0.008	42.7808
3	2.2710	2.0195	22.218	0.008	16.643	0.008	42.7714
4	2.5668	2.3365	22.218	0.008	16.643	0.008	42.7606
5	2.8594	2.5880	22.218	0.008	16.643	0.008	42.7844
6	2.9847	2.6812	22.258	0.008	16.643	0.008	42.7613
7	3.3506	3.0271	22.218	0.008	16.602	0.008	42.7736
8	3.3685	3.0384	22.218	0.008	16.643	0.008	42.7767
9	3.9402	3.4824	22.258	0.008	16.602	0.008	42.7844
10	4.2527	3.7217	22.218	0.012	16.643	0.008	42.7955
11	4.4118	3.8169	22.299	0.012	16.562	0.008	42.7844
12	4.6763	4.0740	22.340	0.012	16.643	0.008	42.7931
13	5.3713	4.7402	22.258	0.016	16.806	0.012	42.7973
14	5.7794	5.1198	22.177	0.016	16.684	0.012	42.7955
15	5.9133	5.2216	22.218	0.012	16.724	0.012	42.7968
16	6.3711	5.6268	22.299	0.012	16.643	0.008	42.7901
17	6.5912	5.8100	22.258	0.012	16.806	0.008	42.7973
18	7.4938	6.4773	22.096	0.016	16.684	0.012	42.7968
19	7.7640	6.7080	22.096	0.024	16.684	0.015	42.7585
20	9.3611	8.0785	22.218	0.028	16.602	0.018	42.7644
21	11.3766	9.8116	21.933	0.036	16.023	0.021	42.7587

Table III-4 - continued

log a	log b	b/a	$\sigma_{b/a}$	Area	σ_{Area}	ϕ in deg.	σ_{ϕ}
9	10	11	12	13	14	15	16
						+79°	
0.2418	0.1904	0.888	0.013	8.4980	0.098	6.9105	3.2588
0.3516	0.2989	0.886	0.006	14.0489	0.077	9.1906	1.4721
0.3562	0.3052	0.889	0.007	14.4082	0.087	9.7248	1.6966
0.4094	0.3686	0.910	0.007	18.8412	0.119	12.3801	2.2204
0.4563	0.4130	0.905	0.005	23.2482	0.111	11.0172	1.5813
0.4749	0.4283	0.898	0.005	25.1408	0.110	8.8927	1.3519
0.5251	0.4810	0.904	0.005	31.8639	0.136	3.0122	1.3877
0.5274	0.4827	0.902	0.004	32.1537	0.116	3.5908	1.1570
0.5955	0.5419	0.884	0.004	43.1069	0.156	-0.0422	0.9732
0.6287	0.5708	0.875	0.004	49.7228	0.204	0.3413	1.0240
0.6446	0.5817	0.865	0.004	52.9025	0.213	-0.7824	0.9163
0.6699	0.6100	0.871	0.005	59.8513	0.267	1.8909	1.0652
0.7301	0.6758	0.883	0.005	79.9882	0.393	0.0409	1.2769
0.7619	0.7093	0.886	0.005	92.9578	0.421	-0.2775	1.2155
0.7718	0.7178	0.883	0.004	97.0028	0.362	0.5700	0.9764
0.8042	0.7503	0.883	0.003	112.6225	0.346	1.4756	0.8080
0.8190	0.7642	0.881	0.003	120.3069	0.352	1.2006	0.7541
0.8747	0.8114	0.864	0.005	152.4916	0.688	3.0276	1.0100
0.8901	0.8266	0.864	0.006	163.6170	0.905	2.1032	1.2420
0.9713	0.9073	0.863	0.006	237.5787	1.234	2.9843	1.1779
1.0560	0.9917	0.862	0.006	350.6729	1.802	3.2176	1.1426

and its error. Columns 13 and 14 give the area within each contour and the corresponding error and columns 15 and 16 give the position angle of the major axis, ϕ and the corresponding error.

In Figure III-1, we have plotted the x and y coordinates of the centres of each contour against their semimajor axis (a) expressed in arc minutes. The centres of blue equidensity contours are marked by crosses and the centres of infrared equidensity contours are marked by filled cycles. The close agreement between the centres of blue and infra-red equidensity contours show that there is no asymmetrical absorption over the cluster due to the presence of dust. Table III-3 gives the mean value of the x and y coordinates of the centre of the cluster for the three wavelength bands (B, V and Infra-red). From the table we can find the location of the exact centre of the cluster with respect to the two reference stars O and M.

ω Centauri

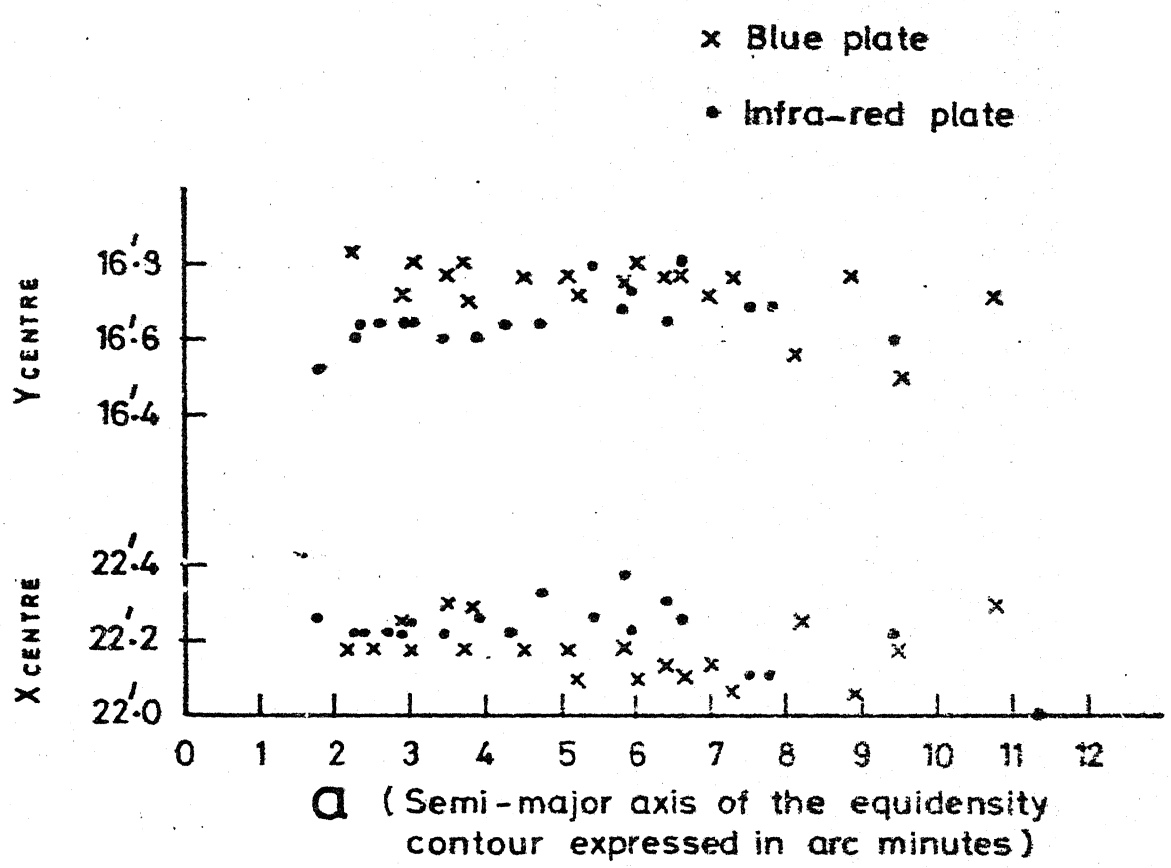

Figure III-1

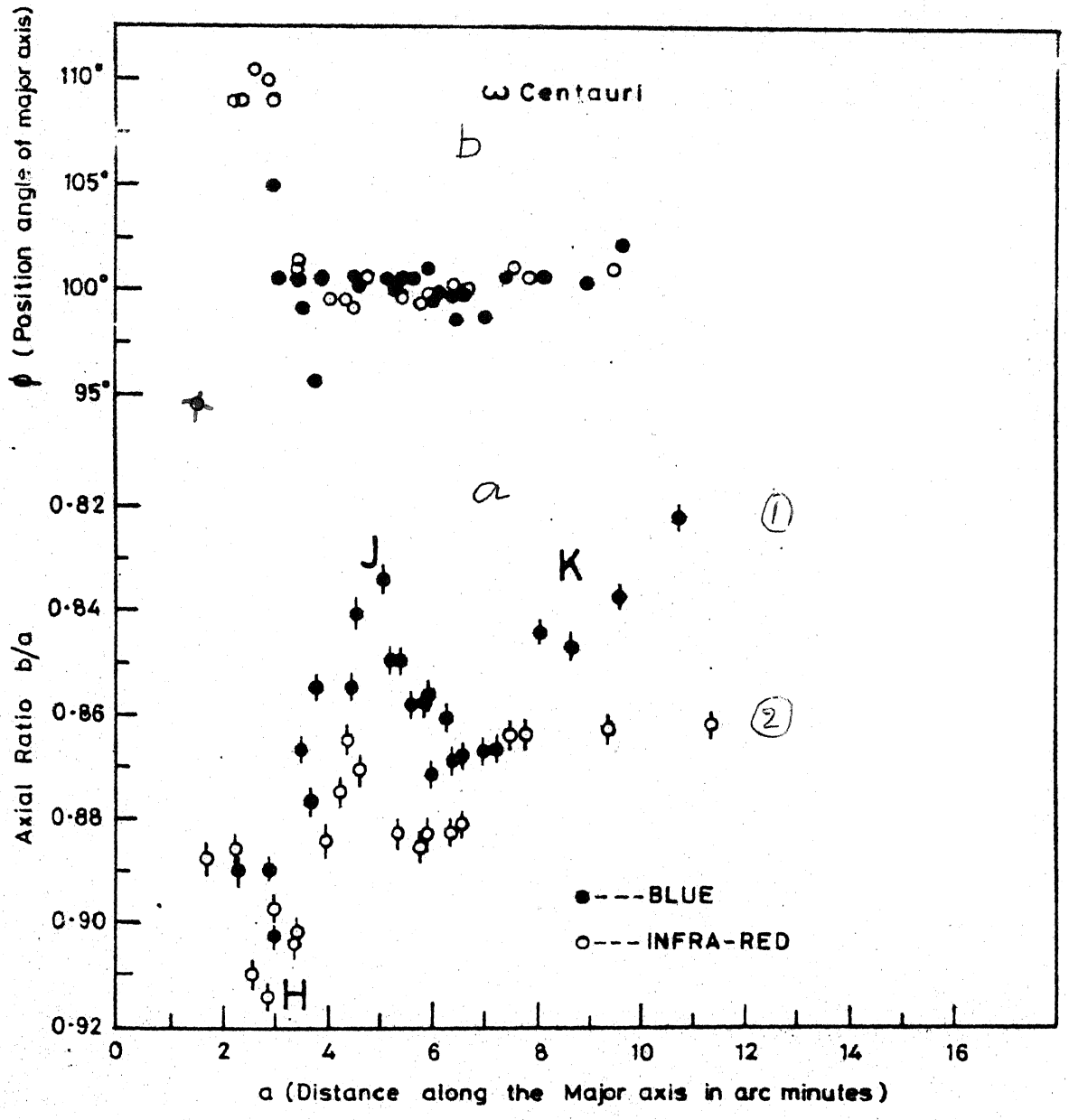
ω Centauri
b
a
J
K
H
1
2
●---BLUE
○---INFRA-RED
φ (Position angle of major axis)
110°
105°
100°
95°
Axial Ratio b/a
0·82
0·84
0·86
0·88
0·90
0·92
0
2
4
6
8
10
12
14
16
a (Distance along the Major axis in arc minutes)

FIG. III-2

Table III-5

Wavelength band	X centre in arc minutes	Y centre in arc minutes
B	22.171	16.741
V	22.114	16.981
Infra-red	22.214	16.624
Mean	22.166	16.781

III.7 Results of Equidensitometry on Omega Centauri: In Figure III-2a, we have plotted the axial ratio b/a against the semi-major axis 'a' for the B and infra-red bands. The values derived for the V band fall between B and infra-red bands. These are closer to those derived from the B band, because the difference in (B-V) colour is not much from the centre to the edge. Our photometric results show large difference in (B-I) colour. The curves show that the cluster is definitely less elliptical in the infra-red band, than it is in the blue band. Both the curves follow the same pattern of increase and decrease in the ellipticity with distance from the cluster centre. Whatever change happens on the B curve, occurs on I curve also, but a little closer to the cluster centre. The curves can be divided into 3 sections. At point H on the curve, the ellipticity

is the lowest in the cluster. From H to J the ellipticity shows a sharp increase and reaches a maximum at J. Between points J and K, the ellipticity shows a sudden dip. Beyond point K, the ellipticity shows an increasing trend. Point H is at 2.5' from the cluster centre, point J is at 5' and point K is at 8' from the cluster centre.

Figure III-2b shows ϕ, the position angle plotted against 'a' the semi major axis. The position angle of the cluster within 2.5' from the centre is definitely different from what the cluster has outside this radius. Beyond 2.5', the position angle shows only slight variations. But these variations, though small, can be connected with the changes in the (b/a - a) curve. Fig. III-3 shows a plot of b/a against 'a' for the cluster M92 and Omega Centauri in the V band. V band is used because we have contours closer to the cluster centre in this band. Data for M92 is taken from Hogner et al (1973) and is given in Table III-6. There is a large amount of similarity between the two curves. Taking the distance of Omega Centauri and M92 as 5.4 kpc and 8.1 kpc (Peterson and King 1975) respectively from the sun, the major axis value of M92 has been brought to the scale of Omega Centauri. The curves do not coincide. But they show that whatever situation prevails in Omega Centauri, also does for M92. The position angles in M92 also change similar

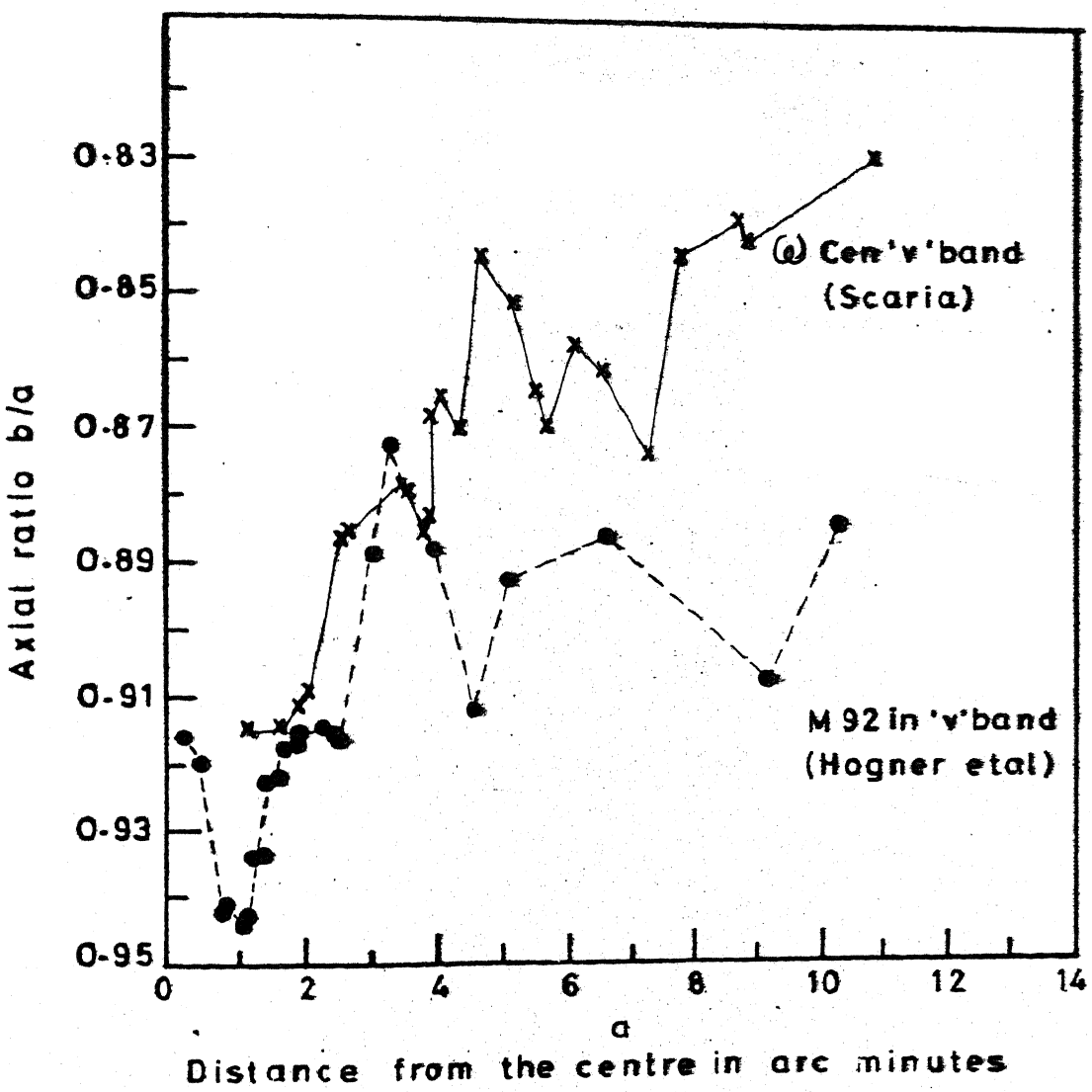
0·83
0·85
0·87
0·89
0·91
0·93
0·95
Axial ratio b/a
ω Cen 'v' band
(Scaria)
M 92 in 'v' band
(Hogner etal)
0
2
4
6
8
10
12
14
a
Distance from the centre in arc minutes

Fig. III–3

Table III-6

Axial ratio b/a and position angle ϕ for M92 in the V Band (Hogner et al 1973)

a in minutes of arc	b/a	ϕ	σ b/a	σ ϕ
0.25	0.919	82.2	0.000	0.0
0.32	0.921	84.1	0.000	0.1
0.49	0.943	85.8	0.002	0.5
0.55	0.942	83.1	0.004	1.0
0.72	0.945	70.4	0.008	3.1
0.77	0.943	66.4	0.011	5.1
0.84	0.934	60.8	0.004	2.0
0.90	0.934	58.3	0.004	1.9
0.97	0.923	56.9	0.005	1.8
1.04	0.923	54.9	0.005	1.7
1.11	0.918	53.2	0.005	1.8
1.18	0.917	52.8	0.005	1.8
1.28	0.916	52.7	0.005	1.8
1.53	0.915	53.5	0.005	1.8
1.59	0.916	57.4	0.006	1.9
1.70	0.917	56.6	0.005	1.8
2.02	0.889	49.3	0.007	1.7
2.20	0.873	46.5	0.007	1.5
2.64	0.888	50.0	0.008	1.9
3.01	0.913	50.9	0.009	2.8
3.37	0.892	51.1	0.009	2.3
4.37	0.886	52.7	0.012	2.9
5.44	0.907	48.6	0.021	6.3
6.92	0.883	19.1	0.023	6.2

to the changes seen in Omega Centauri as shown in Figure III-4 which is copied from Hogner et al (1973). Figure III-5 is the b/a - log a plot taken from Hogner et al (1975) for the cluster M5. The similarity of the curves with that of Omega Centauri cannot be missed at all. All the three clusters show the region of low ellipticity near the centre. Then there is a sudden increase in ellipticity. The ellipticity shows one more drop before increasing again in these three clusters. All the clusters show the sudden change in the position angle of the major axis of the core to that of the outer regions.

Figure III-6 gives the relation between these three regions in the cluster Omega Centauri to the (B-I) colour change from centre to the outer regions. In the figure we have plotted b/a and position angle of the major axis and (B-I) colour against the distance from the centre of the cluster. The (B-I) values are split into four groups. The (B-I) colour along the major and minor axis for the east, west, north and south wings are plotted separately in the figure. The most striking feature in the figure is that the change in ellipticity is connected with change in colour. The core of the cluster which can be identified in the colour curve, matches with the region of lowest ellipticity in the cluster. Between 5' and 8' from the cluster

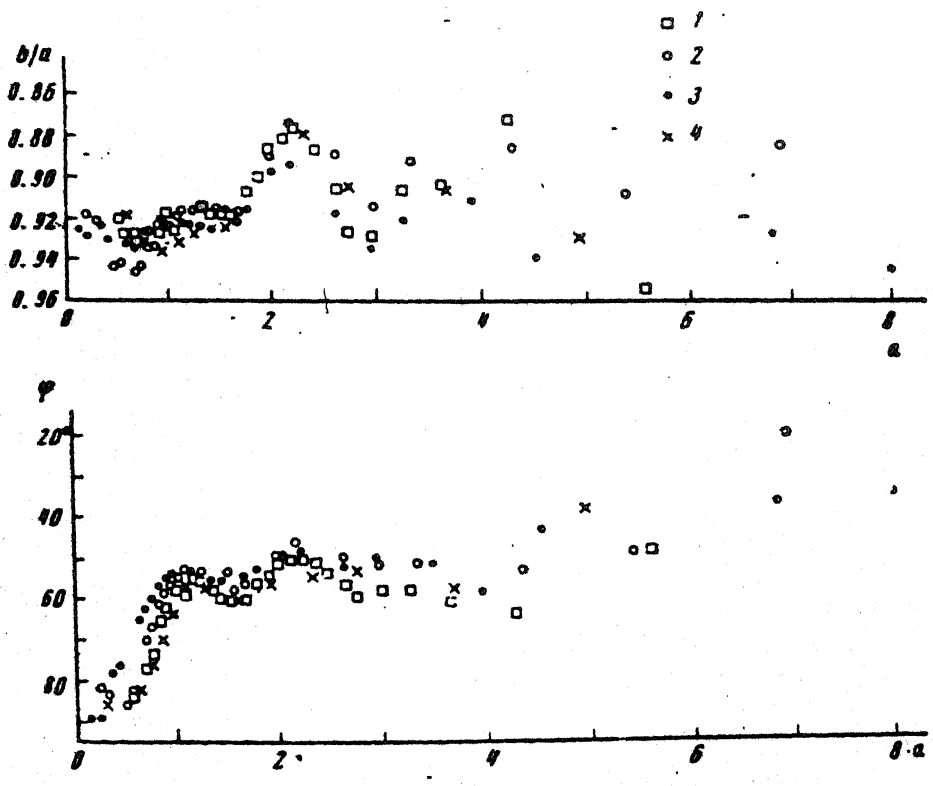

FIG III-IV

Fig. 2. Axial ratio b/a and position angle φ of the major axis as functions of the major semiaxis a. 1) R; 2) V; 3) B; 4) U wavelength band.

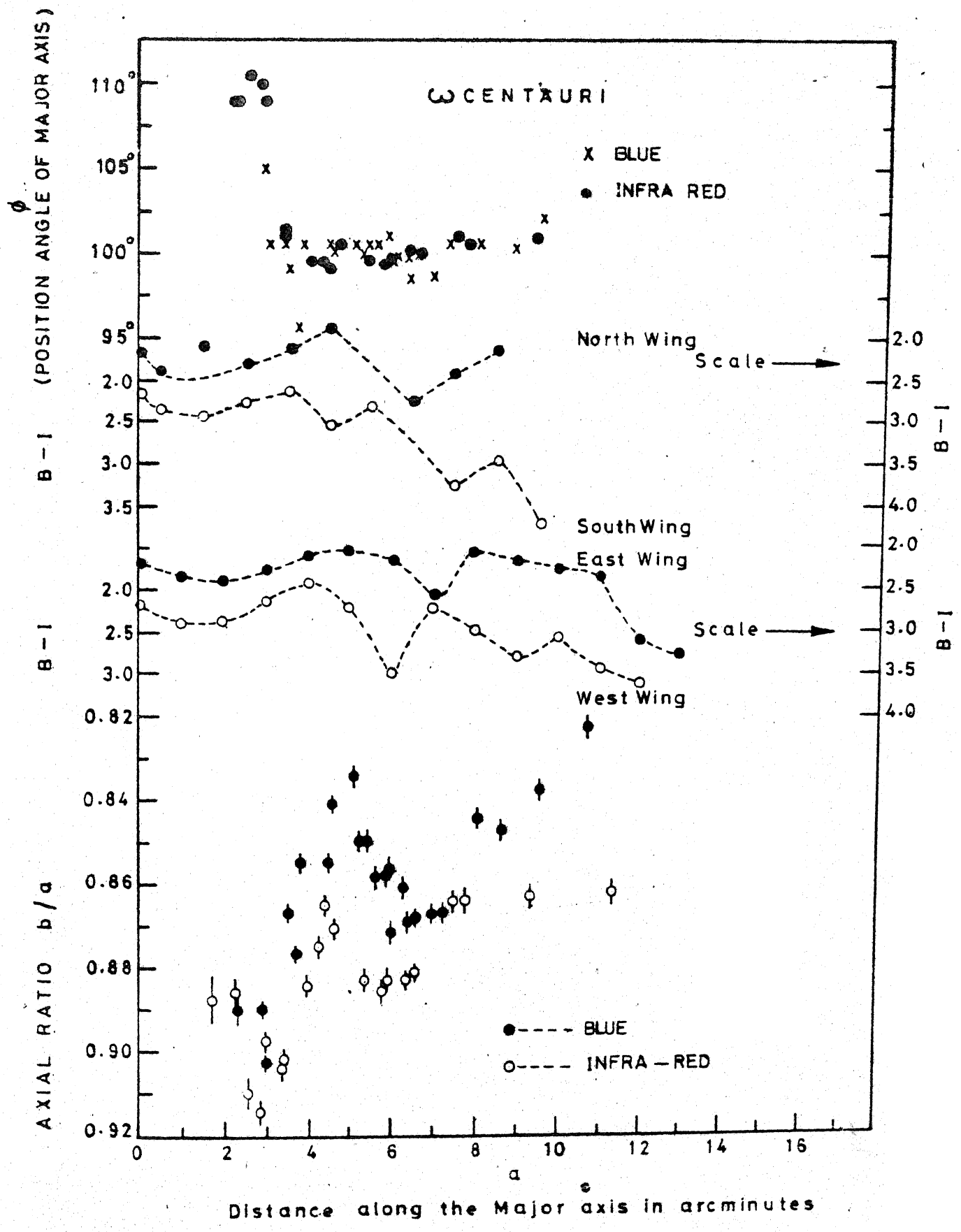
ω CENTAURI
X BLUE
INFRA RED
North Wing
South Wing
East Wing
West Wing
Scale
Scale
BLUE
INFRA – RED
φ (POSITION ANGLE OF MAJOR AXIS)
B – I
B – I
AXIAL RATIO b/a
Distance along the Major axis in arcminutes
a
e

FIG. III-6

centre, (B-I) colour is comparable to what it is at the centre. Here, the ellipticity has suddenly decreased. Between 2.5' and 5', the cluster is bluer and this region in the b/a vs a curve shows large ellipticity. The ellipticity reaches a maximum where the cluster is the bluest. Thus we find that the red stars seen in the cluster showing a distribution more spherical than what the blue stars show. Blue stars appear as a bulge around the red core of the cluster between 2.5' and 5' from the centre and they have a distribution of larger ellipticity when compared to the bright red stars.

III.8 Isodensitometry of 47 Tuc: 47 Tuc is the second largest globular cluster in our galaxy. Basic data on the cluster is taken from Peterson and King (1975) and presented in Table III-7.

Table III-7

1950	1950	l° (deg)	b° (deg)	Conc. Class	Sp. Type	V_r kms/sec	$(m-M)_{app.V}$
$00^h21.9^m$	-72°21'	306	-45	III	G3	-24	13.15

When compared to Omega Centauri, this is a cluster more centrally concentrated and is closer to us. The

47 TUC

PLATE IV

metallicity of the cluster is larger than that for Omega Centauri. Compared to the large core-radius of Omega Centauri ≃2.5', 47 Tuc has a small core-radius = 0'.41 (Peterson and King). Gascoigne and Burr (1956) has made drift scan and concentric aperture measures on the cluster in P and V bands. They show a radial colour change of .17 in P-V colour. Chun and Freeman have studied the cluster photoelectrically, making spot measurements on 81 locations on the cluster in U, B, V bands. Photoelectric measurements of the Mg b lines and the blue CN band also were made on these locations. They report a colour change in the cluster at a distance of about 2' from the centre. The results for the CN bands were not conclusive and Mg b lines did not show any obvious variation. The core-radius of the cluster is only 0'.41. Hence, the 59".4 diaphragm used by Chun and Freeman for the spot measurements is too large a diaphragm, to see the exact location of the colour change in the core. The B-V colour of the inner region of radius 2' is ≃ 0.90 and U-B colour is ≃ 0.39. Outside this region the colour decreases to B-V ≃ 0.81 and U-B ≃ 0.25 at radius 4'.

The plates we have used for equidensitometry on 47 Tuc were taken by the 60 inch reflector at the Harward Observatory Bloemfontein station. The scale of the plate is 26"/mm. The details regarding the plates are given in Table III-8.

Table III-8

Plate No.	Date	Station	Telescope	Exposure time	Scale of the plate
SB 192	Sept. 10/11 1934	Bloemfontein	60" reflector	160 minutes	26"/mm
SB2077	Nov. 9/10 1939	"	"	1 minute	"

The procedure followed for obtaining the isophotes was the same as before. 18 contours have been obtained for the cluster. Following the same procedure as before, b/a the axial ratio, a and b the semi major and semiminor axis and ϕ, the position angle were determined. The first column in Table III-9 gives the contour number, the number increasing outward in the cluster. Column 2 gives a, the semi-major axis. Column 3 and 4 give b/a, the axial ratio and its errors. Column 5 gives the position angle ϕ.

III.9 Results: In Figure III-7 we have plotted b/a and ϕ against the semi major axis 'a'. The change in the ellipticity in the cluster is similar to what is seen in Omega Centauri, M5 and M92. The minimum seen beyond the point of maximum ellipticity is not so prominent as it is in the case of Omega Centauri, M5 and M92. The region of smallest

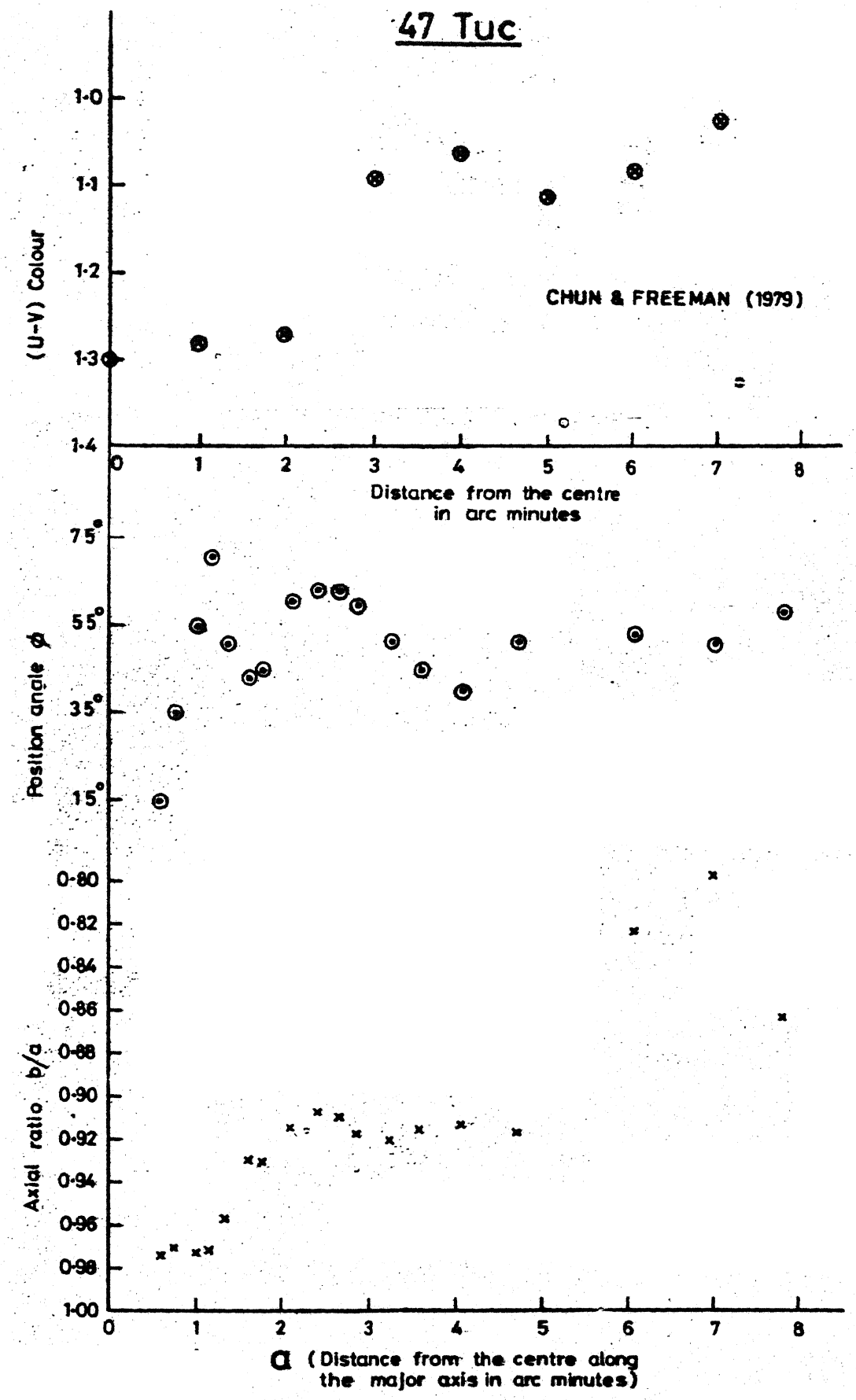
47 Tuc
(U-V) Colour
1·0
1·1
1·2
1·3
1·4
CHUN & FREEMAN (1979)
0
1
2
3
4
5
6
7
8
Distance from the centre
in arc minutes
Position angle φ
75°
55°
35°
15°
Axial ratio b/a
0·80
0·82
0·84
0·86
0·88
0·90
0·92
0·94
0·96
0·98
1·00
a (Distance from the centre along
the major axis in arc minutes)

Fig. III–7

Table III-9

Equidensitometry of 47 Tuc

S. No.	a in minutes of arc	b/a axial ratio	σ b/a	ϕ degrees
1	0.57	0.974	0.001	14.4
2	0.74	0.969	0.002	34.7
3	0.79	0.972	0.002	54.7
4	1.15	0.971	0.003	71.4
5	1.32	0.957	0.003	49.4
6	1.58	0.929	0.004	49.3
7	1.76	0.930	0.004	46.9
8	2.09	0.914	0.005	60.6
9	2.39	0.907	0.005	63.2
10	2.64	0.909	0.006	62.6
11	2.83	0.917	0.006	59.9
12	3.24	0.920	0.006	51.5
13	3.59	0.915	0.007	45.1
14	4.05	0.913	0.008	40.3
15	4.68	0.917	0.008	51.5
16	6.06	0.823	0.009	53.5
17	7.00	0.797	0.010	51.3
18	7.79	0.863	0.015	58.3

ellipticity in the cluster extends upto $\lesssim$ 1.20' from the centre. The ellipticity increases, thereafter, and reaches a peak around 2.4' from the centre. The ellipticity shows a small decrease between 2.4' and 4' and beyond this, the ellipticity is found to increase considerably as seen in the figure. But the results obtained for this region of the cluster are not conclusive, as the plate used for the purpose was not exposed sufficiently long for this faint region of the cluster. Hence, the uncertainty could be quite large. The change in the position angle does not show the kind of change seen in the other three clusters. The position angle changes in a way similar to the change in ellipticity. The third curve in the figure shows the U-V colour variation over the cluster, with mean distance from the centre obtained by Chun and Freeman (1979). The diaphragm used by them was too large and hence the exact location of the colour change cannot be determined from their observations. Anyhow, the relationship between the change in ellipticity and the change in the colour of the cluster to the bluer wavelengths is well established. The extent of the blue region is smaller than what it is in Omega Centauri.

In the next chapter, we have used the photographic subtraction technique to bring out the blue and red regions in the cluster.

-

Many other clusters have been included in our programme of equidensitometry of globular clusters. Some of these for which isophotes have been derived and shown in Plate VII are listed in Table III-10. They show a wide range of the features that we have described in both Omega Centauri and 47 Tuc. The most circular isodensities are obtained in the case of NGC 6093 while the most elliptical contours are seen in NGC 6656. Changes in ellipticity as we proceed outward from the centre are in most cases present as we have seen in Omega Centauri. Position angle changes of the orientation of the major axes are also noticed.

Table III-10

NGC No.	R.A (1950)		DEC (1950)		CONC (Shapley)
	h	m	°	'	
6121(M4)	16	20.6	-26	24	IX
6656(M22)	18	33.33	-23	58	VII
6541	18	04.4	-43	44	III
6090(M80)	16	14.1	-22	52	II
2808	09	10.9	-64	39	I
5927	15	24.5	-50	29	VII
4590(M68)	12	36.8	-26	29	X

PLATE V

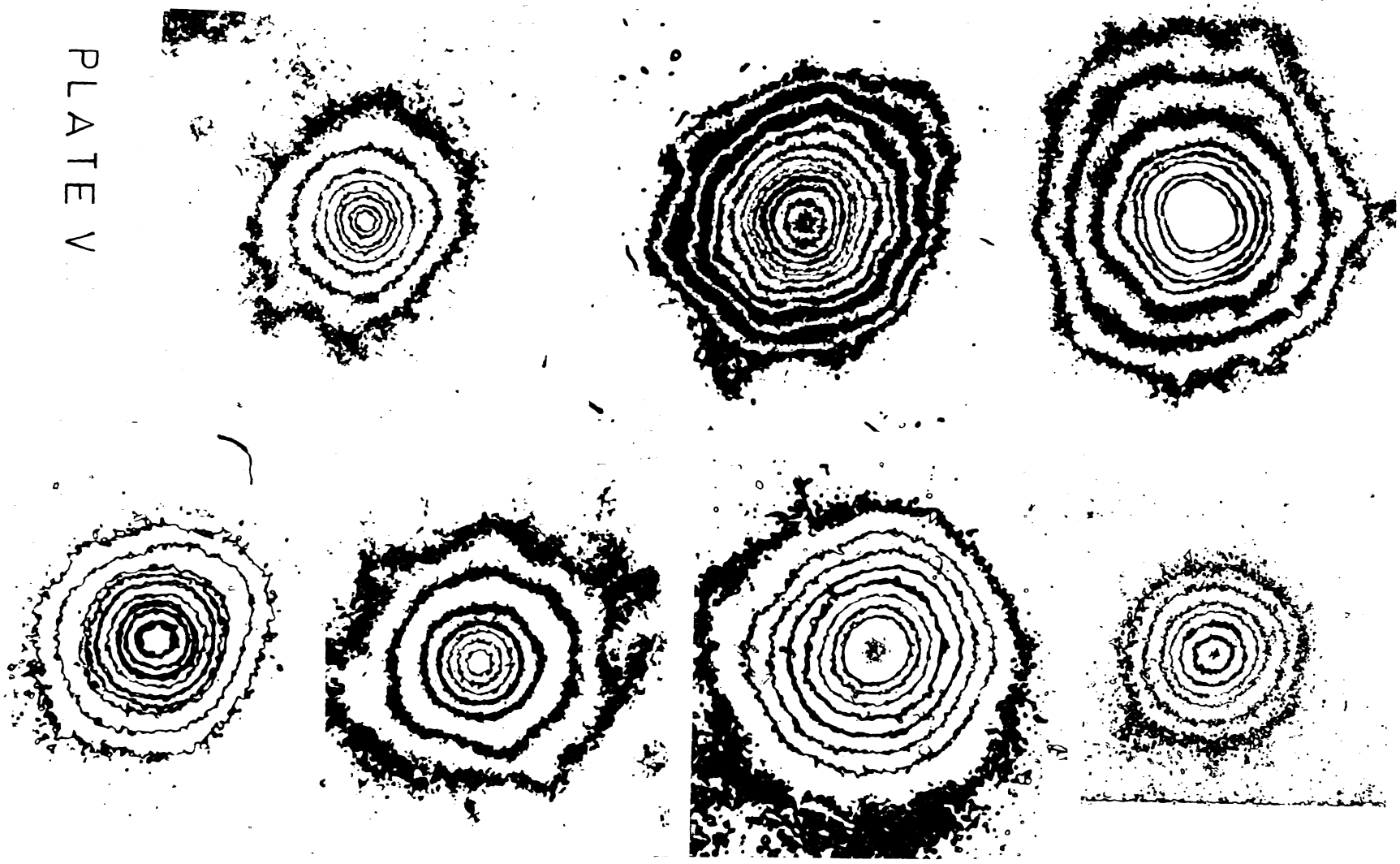

CHAPTER IV

SPATIAL DISTRIBUTION OF BLUE AND RED STARS IN OMEGA CENTAURI

IV. 1 **Introduction:** Composite photography has been extensively used for the study of variable stars. This technique is very useful in determining the colour gradient in a nebula and also in the determination of colours of individual stars. The technique has also been used widely in solar physics for the spatial study of magnetic and velocity fields. Proper exposure photographs are obtained in blue as well as red light. From a set consisting of one red plate and one blue plate, both of proper exposures, we can have two kinds of combinations. One will be a $B^- R^+$ combination where the negative of the blue plate is super-imposed over the positive of the red plate. The other is $B^+ R^-$ combination where the positive of blue plate is super-imposed over the negative of the red plate. Consider first a $B^- R^+$ combination. In the B^- plate, the stars are black dots on a clear background and in the R^+ plate the stars are clear dots on a dark background. Since the blue stars have larger image size on the blue photograph because of a higher brightness, these dark images of the blue stars in B^- plate completely block the smaller and clear

images of the blue stars in R^+ plate. Hence, the blue stars will appear as black dots on the $B^- R^+$ composite photograph. On the other hand, dark images of the red stars in the B^- plate are too small, to cover the larger clear images of these stars on the R^+ plate, and hence in the composite the red stars will appear as a black dot surrounded by a clear ring. A positive of this $B^- R^+$ composite, will show the blue stars as white dots and the red stars will appear as white dots surrounded by a black ring. The relative size of the two superposed images will depend on the colour of the star. The $B^+ R^-$ combination gives the opposite result. When the subtraction process is done on an extended source, like a galaxy, the difference in colour is represented by different shades of gray. If there is no colour difference, the nebula will show a uniformly gray shade. In a $B^- R^+$ combination, very dark surfaces are obtained, for extended sources composed of many unresolved blue stars. Surfaces of lighter gray are the result of larger contributions to the surface brightness, coming from redder stars. On a positive of a $B^- R^+$ combination, shades of darker gray will be for redder regions and shades of lighter gray will be for bluer regions in the extended source. $B^+ R^-$ plate behaves just the opposite way.

IV.2 Application of composite photography to globular clusters: The study of the distribution of the bright red giants and the blue horizontal branch stars, in the cluster, is very important in the field of cluster dynamics and the evolution of the cluster. We have used the above mentioned photographic subtraction process to study the distribution of these red and blue stars in the cluster Omega Centauri. Omega Centauri has a well populated horizontal branch and is well separated in (B-V) colour, from the giant and subgiant branch. All the horizontal branch (HB) stars have colour (B-V) $\leq$.40 and the giant stars have (B-V) $\geq$.60. Because of the large separation of these two groups, it is very easy to separate them out photographically. In the case of HB stars, we have the added advantage that, these stars are within a very small magnitude range and hence will appear as stars with almost the same diameter in the composite photograph. It is, therefore, very easy to identify them. To avoid the main sequence, we have to control the exposure of the original plate while exposing them at the telescope.

We have used two plates, one taken in B band (103aO + GG11) and the other taken in the Infra-red band (IN + RG8) for the subtraction process. The relative exposure times used for the plates are such that for the

bluest stars in the field, the diameters of the stellar images in both the plates are comparable. As explained before B^- I^+ and B^+ I^- composites were made. A positive taken of the combination B^+ I^- will show the features of plate VI and a positive of the combination of B^- I^+ will show the features of plate VII. The cluster looks different in B^+ I^- and B^- I^+ combinations. Blue stars appear as black dots in the positive of B^+ I^- combination and as white spots on the positive of B^- I^+ combination. Red stars will behave just the opposite way. The exposure times of the original plates and of the positives taken from these plates are such that stars bluer than $B-V \leq .50$ appear as black dots in the combination B^+ I^-. The other stars appear as white dots. Central regions show only white dots showing the large density of red stars having $B-V > 0.50$.

IV.3 Results: Table IV-1 gives a list of stars taken from Geyer (1967) with their magnitudes, U-B and B-V colours. These stars have been marked on plate VI. It can be seen that stars bluer than $B-V \leq 0.5$ are seen as perfect round black dots. Since the scales of the two plates are not exactly the same, the stars are not well matched upto the edge of the field. But when the original is seen under a microscope, the red image of one plate cutting into the blue image of the other plate, can be easily seen. Since the

ω CEN

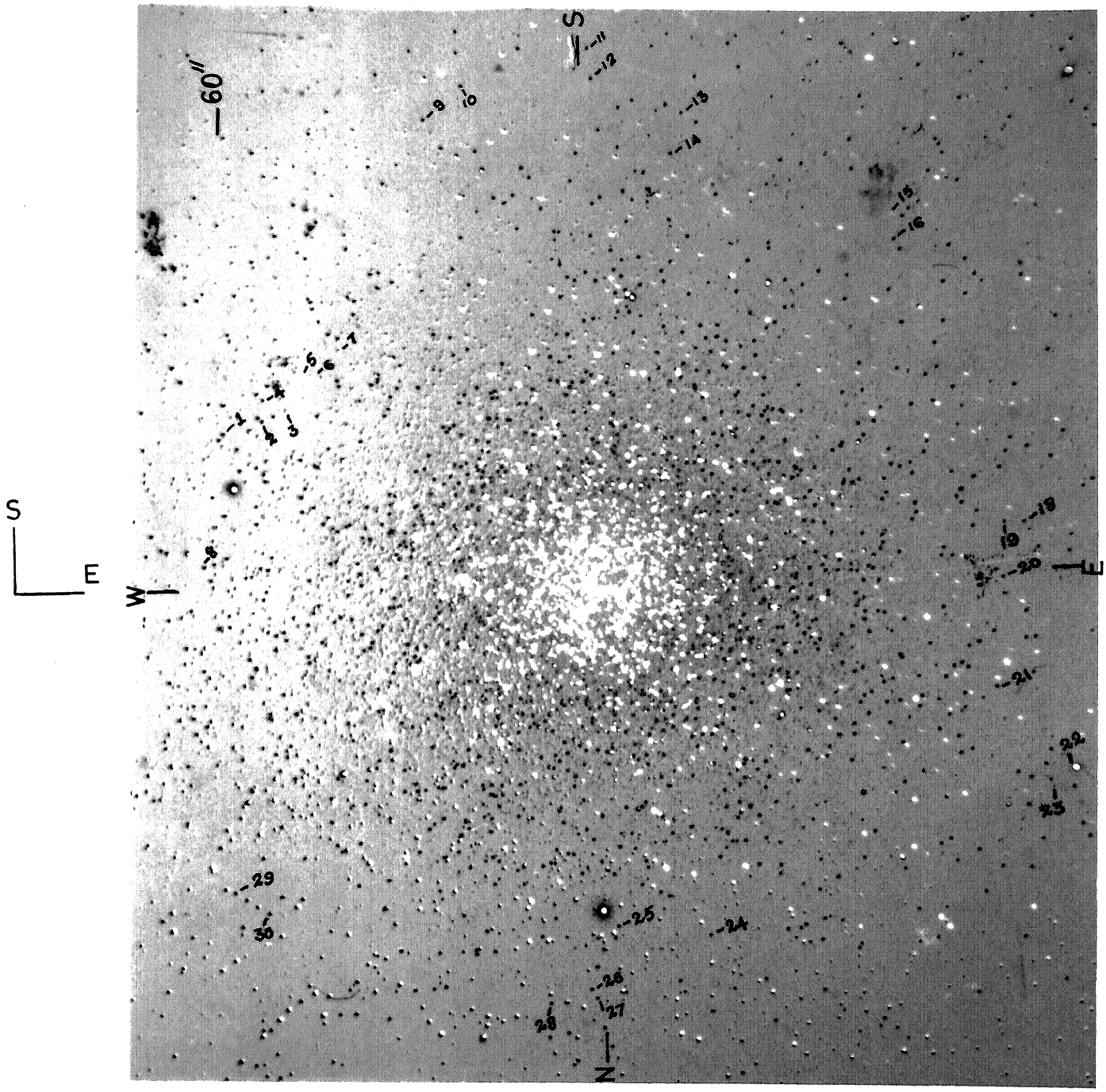

PLATE VI

Table IV-1

No.	Geyer No.	V_{mag}	B-V	U-B
1	30	14.70	+ 0.13	+ 0.02
2	31	14.56	+ 0.22	+ 0.05
3	32	14.23	+ 0.78	+ 0.00
4	33	15.34	- 0.04	- 0.31
5	48	12.21	+ 1.36	+ 1.37
6	49	12.42	+ 1.26	+ 1.01
7	50	13.29	+ 0.78	+ 0.24
8	8	14.59	+ 0.15	+ 0.03
9	76	14.72	+ 0.08	+ 0.04
10	84	15.16	+ 0.00	- 0.14
11	101	14.69	+ 0.09	+ 0.08
12	103	14.78	- 0.02	+ 0.20
13	118	15.30	+ 0.01	- 0.16
14	117	14.97	- 0.05	+ 0.03
15	147	13.54	+ 0.89	+ 0.38
16	148	14.75	- 0.08	+ 0.18
17	184	14.52	+ 0.43	- 0.09
18	194	14.51	+ 0.07	+ 0.00
19	193	14.97	- 0.12	+ 0.00
20	206	14.92	- 0.14	+ 0.05
21	217	14.76	+ 0.16	+ 0.01
22		9.41	+ 0.68	+ 0.33
23		14.59	+ 0.74	+ 0.12
24	288	15.26	- 0.05	- 0.14
25	291	14.49	+ 0.14	+ 0.13
26	310	14.59	+ 0.21	+ 0.02
27	309	15.23	+ 0.00	- 0.26
28	308	14.79	+ 0.08	+ 0.01
29	355	14.87	+ 0.04	- 0.01
30	353	14.84	- 0.05	- 0.01

blue stars have almost the same magnitudes, they all have the same size.

We have made counts of these blue stars in plate V4, dividing them into annular rings. The kind of grid used for the counts, is shown in Fig. IV-1 and the counts obtained for each column are marked on the grid. The black dots marked B, R and Q in the figure are the positions of the reference stars, B, R and Q of plate I. The major axis is almost parallel to OM on plate I. The counts have been treated as concentric aperture measures of brightness and reduced following King (1962) and Illingworth and Illingworth (1976). In Table IV-2 r_e is the effective radius given by $r_e = \sqrt{\frac{1}{2}(r_1^2 + r_2^2)}$ (King 1962). The surface brightness, log f is corrected to the radius r_e, using equation 4 of Illingworth and Illingworth (1976). Correction due to back ground is practically nil (Dickens and Woolley 1966). The innermost circle in the grid has a radius of 4.78 minutes of arc and the outer most circle has a radius of 23.92 minutes of arc. Within this region we have counted 1058 blue stars which accounts for all the HB stars in this field.

In Table IV-2, column (1) gives the inner and outer radii of the annular ring, column (2) gives effective

ω CENTAURI

(Distribution of horizontal branch stars in the region $3.5' < r < 23'$)

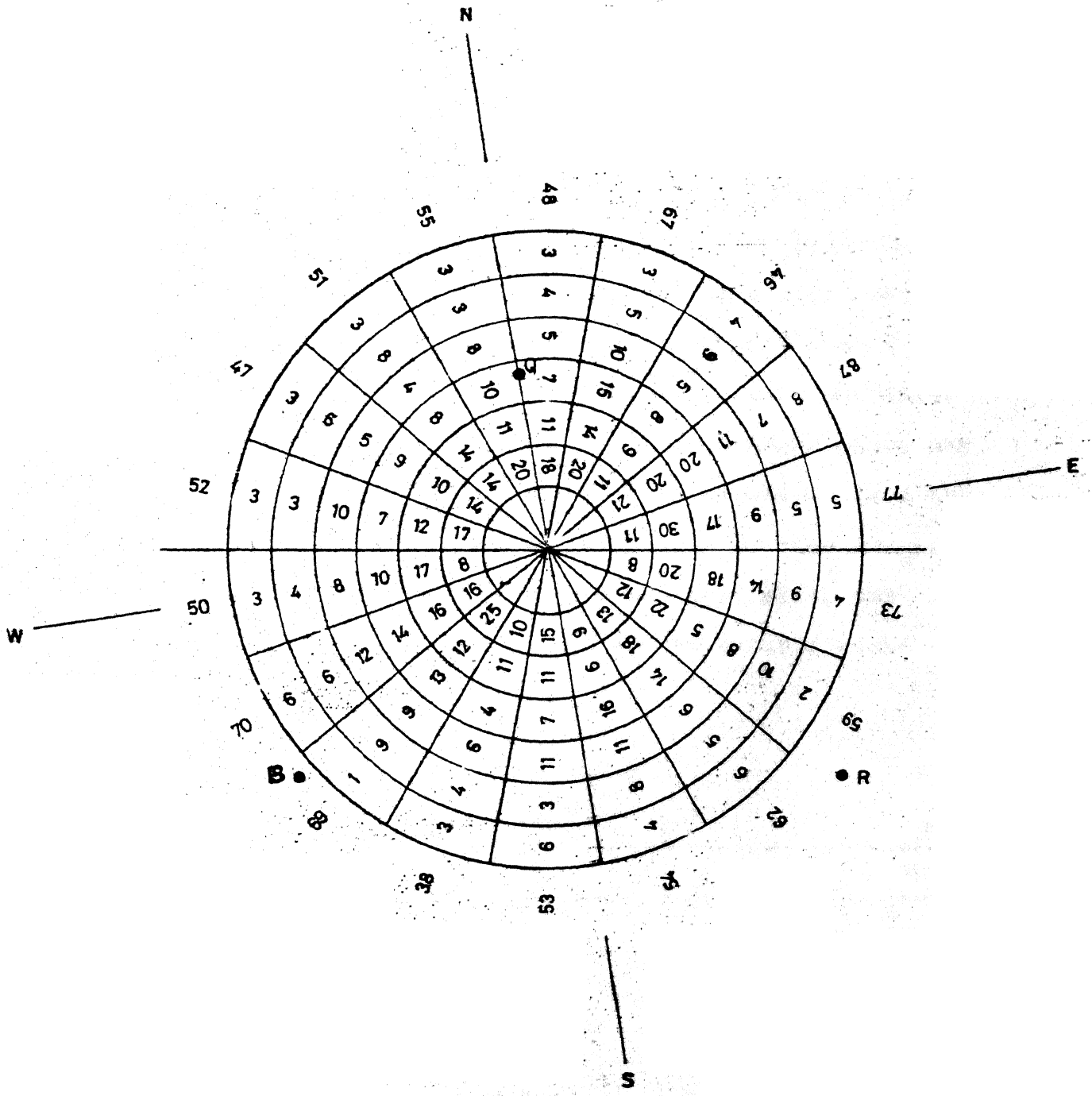

FIG. IV-1

radius r_e, column (3) gives log f, where f is the surface brightness over the annular ring per square minute of arc and column (4) gives log f corrected to the effective radius r_e. In Fig. IV-2 we have plotted r_e against log f (r_e). Counts obtained by Dickens and Woolley from photographic photometry (1966) for the blue stars also have been reduced to surface brightness and plotted on the same figure. Filled circles are our results and open circles are those obtained by Dickens and Woolley. In the outer regions our counts show a larger brightness for the cluster. This is because of the completeness in our counts of blue stars. As plates of proper exposures were not available, the distribution in the inner regions of the cluster could not be studied.

Table IV-2

1	2	3	4
95".7 - 287".0	3.56 arc mts.	0.3249	0.3131
287".0 - 478".4	6.58 arc mts.	0.3116	0.3069
478".4 - 669".7	9.70 arc mts.	0.1391	0.1365
669".7 - 861".0	12.86 arc mts.	-0.1021	-0.1037
861".0 - 1052".3	16.02 arc mts.	-0.3225	-0.3235
1052".3 - 1243".7	19.20 arc mts.	-0.5304	-0.5313
1243".7 - 1435".1	22.38 arc mts.	-0.8058	-0.8066

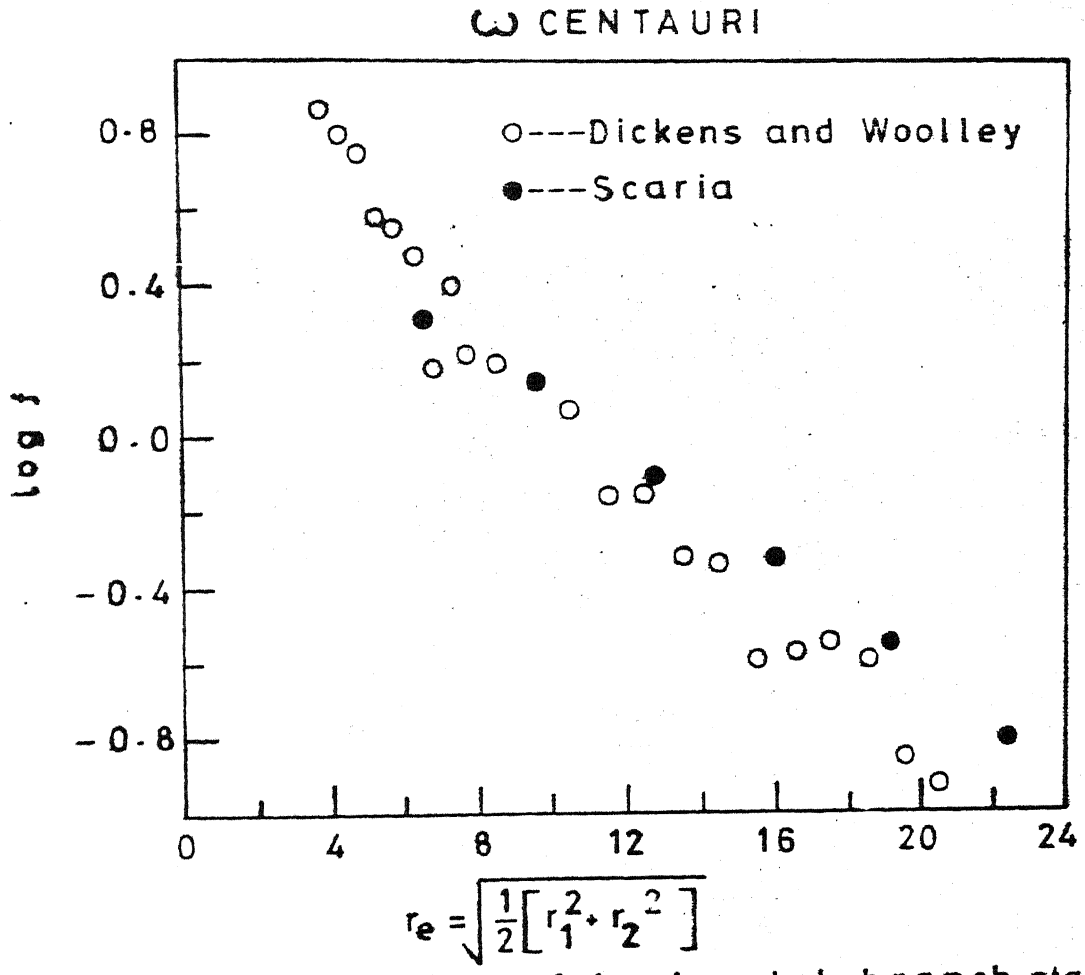

Distribution of horizontal branch stars in the cluster at $3.5' < r < 23'$

FIG. Ⅳ-2

The values marked outside the outermost ring in Fig. IV-1 are the total counts in each sector. These values show the cluster ellipticity very well. The position angle of the major axis is about 90° which is 10° less than the value obtained for the cluster in integrated light. Since the average (B-V) of the cluster is about 0.90, the central region has come out as a white patch.

Plate XVII is the B^- I^+ combination and is entirely different in character when compared to plate VI. In this plate, a blacker region refers to a region of larger (B-V) colour. The infrared plate used for this combination is quite over exposed for the central region and hence the central region appears white in the print. This really does not mean that the centre is blue in colour. For getting the actual colour at the centre, we have to use photographs of lower exposures, so that the density at the centre is of proper range for this work. Table IV-3 gives the B magnitudes and colours of the stars marked in plate XVII

The bulge around the core of the cluster can be seen getting bluer as we go out from the cluster centre as seen from the lighter shades of gray. This is also seen in our photometric results. In the B-I curve we see the cluster becoming bluer from 2.5' of arc to about 6' of arc along the major axis. This change to bluer colour is because of the contribution from the bulge. The scale of this plate

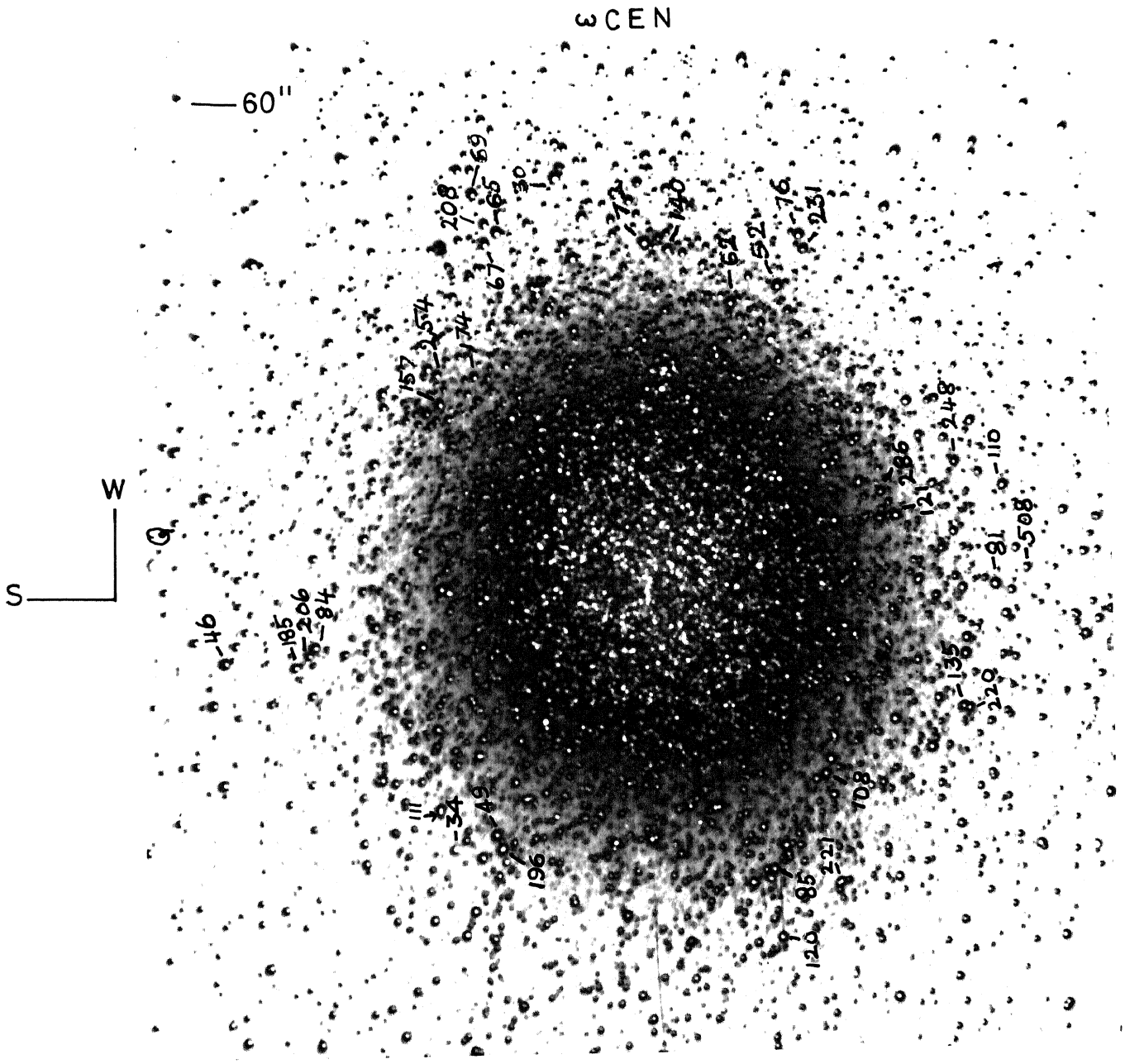

PLATE VII

Table IV-3

B Magnitude and colour of the red stars marked in plate XVII

Royal Observatory Annals No.	B	B-V
46	13.08	1.65
185	13.31	1.27
206	13.37	1.25
84	13.44	1.77
157	13.31	1.34
254	13.49	1.24
174	13.36	1.34
67	12.85	1.29
208	13.43	1.30
65	12.86	1.32
69	13.03	1.46
30	11.89	0.86
72	12.56	0.96
140	12.97	1.07
62	13.05	1.52
52	13.02	1.55
231	13.82	1.63
76	12.93	1.31
116	12.90	1.12
121	12.88	1.07
286	13.90	1.57
248	14.67	1.84
110	13.22	1.46
81	12.91	1.25
508	14.05	1.22
135	13.53	1.66
196	12.5	0.42
49	13.04	1.60
34	11.59	0.44
111	13.15	1.39
108	13.39	1.63
220	13.61	1.45

is about 6 mm/minute of arc and hence the size of the bulge can be easily judged. The cluster becomes redder, when the contribution from the bulge has decreased and the contribution from the red giants dominate the field. The effect of the sudden decrease in the contribution, to the surface brightness, from the bulge, is seen as a kink in the B-I colour curve of Fig. II-8 in the region between 5' and 8' from the centre. They have been marked by arrows in the figure.

CHAPTER V

RESUME OF RESULTS

V.1 Results of the photometric study: The conclusions derived from the observations presented in earlier chapters are described herein. They constitute results from photo-electric aperture photometry on Omega Centauri and photo-graphic equidensitometry of Omega Centauri and 47 Tucane. We have also seen the correlation between the colour variation over the cluster and the change in ellipticity with distance from the centre.

We have in Table II-10 values of log f_o in UBVRI bands for the cluster Omega Centauri where f_o is the surface brightness at the centre in units of U, B, V, R or I = 10.0 magnitude/arc sec^2. In Table II-11, we give core-radii calculated for the major and minor axis separately, using King's theoretical model. The wavelength dependence of the core-radius, is easily seen in the result. Along the major axis, r_c decreases with increasing wavelength and along the minor axis r_c increases with increasing wavelength except for the I band. The ratios of the r_c values for the major and minor axis show that the cluster has less flattening in longer wavelength. Typical values of core radii illustrating the dynamical characteristics of

Omega Centauri are of course obtained from intensity gradients in the 45° direction with respect to the major and minor axes. The differences in wavelength dependence of core radii along major axis and minor axis indicate the contribution to ellipticity by the blue component of stellar population in the cluster. Such studies of globular clusters, especially aimed at derivation of kinematical parameters from brightness distributions, are therefore, best done in the red or near infrared.

Hartwick's luminosity function for M92, alongwith photometric results available in UBVRI bands for the cluster, has been used to calculate the sampling errors in UBVRI bands and also in U-B, B-V, V-R and R-I colours. Tables III-4 and III-5 give these values.

Fig. II-8 gives the distribution of (B-I) colour along the major and minor axis. The curve shows the colour at the centre of the cluster to be uniform over a circular zone of 2.5' radius. This value matches with the value of core-radius for Omega Centauri. Beyond this the cluster becomes bluer by B-I $\simeq$ .45 mag. over a annular zone of $\lesssim$ 3' in width. The cluster again becomes redder beyond this annular zone. The arrow mark in Fig. II-8 show regions where the cluster colour has suddenly changed, beyond the bluer zone. One derives the impression that the distribution

of stars in Omega Centauri can be divided into two groups. The red stars form a system which is quite widespread when compared to the bluer stars; the latter form a bulge around the core of the cluster. These blue objects are mainly the resolved and unresolved stars in the zone 2.5' to 5' which give a background brightness in this region of the cluster. The distribution of bright giants can be seen even beyond the boundary of the blue bulge. When the contribution from the blue bulge has decreased considerably, most of the surface brightness in this region of the cluster, comes from the red giants. They change the (B-I) colour considerably, and produce some depressions in the colour curve. In the intermediate region (2.5' to 5') the bulge has a bigger contribution to the surface brightness than these red giants and hence the colour is bluer there.

A U-B/B-V diagram has been used to find the UV excess, $\delta(U-B)$, over the cluster. In diagram II-10, $\delta(U-B)$ is plotted against the distance from the cluster centre. The cluster in the core has a uniform UV excess $\simeq 0.26$. The UV excess beyond 5' decreases with increasing distance from the centre. The UV excess in the intermediate region shows a sudden increase in the value of ~~colour~~ UV excess $\delta(U-B) \simeq .1$ mag . This is an indication of the difference between the two groups of stars, one forming the

red component of the cluster and the other forming the blue bulge. The red stars seen in the core and also outside the intermediate region show the same UV excess.

The R/R-I diagram in Figure II-6 exhibits the effect of the blue contribution to the integrated light in the intermediate region. (R-I) colour for the giants in M92 (Strom and Strom 1971) is $\simeq$ 0.50 mag. This value is consistent with the value we get for the centre of Omega Centauri. In the fainter outer regions of the cluster, the (R-I) colour gets smaller and smaller, because of the contribution from the blue bulge. Beyond $r \simeq 6'$, the cluster again turns redder as the bulge contribution has decreased.

The results of equidensitometry show the good agreement between the values for the centres in B and infrared bands. Hence, we infer that there is no asymmetrical absorption over the cluster caused by dust.

Fig. II-2 gives the change of ellipticity and position angle with distance from the centre. The figure shows the following details.

a) The core of the cluster which has a radius of $\precsim 2.5'$ is the most spherical region in the cluster. This is consistent with our ideas of cluster dynamics. As the core is

continuously losing angular momentum due to stellar encounters, it should show lower ellipticity.

The observed ellipticity values show sudden increase in the intermediate region of the cluster.

Between 5' and $\lesssim$ 8' the ellipticity decreases and reaches a minimum. The position angle for the core is quite different from that for the outer regions.

The above four characteristics of the ellipticity curve can be seen in the ellipticity curves for M5, and 492 (Kadla et al 1976).

Equidensitometry on 47 Tucanae also shows similar results as seen in the figure III-7.

In Fig. III-8, we have compared the results of photoelectric photometry with the results obtained from equidensitometry of Omega Centauri. The ellipticity is low for the zones where the cluster is red. The ellipticity shows sudden increase where the cluster is bluer. The blue bump in the colour curve matches well with the region where the ellipticity suddenly increases. The ellipticity reaches a maximum where the cluster is the bluest.

Chun and Freeman (1979) give photometric results for the cluster 47 Tuc. They report that the cluster colour becomes bluer by B-V $\simeq$ 0.1 mag. around 2' from the centre. This matches well with the region of increase in ellipticity in 47 Tuc.

The presence of such bulge for M92 can be inferred from available data. Sandage and Walker (1966) have shown that the red giants and asymptotic giant branch stars in M92 show different UV excess and that they can be easily separated in a colour-colour diagram. Strom and Strom (1971) have made detailed spectroscopic studies of these stars, but could not see any evidence of UV excess in the spectral energy distribution. They show the dependance of δ(U-B) on the distance of the star from the centre. From our earlier results, we have found that the increase in ellipticity is due to the bulge around the core. In Fig. III-4, the ellipticity in M92 increases from $\simeq$100" from the centre and remains large upto a distance of $\simeq$160". This is the zone where the anomalous difference in the UV excess is the largest for the giant and asymptotic branch stars. The chances are that the photometry in this region is being affected by the bulge which has a large colour excess. This UV excess does not exist outside 200". One objection to this argument will be that both the groups

of stars are measured in the same region. But we should keep in mind that the giants are very much brighter than the asymptotic branch stars and hence the UV excess will not be so easily seen in the measurements of giants. UV excess of this type has been noticed in several globular clusters. This may probably mean that many of these clusters have blue bulge around the core.

Strauss (1978) has done strip photometry on 14 globular clusters in UBVRI colours. All his clusters show "red kinks" similar to what we have seen for Omega Centauri, in the B/I curves. Whether a blue bulge in these clusters exist can only be settled on the basis of further observations of the kind reported herein.

V.2 Nucleus of M31 and Omega Centauri: Using stratoscope pictures of M31, Light et al (1974) have shown that the nucleus of M31 is a separate and distinct feature of the galaxy. It is found elliptical (1" x 1.6") with its major axis lying in position angle 63° ± 5°. The position angle of M31 is usually taken as 38° (Lindblad 1956, Hubble 1929, and de Vaucouleur 1958). Johnson (1961) has shown this difference in the position angles of the nucleus and the outer parts of the galaxy. Light et al find a sharp discontinuity of the nucleus from the nuclear bulge. They

suggest that, as the nucleus and bulge are separate features, they would exhibit different velocity dispersion, colour, metallicity etc. which could be detected from ground based observations.

Walker's (1974, 1975) rotation curve, for the nucleus of M31, peaks with V $\lesssim$ 100 kms/sec at r = 2".2. Beyond r = 2".2, the rotation curve varies in a Keplerian manner. Peterson (1978) has measured the rotation in the nuclear region of M31 and got a peak velocity of V $\lesssim$ 60 kms/sec. at 1.5" of arc from the centre. He finds the velocity then dropping down to $\lesssim$ 0 kms/sec between 3" and 6" before rising again. This rotation curve was explained using a 2 component dynamical model, one component representing the nucleus and the second representing the nuclear bulge. The bulge component which dominates the surface brightness beyond 2" ($\lesssim$ 6.5 pc) has a major axis luminosity profile with core-radius $\lesssim$20" (from King's model fit).

The core of Omega Centauri can be seen dominating the bulge better in infrared light, since the bulge is found to be bluer. The bulge in Omega Centauri seems to contain large number of asymptotic branch stars as derived from their δ (U-B) characteristic. If we assume that larger ellipticity is the result of higher rotation speeds, then the bulge in Omega Centauri should be rotating faster than

the core. In the results obtained by Walker, the region of maximum rotational velocity falls well outside the nucleus, whereas Peterson's observation shows that this region is at the boundary of the nucleus. The core-size of Omega Centauri in B light $\simeq$ 4 pc in radius whereas the radius of the nucleus of M31 is 5 pc. The maximum ellipticity in Omega Centauri is seen at 7.5 pc and the maximum rotational velocity in the nucleus of M31 is also at 7.5 pc when Walker's results are considered. Peterson shows a dip in the velocity between 10 pc and 20 pc from the centre. For Omega Centauri also we see a dip in the ellipticity curve 8 pc and 12 pc from the centre. Beyond this the ellipticity is increasing in Omega Centauri and so is the case of rotation in the nucleus of M31.

The analogy between the nucleus of a galaxy and the globular clusters is not well understood. In Omega Centauri, the bulge consists of evolved horizontal branch stars. Because of mass-loss, during the star's evolution through the giant branch, these stars should attain larger velocity dispersion and in a rotating cluster, larger angular momentum. Hence, from dynamical considerations, the chances are that the bulge which contains stars thrown out from the core, should have larger rotation than the core and hence larger ellipticity. In the case of Omega

Centauri, the boundary of the blue bulge is shown by the "red kinks" in the (B-I) curve. For Omega Centauri these kinks match with the region of low ellipticity. The reasons for the low rotation between 10 pc and 20 pc in the M31 nucleus are not clear. Perhaps there may be a similarity between the observed phenomena in Omega Centauri and the M31 nucleus. A multi-colour study would shed much light on this problem.

REFERENCES

Arp, H.C. 1959, A.J., 64, 441.

Arp, H.C. 1965, Galactic Structure, ed. A. Blaauw and M. Schmidt (Chicago : University of Chicago Press, Chap. 19, p. 401.

Arp, H.C., Baum, W.A., and Sandage, A.R. 1953, A.J., 58, 4.

Bappu, M.K.V. 1977, Kodaikanal Observatory Bulletin, 2, 64.

Bappu, M.K.V. 1978, Paper presented at ESO Symposium on Astronomical photography conducted at Geneva.

Baade, W. 1944, Ap. J., 100, 137.

Baum, W.A., Hiltner, W.A., Johnson, H.L., and Sandage, A.R 1959, Ap. J., 130, 749.

Bell, R.A., and Dickens, R.J., 1974, M.N.R.A.S., 166, 89.

Bohm-Vitense, E., Holweger, H., and Kohl, K. 1963, Ap.J., 130, 604.

Cannon, R.D., and Stobie, R.S. 1973, M.N.R.A.S., 162, 207.

Cathey, L.R. 1974, A.J., 79, 1970. 1370.

Chun, M.S., and Freeman, K.C. 1979, Ap.J., 227, 93.

Da Costa, G.S. 1979, A.J., 84, 505.

de Vaucouleurs, G, 1958, Ap.J., 128, 465.

Dickens, R.J., and Bell, R.A. 1976, Ap.J., 207, 506.

Dickens, R.J., and Rolland, A. 1972, M.N.R.A.S., 160, 37.

Dickens, R.J., and Woolley, R.vd.R. 1967, R.O.B., No.128.

Eggen, O.J. 1971, Ap. J., 163, 313.

Eggen, O.J., and Sandage, A.R. 1965, Ap.J., 141, 821.

Feibelman, W.A. 1979, A.J., 84, 497.

Fernie, J.D. 1974, P.A.S.P., 86, 837.

Freeman, K.C., and Rodgers, A.W. 1975, Ap.J (Letters)., 201, L71.

Gascoigne, S.C.B., and Burr, E.J. 1956, M.N.R.A.S., 116, 570.

Geyer, E.H. 1966, Z. Astrophys., 66, 16.

Gott, J.R. III. 1973, Ap.J., 186, 481.

Gott, J.R. III. 1975, Ap.J., 201, 296.

Greenstein, J.L. 1939, Ap.J., 90, 387.

Harding, G.A. 1962, Observatory., 82, 205.

Harding, G.A. 1965, R.O.B., No.99.

Hartwick, F.D.A. 1970, Ap.J., 161, 845.

Hodge, P.W., and Brownlee, D.E. 1966, P.A.S.P., 78, 125.

Hogner, W., Kadla, Z.I., Richter, N., and Strugatskaya, A.A. 1973, Sov. Astron., 16, 843.

Hubble, E. 1929, Astrophys. J. 133, 309.

Iben, I. 1974, Ann. Rev. Astr. and Ap., 12, 215.

Illingworth, G. 1977, Ap.J (Letters)., 218, L43.

Illingworth, G., and Illingworth, W. 1976, Ap.J. Suppl., 30, 227.

Iriarte, B., Johnson, H.L., Mitchell, R.I., and Wisniewski, W. 1965, Sky and Telescope., 30, 21.

Johnson, H.M. 1961, Ap.J., 133, 309.

Kadla, Z.I. 1966, Sov. Astron., 10, 97.

Kadla, Z.I., Richter, N., Strugatskaya, A.A., and Hogner, W. 1976, Sov. Astron., 20, 49.

King, I.R. 1962, A.J., 67, 471.

King, I.R. 1966, A.J., 71, 64.

King, I.R. 1966, A.J., 71, 276.

King, I.R. 1975, Paper presented at IAU Symposium No.69.

King, I.R. 1978, Ap.J., 221, 1.

Kraft,R. 1978, Paper presented at IAU symposium No.80,167.

Kron, G.E., and Mayall, N.U. 1960, A.J., 65, 581.

Larson, R.B. 1975, M.N.R.A.S., 173, 671.

Lau, E., and Krug, W. 1957, Die Aquidensitometric, Akademie-Verlag., Berlin.

Lin, C.C., and Shu, F.H. 1964, Ap.J., 140, 646.

Lin, C.C., and Shu, F.H. 1966, Proc. Natl. Acad. Sci., 55, 229.

Light, E.S., Danielson, R.E., and Schwarzschild, M. 1974, Ap.J., 194, 257.

Lindblad, B. 1956, Stolkholm Obs. Ann., 19, No.2.

Lindsay, E.M. 1956, Vistas in Astronomy., A. Beer, ed. (Pergamon Press, Inc., New York), Vol.2, p. 1057.

Mallia, E.A. 1977, Astron. and Astrophys., 60, 195.

Martin, W.Chr. 1937, "Photographische Photometric van veranderlijke Sterren in Omega Centauri" (Thesis, Leiden).

Martin, W.Chr. 1938, Ann. Sterrew. Leiden, XVII, Part 2.

Michie, R.W. 1964, Ann. Rev. Astron. Ap., 2, 49.

Morgan, W.W. 1959, A.J., 64, 432.

Norris, J., and Bessell, M.S. 1975, Ap.J., 201, 175.

Oort, J.H., and van Herk, G. 1959, Bull. Astr. Inst. Netherlands, 14, 299.

Peterson, J.A. 1977, Ap.J., 214, 550.

Peterson, C.J. 1978, Ap.J., 221, 80.

Peterson, C.J., Ford, W.K., and Rubin, V.C. 1977, A.J., 82, 32.

Peterson, C.J., and King, I.R. 1975, A.J., 80, 427.

Richter, N., und Hogner, W. 1963, Astron. Nachr. 287, 261.

Rusev. 1972, Sov. Astron., 18, 71.

Sandage, A.R. 1953, A.J., 58, 61.

Sandage, A.R. 1957, Ap.J., 125, 422.

Sandage, A.R. 1970, Ap.J., 162, 841.

Sandage, A.R., and Walker, M.F. 1966, Ap.J., 143, 311.

Shapley, H. 1917, Ap.J., 45, 118.

Shapley, H. 1930, "Star Clusters" (Harward University Press, Cambridge, Massachusetts).

Sistero, R.F., and Fourcade, C.R. 1970, A.J., 75, 34.

Stebbins, J. 1950, M.N.R.A.S., 110, 416.

Strauss, F.M. 1978, Astron. Astrophys. Suppl., 33, 315.

Strom, S.E., and Strom, K.M. 1971, Astron. Astrophys. 14, 111.

Strom, S.E., Strom, K.M., and Goad, J.W. 1976, Ap.J., 204, 684.

Toomre, A. 1977, Ann. Rev. Astron. Astrophys., 15, 437.

Walker, M.F. 1974, P.A.S.P., 86, 861.

Walker, M.F. 1975, P.A.S.P., 87, 479.

Wallsistein and Pallachowski. 1978, Paper presented in the IAU Symposium No.80, p. 173.

Wilson, C.P. 1975, Astron. J., 80, 175.